Development of a global spatio-temporal seismicity model and its application to the Vrancea Seismic Zone, Romania

by

Nastasja Anais Scholz

A thesis submitted to the Victoria University of Wellington in fulfilment of the requirements for the degree of Master of Science in Geophysics.

Victoria University of Wellington 2007

Abstract

This study investigates the temporal behaviour of major earthquakes in the Vrancea Seismic Zone (VSZ)in Romania. I used the Romplus catalogue, which is a compilation of several sources and spans the time from 984 AD to the year 2005 and in which the data are of different quality. This catalogue contains only Vrancean earthquakes and consists of more than 8000 events. Qualities 'A', 'B' and 'C' were used to model the data. 'D' and '=' were found as too unreliable for modeling. Using the b-value, I concluded that 3.5 is the correct cut-off magnitude for earthquakes after 1980 and at depths of 60 km and greater. Thereby I detected an increase in the b-value after 1986 of about 0.2 units. The reason for this increase could not be found. Plotting the Gutenberg-Richter relation for several time and depth intervals, it was found that at larger depths than 60 km, there are too many M7 earthquakes as compared to small shocks. The shape of the Gutenberg-Richter relation is similar as to the one expected by the characteristic earthquake model (Schwarz and Coppersmith, 1984; Wesnousky, 1994). A strike of 53° was found and the earthquake coordinates were rotated correspondingly. The resulting view on the slab showed the confined volume in which the earthquakes happen and well as the 'aseismic part' of the slab between 40 km and 60 km of depth. The seismicity seems to reach a depth of 180 km. Only the earthquakes in the slab, below a depth of 60 km, show clustering behaviour. Furthermore, the M7 earthquakes all happened in the slab. Thus, a depth limit of 60 km was introduced for modeling. In order to find aftershocks in the catalogue, the temporal behaviour of the Vrancea earthquakes was examined. The mean magnitude increases after each major earthquake, indicating an aftershock process. This was confirmed by the rate of occurrence, which showed an increase in rate after the 1990 earthquakes. The rate of occurrence is too low for the first 580 days after 1980, possibly due to insufficient earthquake detection in this period of time.

All the damaging M7 earthquakes all happened in the slab. Thus, shallow earthquakes had to be considered separately. A depth limit of 60 km was introduced and earthquake in shallower and deeper depths were considered separately. For the shallow earthquakes there was a sharp increase in the apparent b-value below the cut-off magnitude of 3.5. After reaching a value of 2.4, the b-value starts to fall steeply. This was attributed to biases in the magnitude calculation. I used the rounded value of 3.5 as a cut-off magnitude for the shallow earthquakes. Having found the magnitude cut-off, depth and time limit, modeling could be started. The model gives two important parameters: the proportion of aftershock and the time to the next earthquake. Using the Maximum Likelihood Method, a best fit was found for a data set starting at 1980 and consisting of earthquakes with a cut-off magnitude of 3.5 and a depth equal and greater than 60 km. According to the model, this data set consists of 13 ± 5% aftershocks and has an inter-event time for new earthquakes of 13 ± 1 days. Using several cut-off magnitudes, it was found that the calculated inter-event time for these earthquakes is consistent with the Gutenberg-Richter law. In contrast, the predicted value for the inter-event time of M7 earthquakes does not match the one found in the catalogue. While the Maximum Likelihood Method leads to 814 years as recurrence time, the data shows a recurrence time of only 23 years. The model fits the data set of the 1990 aftershocks very well, too, leading to a aftershock proportion of 58 ± 15%. The data set for the 1986 did not lead to good results, probably due to missing aftershocks shortly after the main shock. Comparing model and data with a pure Poisson model I could see that earthquakes tend to cluster in the first days after the major event. Several days later, their behaviour changes and then is similar to the one proposed by the seismic gap model. Looking at the ratio between the probabilities of the model of Smith and Christophersen and of the Poisson model, a clustering behaviour in the first 24 hours after the main shock was found, followed by a decreased seismicity, which reverts to be Poissonian after 100 days. Thus, I concluded that aftershock behaviour is only relevant after the first 24 hours following a major earthquake. After 24 hours, seismic hazard decreases to be less than as expected by the Poisson model in the following 100 days, until seismicity returns to be Poissonian again. Additionally, I suggest that the 1990 earthquake and its aftershocks should be considered as a ’model earthquake’ for future earthquakes as it seems to be representative for earthquake behaviour in the VSZ.

CONTENTS

LIST OF FIGURES

1. INTRODUCTION

Earthquakes are non-linear, chaotic, and scale-invariant and because they are self-similar, they are impossible to predict precisely (Geller et al., 1997). This means that it is not possible to give the exact date, location, and magnitude of a future earthquake, because of the continuum and fractal nature of it. Allen (1976) says that an earthquake prediction can only be considered as valid if time, magnitude, and area of occurrence are specified. They have to be within well-defined limits, such that the prediction can be judged in terms of its success or failure. He states that very generalized predictions, like saying that an earthquake could happen within 25 years, can lead to a development of realistic building codes and land-use planning. But short-term predictions are those which are commonly more in demand regarding alerting emergency forces and evacuation. Here, I cite Allen (1976) who gives six attributes a valid earthquake prediction should have:

- It must specify a time window
- It must specify a space window
- It must specify a magnitude window
- It must give some sort of indication of the author's confidence in the reliability of the prediction
- It must give some sort of indication of the chances of earthquake occurring anyway, as a random event
- It must be written and presented in some accessible form so that data on failures are as easily obtained as data on successes

It is common to formulate earthquake prediction in terms of probabilities and that makes it a statistical problem. Kagan (1997) defined earthquake prediction as (probabilistic) statement about future earthquakes, which reduces the uncertainty of their occurrence compared to present knowledge. This statement should be testable. Ideally, the time-dependent prediction should be a formal rule that predicts the rate of occurrence of earthquakes over some interval of time and space, include the seismic moment tensor and it should have

better results than the Poisson estimate. The testing of these predictions must include the comparison with the null hypothesis that states that prediction successes are due to chance, and it should include spatial variations and temporal clustering of seismicity (Kagan (1997) and references therein). There are no reliable precursors of earthquakes. However, Kagan (1991) suggests that increased seismic activity indicated future large earthquakes. In my work I will use a spatiotemporal model and apply it to the Vrancea Seismic Zone (VSZ) which is located in Romania, Eastern Europe. This model should give me probability estimates for next major earthquakes, which is of huge concern regarding the poverty of this country and its vulnerability to earthquakes.

1.1 Romania

Fan et al. ((1998) and references therein) describe the Carpathian Mountains as a part of the northern branches of the Alpine fold-and thrust system. The Alpine-Carpathian orogenic belt reaches from Eastern-France to the Black Sea. In the early Jurassic, the collision between the African, Arabian and Eurasian plates formed this belt, consisting of a large number of plates and subplates. Their movement resulted in extremely complex structures. The Carpathian arc in Romania is a result of the suturing of continental fragments against the irregulary boundary of the Eastern European Platform and ongoing continental convergence. Wenzel et al. (2002) and Sperner et al. (2001) give a good overview of the tectonic history and the formation of this area. Seismicity in the Romanian Carpathians consists of earthquakes at shallow and intermediate depths. While the shallow seismicity is more diffuse and can be attributed to known fault zones and mountain areas, the intermediate-depth seismicity takes place in the Vrancea Seismic Zone (VSZ), with a deepest event on May 16, 1982, with a M_L of 4.3 and a focal depth of 221 km (ISC). Less seismicity is found between 40 and 70 km, which was attributed to the rheology condition of

the descending slab by Fan et al. ((1998) and references therein). The subducted lithosphere is continental (Necea et al, 2005) which leads to more defuse and broadly distributed internal deformation. Van der Hoeven (2003) states that subduction started 16 M years ago, involving slab roll-back and (hypothesized) slab break-off which started in the Norther Carpathians and migrated to the VSZ, where the slab still seems to be attached to the surface. This is also suggested by Wenzel et al. (2002).

1.1.1 Vrancea Seismic Zone

The Vrancea Seismic Zone (VSZ) (Fig. 1) is potentially the most hazardous source area not only for Romania but also for a large part of eastern and southeastern Europe. Although its strongly confined seismicity makes it unique in Europe, it is not well understood yet. Many strong earthquakes have occurred in the VSZ, e.g. November 10, 1940, M_W = 7.7, 160 km depth; March 4, 1977, M_W = 7.5, 100 km depth; August 30, 1986, M_W = 7.2, 140km depth; May 30, 1990, M_W = 6.9, 80km depth; (Wenzel et al., (2002)). These events caused immense damage and fatalities. The VSZ lies beneath two corner forming mountain belts consisting of the Eastern and Southern Carapthians. From Vrancea the Eastern Carpathian Mountains reach into the Ukraine and Slovakia in the Northwest and the Southern Carpathian Mountains reach towards the Southwest. Northeastern and southwestern crustal bounds are the Trotus-Pecebeaga Camena fault zone and the Intramoesian fault, respectively. Three lithospheric blocks take part in the tectonic evolution and continental collision near the Vrancea region: the East European Platform, the Moesian subplate, and a subplate consisting of the intra-Carpathian basin system. This system includes the Pannonian Basin, the Apuseni Mountains, and the Transylvanian Basin. The Pericarpathian fault zone, in front of the Carpathian arc, and the Peceneage-Camena fault zone long the axial extension of the Eastern Carpathians form the major fault zones.

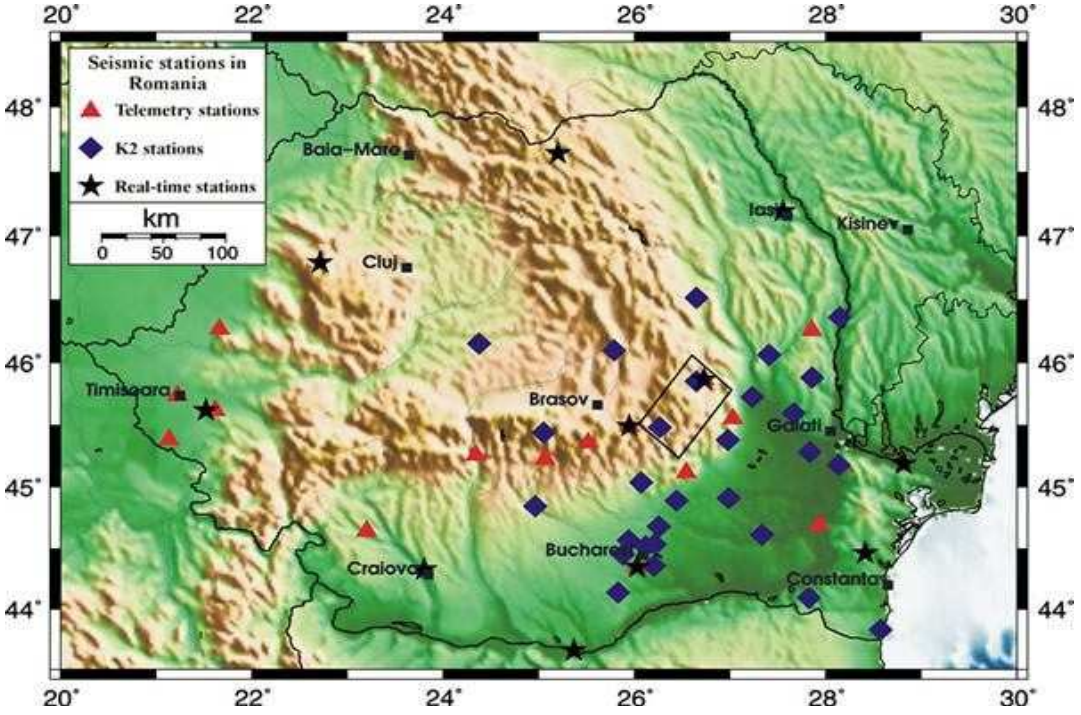

***Fig.1.1**: Location of the VSZ in Romania as well as the recording stations. Plotted by Radulian M. et al. (2007)*

Wenzel et al. (2002), who synthesize interpretations of plate kinematics, seismic tomography and the features of the stress and strain field into a geodynamic model, see this seismicity, like van der Hoeven (2003), as a result of plate break-off beneath Vrancea. The authors say that all earthquakes of intermediate depth have a compressive, thrust faulting regime and that the fault plane solutions of the large earthquakes are very similar, with a strike SW-NE, a dip of 60° to 70° to the NW and a slip angle of about 90°. The use of the Gutenberg-Richter law with a b-value of 0.78 leads to recurrence times of 10 years for M_w > 6.5, 25 years for M_w > 7.0 and 50 years for M_w > 7.4, three earthquakes with M_w = 7.0 per century and six events with M_w > 6.8 per century. Wenzel et al. (2002) conducted several tomographic studies of the VSZ and found weak indications of slab detachment. It seems that the slab extends deeper than 200 km, the level at which seismicity stops, with an

additional 150km of aseismic slab. Sperner et al. (2001) calculated a 3D model of the velocity-depth structure by inverting teleseismic P-wave traveltimes residuals and found, too, that the maximum depth has to be larger than the maximum depth of the earthquakes. The volume of elevated velocities shows a change in strike from top to bottom from a strike orientation SW-NE at the location of the shallowest material and S-N for the deeper portions of the high-velocity material. Wenzel et al. (2002) also examined the strain and stress beneath Vrancea. From geological evidence they concluded that the active subduction ended about 10 million years ago and that the only forces which still are acting on the slab are the gravitational force and pressure. The geodynamic model of Wenzel et al. (2002, and references therein) assumes that the Miocene subduction consisted of roll-back of the subducting slab, so that the intra-Carpathian blocks moved (independently with different directions and velocities) to the Northeast and East, accompanied by counterrotation of these blocks. Slab steepening produced along-strike extension and the curved geometry of the Carpathian arc caused a segmentation of the slab. After this, the continental collision started, followed by the plate break-off of the slab segments. Bazacliu et al. (1999) separated the slab into different segments. These segments are the following: Zone A: 60-100 km with the highest magnitude of 7.4; Zone B: 100-120 km, a probable transition zone; Zone C: 120-180 km with the highest magnitude of 7.6. They assume that the earthquake generation process in the segments develops almost independently from each other. There is also a sharp decrease in the b value to 0.4 at depths below 160km. It agrees with stress drop increase in the lower part of the slab, but it also could mean that they did not choose the right cut-off magnitude, which has influence on the b-value. At around 100 km depth, the slope b has a value of 1.4, which characterizes the asperity-like seismic activity and this is assumed to be caused by the presence of a dehydration reaction in this zone (references in Bazacliu et al. (1999). Ardeleanu (1999) also mentions the segmentation into three zones:

- Within the foredeep region, in front of the bending zone of the Carpathian arc, is the zone of crustal, moderate earthquakes with a maximum magnitude M_S = 5.2 and hypocenters at depths between 0 and 40 km.
- There is a zone of low seismicity at depths between 40 and 60 km.
- At depths of 60 to 200 km, there is the zone of well-confined, subcrustal earthquakes. Here happened about five major events in each century with a value of M_W of about 7.0.

(see references in Ardeleneanu (1999)). Her tests indicated that shallow events can be modeled by a clustered pattern in space and time and that the mainshocks at intermediate depths are completely random, which is related to the heterogeneity of the segment. She assumes that the shallow activity is related to the NW-advancement of the Black Sea platelet. References in Ardeleneanu (1999) suggest bi-axial, homogeneous stress in the crust, and the vertical principal stress is the minimum compression axis. In the subcrustal zone, it is suggested that the minimum compression axis acts vertically and the maximum compression axis acts from NE to SW. This is related to the occurrence of different space and time seismicity patterns, which are seen as other evidence for a decoupling slab.

Hurukawa et al. (2006) state that historical M7 earthquakes show a clear dependence of focal depth on the particular active time in each century. They mention a ”quasi-cycle” of about 100 years, in which the first M7 earthquake occurs in a deeper segment (140-160 km) during the first 10 years. The second event occurs in the midst segment (110-140 km) between the years 30 and 40, and the last M7 earthquake occurs in the middle segment (80-110 km) between 70 and 90 years after the start of the ”century”. The Romplus catalogue does not show these ”quasi-cycles”. Only once there is a match concerning the focal depths of three consecutive M7 earthquakes, but these events all happened within a time period of 60 years.

1.1.2 Stations in the VSZ

Wenzel et al. (1999) give a good description of the stations in the VSZ. The systematic monitoring of earthquakes started in 1892, when S. Hepites set up a network of macroseismic stations with 320 observation points. This network was working until World War I, and again from 1921 to 1926. Since the M_W = 7.4 earthquake the 4th of March 1977 the distribution, the number and the dynamic range of free-field accelerometers in seismic regions has increased considerably and digital instruments are now used. There are now over 70 strong motion accelerometer stations in Romania and the data base of seismic ground motion records is accumulating. The accelerograph network of Building Research Institute INCERC (Institutul National de Cercetari) Bucharest, the National Institute of Research and Development for Earth Physics (NIEP) and ISPH-Geotec (Institute for Hydro-energetic Studies and Designs) consists of 71 strong motions accelerographs (SMA-1) in the seismic zones of Romania. This network produced more than 110 useful records during the Vrancea earthquakes of 1977, 1986 and for both earthquakes of 1990. In 1997, the geophysical institute of Karlsruhe, Germany, and the NIEP started to install a modern network with digital Kinematrics-K2 instruments in Bucharest and the Southeast of Romania. This network did not record stronger earthquakes than M_W = 5.3 to the time the paper was written. Only in 2005 a new M6 earthquake happened in the VSZ. Periods of sampling are 0.01s and 0.02s and the measurements are in cm/s^2. Due to the very confined focal volume of the VSZ, the source-receiver geometries remain almost constant. For the sites in Bucharest, with an average epicentral distance of 170 km, the backazimuths as well as the angles of incidence at the free surface vary less than 10 degrees.

2. CATALOGUE AND DATA DESCRIPTION

2.1 Catalogue and Data Quality

2.1.1 Romplus-Catalogue

I worked with the data of the Romplus-catalogue (Onescu et al., 1998) which reaches back to the year 984 AD and ends in the year 2005. It includes the time, location, depth, magnitude, number of stations, RMS time residual, quality and errors of 8148 earthquakes (see Appendix). The Romplus catalogue is based both on compiled data and on new locations. For the period 984 to 1979, the data are compiled from the catalogue of Constantinescu and Marza (1980). According to Oncescu et al. (1999, Wenzel et al., Vrancea Earthquakes: Tectonics, Hazard and Risk Mitigation), the events are relocated or newly relocated between 1980 and 1997, and the locations based on picks from digital data are preferred. Magnitude evaluation is based on the measurement of the amplitude of seismic waves. But one of the features of magnitudes is the saturation of all magnitude scales for strong events. Kagan (1991) mentions the causes: (1) the complexity of the source-time seismic moment tensor release; (2) filtering of a seismic signal through the structure of the earth; (3) filtering through the seismometers. Mostly, high frequencies are used to estimate magnitudes, but the waves undergo scattering, multipathing, focusing and unfocusing. The higher the frequency, the stronger are these effects. The magnitude used in the catalogue, is stated to be the moment magnitude. The moment magnitude is a successor to the Richter scale and is used to be consistent over a large magnitude range. It is dimensionless and defined by

$$Mw = \frac{2}{3}(log10 * \frac{M0}{Nm} - 9.1) \qquad (2.1)$$

where M_0 is the seismic moment and Nm is the unit of the moment. Thus, the different magnitude scales were converted into the moment magnitude *Mw*, because in contrast to

the surface wave magnitude, the body wave magnitude and other magnitudes in the original data, the moment magnitude does not saturate, and should be known with an accuracy of 0.5 units (Oncescu et al, 1999, Wenzel et al., Vrancea Earthquakes: Tectonics, Hazard and Risk Mitigation). The fact that it does not saturate, means that there is no particular value beyond which large earthquake all have the same magnitude. Oncescu et al. (1999) state that, for earthquake of medium or small sizes, the catalogue is not complete before 1400. According to them, it should be complete between 1411-1800 for M_W = 7.0 , between 1801-1900 for M_W = 6.5, between 1901-1935 for M_W = 5.5, between 1936-1977 for M_W = 4.5 and they even state that between 1978-1997 the catalogue should be complete for M_W = 3.0. Results of my own work cast some doubts on this assumption.

2.1.2 Data Quality

The quality of the data in the Romplus catalogue has five different values: 'A', 'B', 'C', 'D' and '='. These labels refer to different authors. 'A' has 14 phases, an RMS of the location of 0.2s, a GAP (the biggest azimuth angle of separation between stations) of 140 degrees and 10 S-phases. 'B' has 8 phases, an RMS of location of 0.3s, a GAP of 240 degrees and 8 S-phases. 'C' represents the lower quality and for macroseismic measurements ,'D' was automatically given. '=' was used to indicate missing statement about the quality of an earthquake. First I decided to exclude only earthquakes with quality '=' in this work. In the following plots I used numbers for the quality values A, B, C and D, so that no given value is Zero, and A= 1, B = 2, C = 3 and D = 4. I plotted the quality against the three factors RMS, number of stations (NS) and GAP. In Fig. 2.1, it is obvious that quality 'D' is unrestrained and thus these earthquakes should not be used. The earthquakes of the qualities 'A', 'B', and 'C' all have an RMS of approximately 0.5 and smaller. The Fig. 2.2 shows that there is no relation between the quality and the number of stations. For example, quality 'B' is assigned to earthquakes with the fewest stations. In contrast, the Fig. 2.3 shows that the GAP increases with decreasing quality and gets unreasonably large for earthquakes of

quality ’D’. So I decided not to use the earthquakes which are of quality ’D’ either.

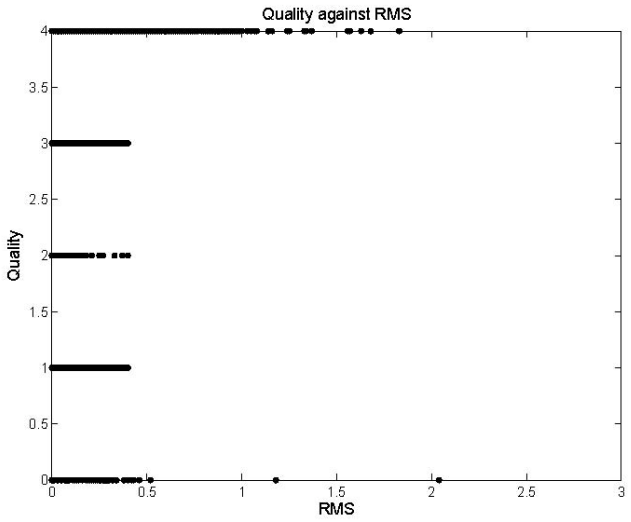

Fig. 2.1*: Relation between the quality and the RMS residual*

2.2 Catalogue Incompleteness

Catalogues that are based on longer period waves miss many early aftershocks, even when their magnitudes are above the stated magnitude threshold. This may introduce significant biases in the statistical analysis of seismicity. The behavior of aftershock sequences during

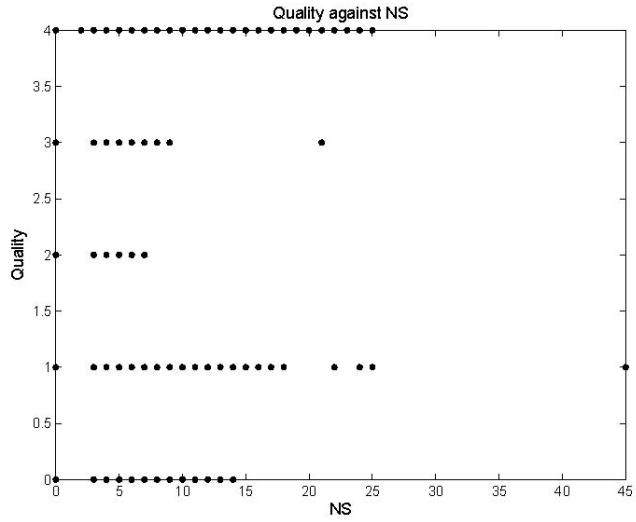

Fig. 2.2: *Relation between quality and the number of station*

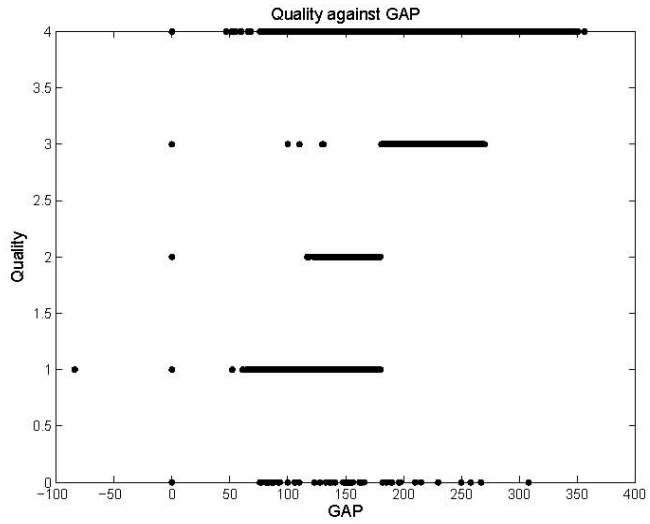

Fig. 2.3: *Relation between the quality and the biggest Azimuth Angle of Separation (GAP) between stations*

the first minutes and hours after the triggering event can be significant for seismicity models, where it is major issue whether the parameter c in Omori's law is a physical parameter (i.e. independent of methods of registration and interpretation), or if it is a result of measurement and technique deficiency (e.g. Lindman et al., 2006; Kagan et al., 2005; Shcherbokov et al., 2004).

Omori's law is given by

$$n(t) = \frac{K}{(t+c)^p}$$

In this formula, *n* is the number of aftershocks, *K* and *c* are constants, whereas *c* can have a value between 0.01 several days and *p* is around 1.

Thus, the next chapter is about the completeness of the data and which magnitude can be taken as the cut-off magnitude for several time intervals.

3. MAGNITUDE DISTRIBUTION, CATALOGUE CUT-OFF MAGNITUDE AND B-VALUE OF THE VSZ

3.1 Magnitude distribution of the VSZ

3.1.1 Average magnitude

I plotted the average magnitude against time first for the whole catalogue and then for the time intervals between 1900 and 2005 as well as between 1980 and 2005 (see Fig. 3.1a,b and c). To calculate the average magnitude the following formula was used:

$$Mav = \sum_{i=0}^{n} \frac{Mw(i)}{i} + \frac{(i-l)*Mav(i-1)}{i} \qquad (3.1)$$

The first plot shows how the average magnitude decreases through time (Fig. 3.1a). From about 1800 on, it falls rapidly from about 6.8 to less than 3 after the year 2000. This certainly has again to do with the increasing capabilities of earthquake recording. The average of the magnitude decreased in the second half of the 20th century, probably due to better and more instruments, which are able to detect smaller earthquakes. To get a better picture of the part of the catalogue I used, I plotted the average magnitude only for the time from 1980 till the end of the catalogue (see Fig. 3.1c), which shows a quite stable value of the average magnitude with time. This again shows that the catalogue can be used from 1980 on, because the data seem to be consistent from this point on. The recording 27 of earthquakes is from then on able to detect the small earthquakes which accounts for the low and stable value of the average magnitude.

The average magnitude over time has some interesting features. In Fig. 3.1a it is shown for the whole catalogue. The average magnitude stays at a magnitude level of about 7 for a

very long time, starting to fall only after 1800 with a steep decline in the second half of the 20th century. In Fig. 3.1b, which shows the part of the catalogue from 1900 on, the average magnitude over time fell from 4.6 to 3.8 at the start of the First World War and then increased to 4.4. This level was held until 1980, which led to the conclusion that only data after 1980 should be used. This is fortified by Fig. 3.1c which shows a very stable average magnitude after 580 days following 1980. In the first 580 days after 1980, the average magnitude is higher, possibly due to missing earthquakes (see chapter 5).

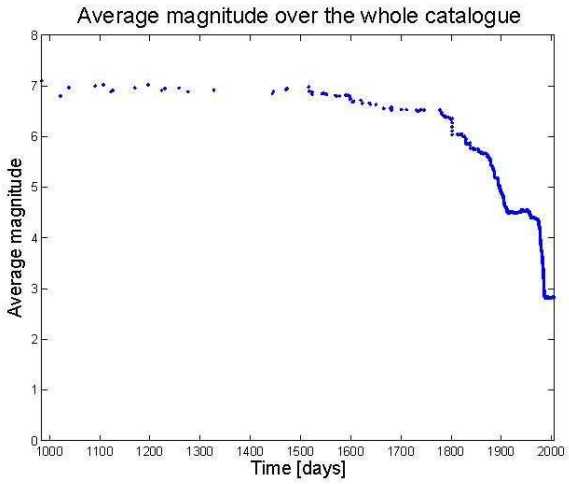

Fig 3.1 a) Average magnitude with time

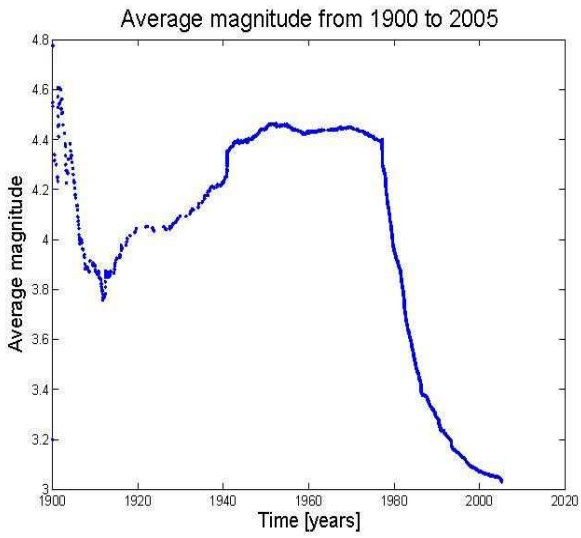

Fig. 3.1 b) Average magnitude against time from 1900 till the end of the catalogue

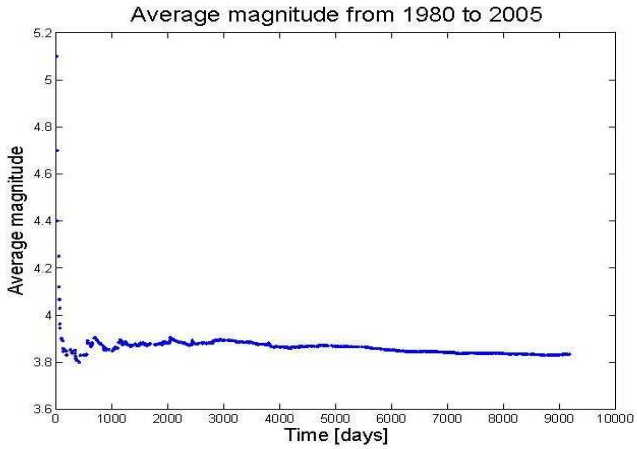

3.1 c) Average magnitude with time; cut-off magnitude is 3.5

***Fig.3.1**: Average magnitude with time*

3.2 Kagan's discussion of the Gutenberg-Richter Law, universality of the β-value

Gutenberg and Richter (1944) have found that the number of earthquakes of magnitude M is proportional to 10^{-bM}, with a worldwide value of *b* close to 1. The b-value can vary noticeably on a regional scale. Gutenberg and Richter (1944) gave the following formula:

$$log_{10}N(m) = a - bm \qquad (3.2)$$

N is the number of earthquakes and the parameter *a* characterizes the seismic activity of a region. The parameter *b* is the slope of the graph and has a value close to one. For the energy of an earthquake, or the seismic moment M, this relation can be changed into a power law relation or into the Pareto distribution, with the power exponent $\beta = \frac{b}{1.5}$ (references in Kagan (2005)). According to the Gutenberg-Richter law, the number of

earthquakes increases as their size decreases. Kagan (1991) mentions a catalogue completeness threshold M_t because of the limited sensitivity of networks. So the law can be written as

$$\Phi(M) = \beta M_t^{\beta} M^{-1-\beta} \tag{3.3}$$

Thus, the Gutenberg-Richter law is written as a power law distribution $\Phi(M)$, where Φ is the probability density function. The Gutenberg-Richter distribution can also be written as

$$\Phi(M) = C^{-1} M_t^{\beta} M^{-1-\beta} exp\left(\frac{-M}{M_{xg}}\right) \tag{3.4}$$

where C is a normalizing coefficient. This equation has an exponential roll-off at large magnitudes with M_{xg} as the maximum moment parameter (the effective maximum seismic moment) (Kagan (1991)). This tapered distribution is called the Gamma distribution and assures that the total moment rate is finite and the total moment rate depends on the corner magnitude. Kagan (1991) compared the size distribution of earthquakes for different depths. He found that β is smaller for deep and intermediate earthquakes than for the shallow ones, but the author states that it is a small effect with a value between 0.45 and 0.65 for all depth ranges. Kagan (1991) found that among various subduction zones, little if any variation in maximum earthquake seismic moment is observed, because of the high levels of correlation between the numbers of seismic events at different depths and the correlation of the tectonic deformation rate and seismic activity, which suggests that seismic activity indicates tectonic deformation rate in subduction zones. For earthquakes with a reverse mechanism and mid-ocean ridge earthquakes, Kagan (1991) found a β value of 0.638 ± 0.015 and 0.833 ± 0.036, respectively. Kagan (1999) states that the magnitude-frequency relation, unlike the moment-frequency relation, cannot be universal, because the b-value depends on the magnitude scale, in which the magnitude is not a physical quantity, and because the decay of the high-magnitude distribution tail is produced by a magnitude saturation effect.

The knowledge of universality of the moment-frequency relation can be very important for seismic hazard estimation. Kagan (1999) argues that the difference in the b-values for subduction zones and mid-ocean earthquakes may be due to a mixture of several earthquake mid-ocean ridge populations with a different maximum magnitude scale. He explains this with the thickening of the brittle crust while it moves away from the mid-ocean ridge. Kagan (1999) explores whether the β-value differs for earthquakes deeper than 70 km and also in respect to shallow earthquakes. He found $\beta = 0.661 \pm 0.011$, $\beta = 0.619 \pm 0.025$ and $\beta = 0.597 \pm 0.036$ for shallow, intermediate and deep earthquakes, respectively. He states that worldwide values for shallow earthquakes are influenced by mid-ocean ridge earthquakes, which have a higher β-value. Kagan (1999) says that the β-value depends on the magnitude threshold and when this threshold is smaller, it could be that the mid-ocean ridge earthquakes obey an universal moment-frequency relation similar to the one of the other earthquakes with a compressive regime. Kagan (1999) gives possible reasons for regional variations in the β-value:

- They could be due to random fluctuations due to a number of earthquakes in a catalogue which is too small.
- They could be due to systematic errors. Examples are the saturation of magnitude scales and magnitude round-off, insufficient knowledge of earth structure or nonuniform distribution of seismic stations.
- He also states that seismic regions may have different physical properties which may influence the β-value, such as the age of the subducting slab, the plate convergence rate, slab composition or the dip angle.

Kagan (1999) assumes that the last point can be omitted and that variations in the β-value are due to systematic errors. He considers two kinds of seismic-moment frequency relation universality: a “weak universality” for the long-term, worldwide seismicity distribution, and a strong universality in which there is uniformity of earthquake size statistical distribution for a

seismicity divided into seismic regions and time spans. Kagan (1999) states that only the first universality could be proposed for the deep earthquakes (close to the 660 km discontinuity). He sees the reasons for a higher β-value in the deeper regions and in the higher spatial fluctuations. Deep seismicity is characterized by discontinuous 'hot spots' of seismic activity. Kagan (1999) cites Giardini (1988) and Okal and Kirby (1995) who suggest that the β-value of deep earthquakes depends on the spatial fractal dimension of earthquakes and quasi-turbulent motions of fluids producing patterns of fractally distributed regions of high strain (citation of Mandelbrot (1983)). Kagan (1999) sees it as possible that mantle convection near subducting slabs is uniform, causing strains in the slabs, which cannot accommodate these plastically. This could cause a distribution with a fractal pattern.

3.3 Gutenberg-Richter Law applied to the VSZ

I plotted the cumulative number of all earthquakes in the catalogue against the magnitude and then for all earthquakes with magnitude = 3.5 (Fig. 3.2a and b). Both plots are for the whole time range of the catalogue. I regard this magnitude as the cut-off magnitude and will give the explanation later in the text. For reference, I also plotted a straight line with a b-value of 1.0, representing the slope.

The gradient of the graph in Fig. 3.2a is not equal to one as would it be expected from global studies. This indicates that several medium sized earthquakes are missing, while Fig. 3.2b (after 1980) shows a number of medium and larger earthquakes which is rather too high, especially earthquake with magnitudes of 6.5 and higher.

3.4 Catalogue-cut-off magnitude and b-value and their changes with time

3.4.1 Cut-off magnitude and b-value for deep earthquakes

I plotted the b-value against a range of cut-off magnitudes for the first 2900 days after 1/1/1980. Fig. 3.3a shows the b-values for each step in the cut-off magnitude and the number of data at each magnitude. Fig. 3.3b shows the error bars of the b-value at each magnitude step. The standard deviation was calculated with the following formula:

$$sd = \frac{b}{\sqrt{n}}$$

(see Aki, 1965). There is a strong decrease for magnitudes smaller than 3.7 and the b-value seems to fall under a value of 1.0 for magnitudes smaller than 3.5 and then decreases steadily.

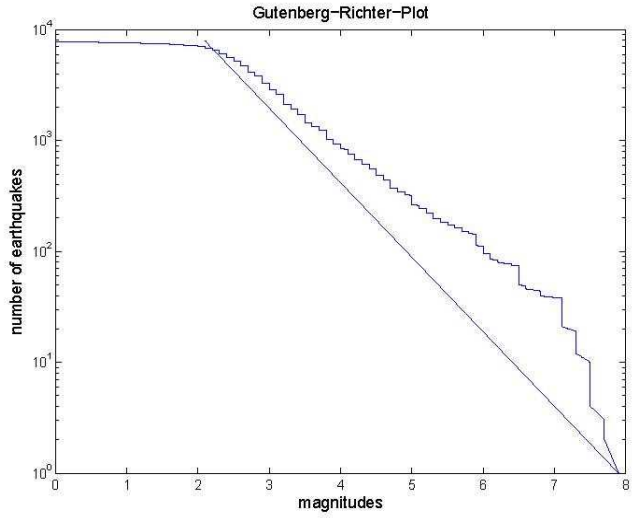

Fig. 3.2 a) Gutenberg-Richter Relation for all earthquakes

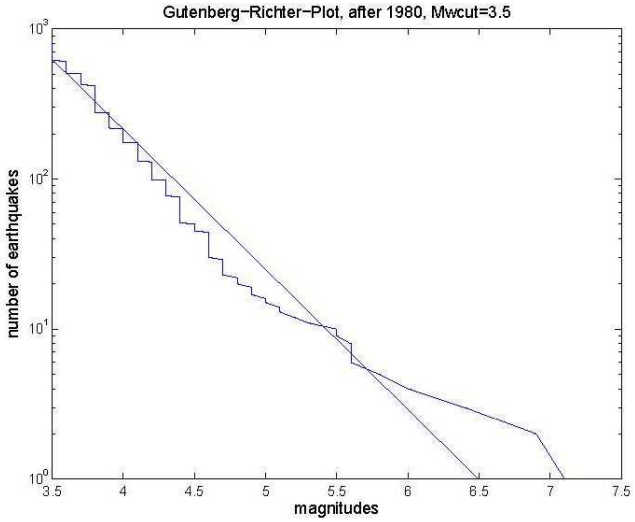

Fig. 3.2 b) Gutenberg-Richter Relation for earthquakes with cut-off magnitude 3.5 and higher

Fig 3.2: *Gutenberg-Richter Relation a) for all earthquakes and b) for all magnitudes with magnitude 3.5 and higher and the whole time range of the catalogue; the straight line represents the slope with b = 1.0 of the Gutenberg-Richter Relation, as reference*

I made similar plots for the time following 2900 days from 1/1/1980 which corresponds November 1986 (Fig. 3.4a and Fig. 3.4b) and it can be seen that the b-value starts to fall from magnitudes smaller than about 3.0. The cut-off magnitude can be seen if one looks where the b-value in Fig. 3.3b and 3.4b have a stable value.

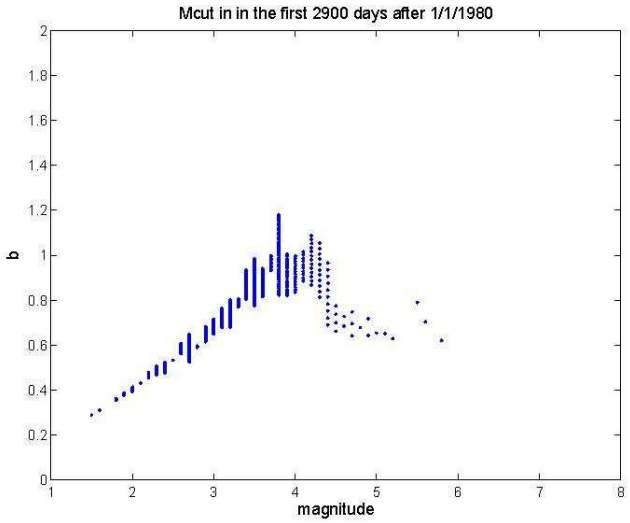

Fig.3.3 a) change of the b-value with cut-off magnitude and number of data

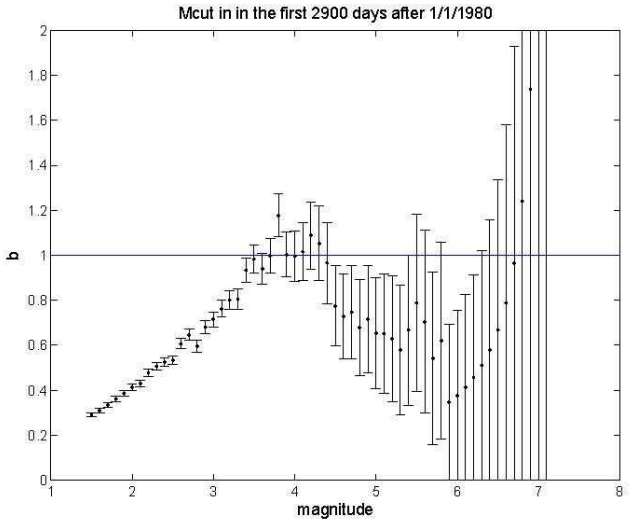

Fig. 3.3. b) change of the b-value with magnitude and error bars

Fig 3.3 *: b-value against cut-off magnitude in the first 2900 days after 1/1/1980; blue line shows where b = 1.0*

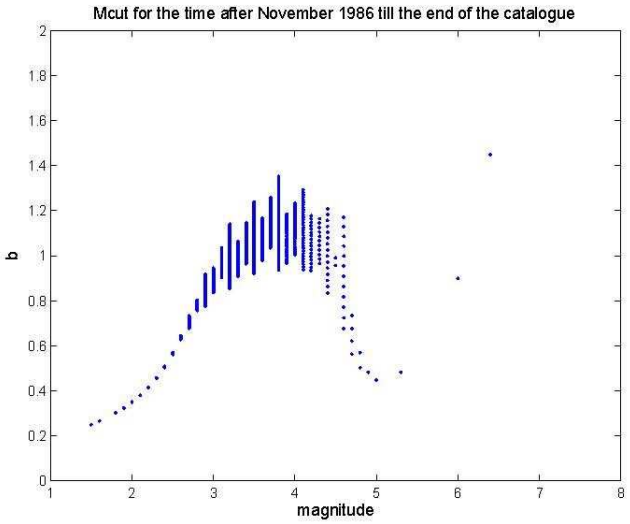

Fig. 3.4 a) change of the b-value with cut-off magnitude and number of data

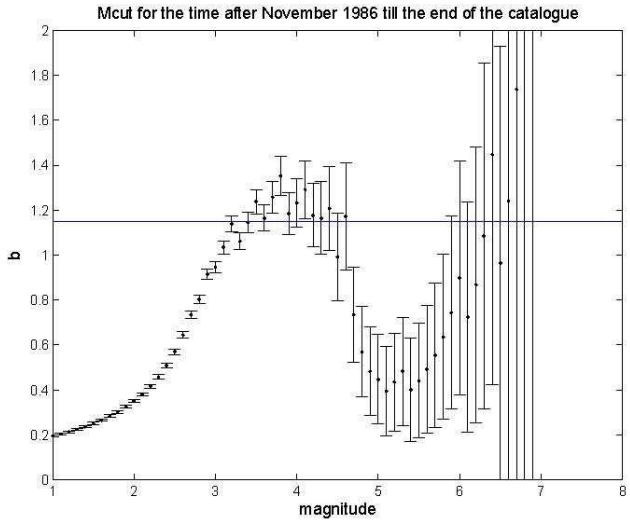

Fig. 3.4 b) change of the b-value with cut-off magnitude and error bars

Fig 3.4: *b-value against cut-off magnitude from November 1986 till the end of the catalogue; blue line shows where b = 1.0*

While the cut-off magnitude in Fig. 3.3b seems to be 3.5, the cut off-magnitude after November 1986 decreases to 3.2. I suggest that the catalogue for the time after 1980 is complete above *Mw* = 3.5 and then *Mw* = 3.2 after November 1986. A striking feature of the figures 3.3a and 3.4a is that several magnitudes seem to be favoured. There is an unusually high number of the magnitudes 3.2, 3.5, and particularly 3.8. The high number of earthquakes with magnitudes of 3.2, 3.5, and 3.8 could be due to a rounding process. It could be that the original magnitudes have been determined to a quarter of the magnitude unit, so that 3 3/4 was rounded up to 3.8, for example. This explains the feature in those two plots. An interesting observation in the plots of the b-value and its error bars is the increase of the b-value between the two time intervals. The b-value for the time between 1986 and the end of the catalogue is about 0.2 units higher than for the time between 1980 and 1986. This change coincides with the occurrence of a *Mw* = 7.1 earthquake on the 30th of August, 1986.

Possible explanations for the change in the b-value: Concerning the change in the b-value, authors of several papers have different explanations for this feature in connection with large earthquakes. Tebbens et al. (2003) see the reason as a consequence of temporal truncation of the analyzed data sets. Zuniga et al. (1995) see the change of the b-value as due to a transformation of the magnitude scale between two periods. The authors mention reasons like (a) a change of the agency operating the network, (b) the introduction of a new software, (c) the introduction of new hardware for the analysis, (d) the removal or addition of seismograph stations, and

(e) changes in magnitude definitions. Also mentioned are differences in station corrections, inclusion or deletion of data from local networks. Wyss et al. (2000) studied the Landers Earthquake and stated that the increase in the b-value was due to a larger production of small earthquakes. They connect high b-values with low ambient stress after the major earthquake, because there is a higher probability of small earthquakes. Matsumura (2005) also sees the reason of a change in b-value due to high or low stress. An increase coincides with low stress, a decrease with high stress. Bowman et al. (2004) connect

changes in the b-value to the changes of the largest magnitude M_{max} in a region, which grows prior to a large earthquake and decreases following it. Volant et al. (1992) see no connections between a change in b-value and the stress history for the spatial migration of seismicity. They did not find any correlation with stress or stress intensity factor changes, nor with rock property changes in their study. An explanation is the simultaneous occurrence of both aseismic slips and earthquake fractures. The authors mention studies in which a b-value increase is associated with stable crack coalescence during experiments on wet core samples. I think it is not quite clear what caused the higher b-values in my plot. On the one hand, the high number of magnitudes of 3.2, 3.5 and 3.8 in 4.12a and 4.13a biases the b-values, making them higher than expected. There also was a change in the network used to record these earthquakes, which could have biased the data, too. On the other hand, the occurrence of a large earthquake in the time of the obvious change in the b-value coincides with the theses of Bowman et al. Thus, this would need further research to make it clear what the reasons really are.

3.4.2 Cut-off magnitude and b-value for shallow earthquakes

I plotted the b-value against cut-off magnitude for shallow earthquakes in order to find the cut-off for these. I did this to find out if I could use the model for shallow earthquakes, too.

In Fig. 3.5b it is especially clear that there are too many small earthquakes. The b-value stays at his global value of about 1.0 until the cut-off magnitude for the deep earthquakes is reached and then rises to values of about 2.4 before it falls steeply. This phenomenon was already discussed by Felzer (2006). She discusses the errors that can influence the b-value. She mentions that already the rounding of magnitudes can affect the b-value in two ways. She gives an example for the first way and supposes that magnitudes are rounded to the nearest tenth. Then a collection of earthquakes with M = 2.0 will actually include earthquakes with M = 1.95. This could lead to overestimations of b. Second, she mentions that earthquakes often are rounded to M_R with $M_R - \delta = M_R = M_R + \delta$. She states that the

Gutenberg-Richter distribution has more earthquakes with $M_R - \delta = M = M_R$ so that the true magnitude is lower than M_R. This could lead to an underestimation of the b-value. She also mentions catalogue incompleteness due to not adequately recorded and not listed earthquakes or changes in magnitude scales. Felzer found the same feature of high b-values for small magnitudes for a sample of earthquakes in Southern California from 1984 to 1999. She alludes to sample size, catalogue incompleteness and magnitude error to be possible reasons for the developing of the b-value. She states that this pattern is expected regarding an increasing magnitude error with decreasing magnitude combined with magnitude incompleteness. Thus, the high b-values for small magnitudes in Fig. 3.5b could be due to bias in magnitude calculation. From Fig. 3.5b I infer that the cut-off magnitude should be 3.6. Because of the rounding effect, I will use 3.5 as the cut-off for the shallow seismicity.

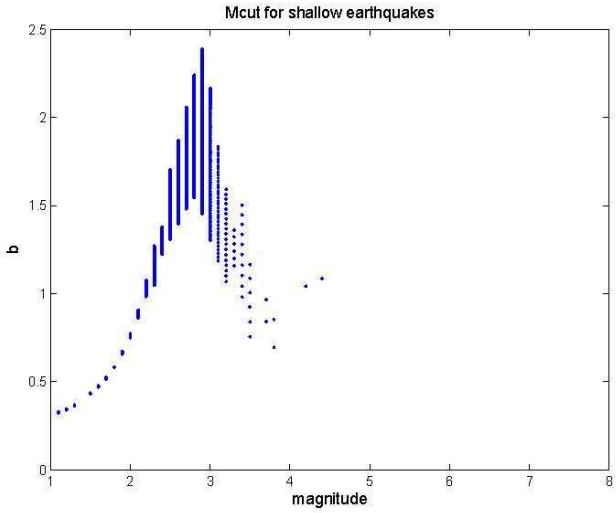

Fig. 3.5 a) change of the the b-value with cut-off magnitude and number of data of shallow earthquakes

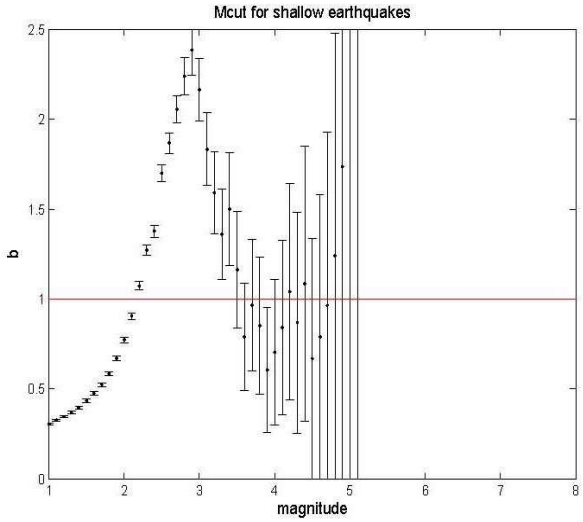

Fig. 3.5 b) change of the b-value with cut-off magnitude and error bars for shallow earthquakes

Fig. 3.5*: b-value against cut-off magnitude for shallow earthquakes; red lines shows where b = 1.0*

3.5 Gutenberg-Richter Relation for several depth and time intervals

I plotted the Gutenberg-Richter-Relation and the earthquake distribution for several time and depth intervals due to increasing quality in the measurements for the whole catalogue and from 1980 on (Fig. 3.6a, b, c, d).

There is a remarkable high number of large earthquakes in Fig. 3.6a. I could not determine if this is a physical fact or if it is due to catalogue incompleteness. The earthquake distribution does not really get sharper with increasing time. In the plot of the Gutenberg-Richter relation for shallow events in the time from 1980 to the end of the catalogue (Fig. 3.7b) there are outstanding variations in the number of earthquakes of different magnitudes. There seem to be a lower number of medium sized earthquakes and then a high number of earthquakes with large magnitudes. According to this figure, there should be ten times too earthquakes with Mw = 7.

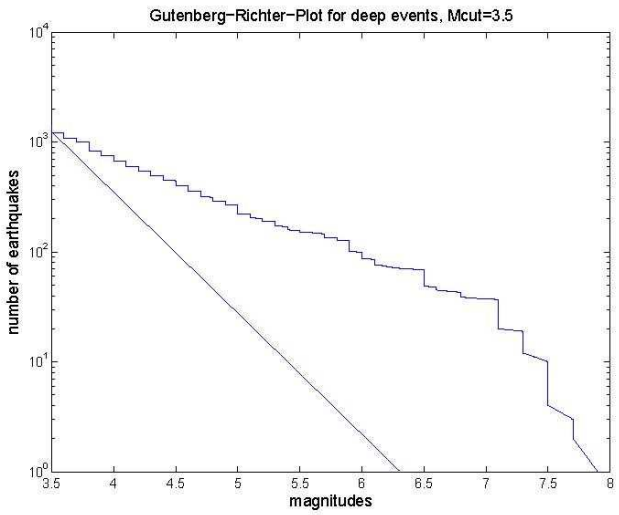

Fig. 3.6 (a) Gutenberg-Richter Relation for deep earthquakes in the catalogue with *Mcut* = 3.5 and deeper than 60 km

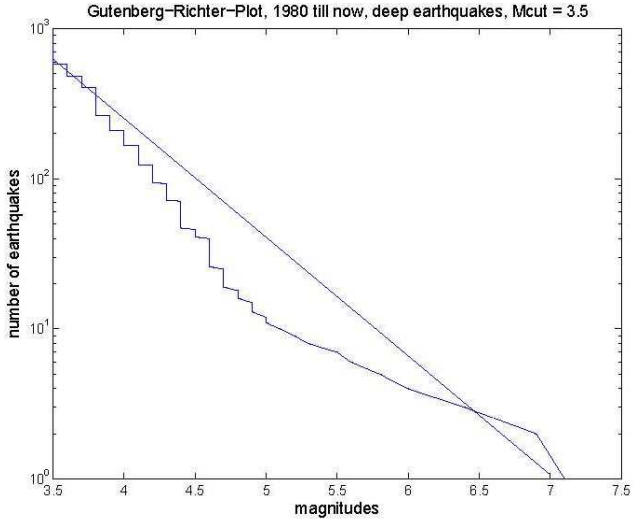

Fig. 3.6 b) Gutenberg-Richter Relation for deep earthquakes (≥ 60 km) after 1/1/1980 with Mcut ≥ 3.5

Fig. 3.6: *Gutenberg-Richter Relation for deep earthquakes; slope of the straight line given by a b-value of 1.0*

I plotted the Gutenberg-Richter relation only for the time between January, 1980 and May, 1985 (Fig. 3.8). Fig. 3.8 was made because I found interesting characteristics for this time interval in other plots (see Fig. 5.4b). But it does not show any distinctive features in the occurrence of intermediate magnitudes.

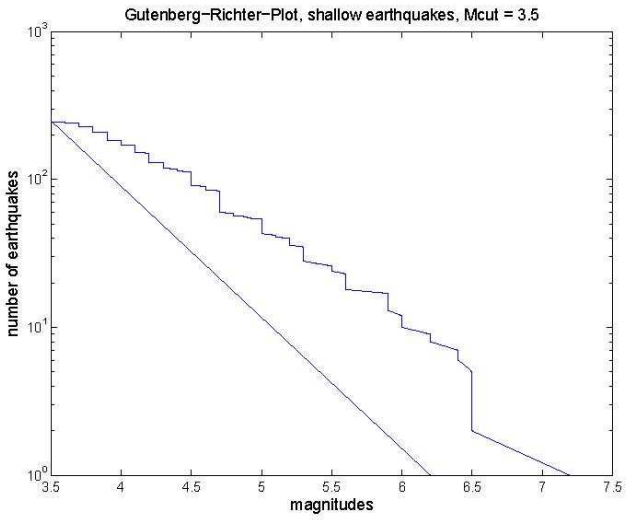

Fig. 3.7 a) Gutenberg-Richter Relation for shallow earthquakes (≤ 60 km) and magnitudes of ≥ 3.5

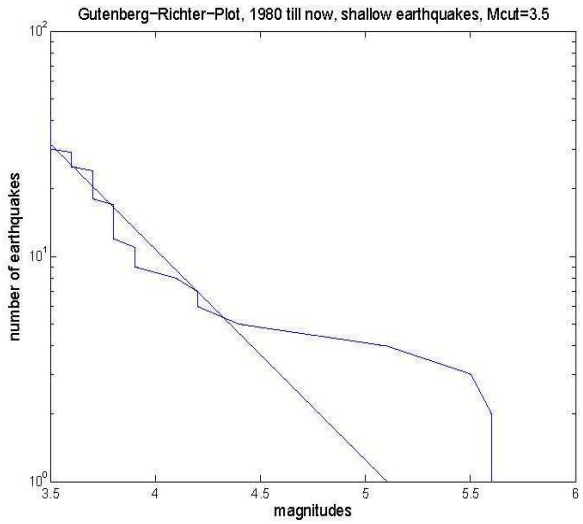

Fig. 3.7 b) Gutenberg-Richter Relation for shallow earthquakes (≤ 60 km) after the 1/1/1980 and magnitudes of ≥ 3.5

Fig. 3.7*: Gutenberg-Richter Relation for shallow earthquakes (≤ 60 km), with Mcut ≥ 3.5 ; the slope is given by a b-value of 1.0*

In this chapter, I plotted the Gutenberg-Richter relation of several depth and time intervals. These plots show that there are clearly too many M7 earthquakes with respect to earthquakes with small magnitudes. The shape of the Gutenberg-Richter relation, with its bulge at high magnitudes, is very similar to the Gutenberg-Richter relation of characteristic earthquakes (Wesnousky, 1994). Wesnousky states that the characteristic earthquake model of Schwarz and Coppersmith (1984) implies regional distributions of seismicity that satisfy equation 3.2 are in part a reflection of the size distribution of faults in a region.

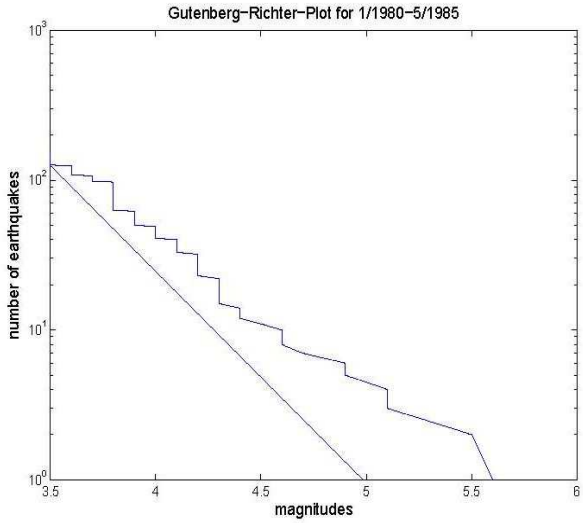

Fig. 3.8: *Gutenberg-Richter Relation for all earthquakes with Mcut ≥ 3.5 and the slope of the straight line given by a b-value of 1.0*

4. SLAB GEOMETRY AND EARTHQUAKE DISTRIBUTION

4.1 Slab geometry and stresses

Radulian et al. (2007) speak about the Vrancea as the most concentrated seismic active area in Europe, with an unusual concentration of seismic energy released at intermediate depth (60 - 180 km). This seismic energy release is located in a narrow lithospheric body pulled into the asthenosphere. They mention tomographic studies identifying an extended high-velocity body beneath the Carpathian arc, with the earthquake distribution constrained to a small region at the NE-border to this body.

Martin et al. (2006) have used non-linear teleseismic bodywave tomography which provided them with high-resolution images of the upper mantle structure. Their image shows a high-velocity body beneath Vrancea and the Moesian platform with a NE-SW orientation between 70 and 200 km depth. Beneath 200 km the orientation changes to N-S up to a depth of 350 - 370 km. They interpret this high velocity body as the subducted not yet detachted slab. The NE-part seems to be coupled to the Moesian lithosphere and contains the intermediate depth seismicity. The SW-part appears to already be detached and pull into depth from the material underlying it. The authors see the low-velocity anomalies in agreement with the lithosphere-asthenosphere boundary between 110 and 150 km beneath the Moesian platform and deeper than 200 km beneath the East European platform. The authors' images support models suggesting slab rollback during subduction/collision, followed by slab steepening and lithosphere delamination. The authors state that the different degrees of mechanical coupling between slab and lithosphere help understand the loci of seismicity as volumes of stress concentration.

Wenzel (2005) speaks about the stress in Vrancea. He cites other authors who showed that the maximum shear stress in a descending slab accumulated in a depth range of 70 to 160 km in a narrow area and the depth distribution of the annual average seismic energy

released in earthquakes has a shape similar to that of the depth distribution of the stress magnitude in the slab. He also cites the results of tomography studies revealing the high-velocity body beneath Vrancea, which exceeds the dimensions of the seismogenic region by far. The seismic gap at about 50 km of depth is seen as a zone of weakened mantle material. The spatial changes in seismicity are seen to be related to changes in the dynamics of the descending slab, which results in a significant redistribution of shear stresses.

Ismail-Zadeh et al. (1996) mention a double subduction tectonic model for Vrancea. They cite Onecscu(1984) and Oncescu et al. (1984) that the decoupling of the sinking slab could be caused by the NW push of the Black Sea plate. According to models, a cold, denser and more rigid relic slab beneath the VSZ sinks due to gravity. The hydrostatic buoyancy forces help the slab to subduct, and viscous and frictional forces work against the descent. At intermediate depths, these forces produce an internal stress with one principal axis which is directed downward, thus causing earthquakes. In their work, Ismail-Zadeh et al. (1996) show that the average stress magnitude peaks in the depth range from about 70 km to 150 km. The maximum viscous stress is reached at a depth of 90 km, the maximum number of shocks is at a depth of about 140 km. The models also show that these forces are not the only source of stress that leads to seismicity. Ismail-Zadeh et al. (1996) conclude from their observations that the basalt-eclogite phase transition in the descending slab is likely to have no fundamental effects on the production of stress at intermediate depths in the VSZ. They also say that the generation of a pore fluid by dehydration of hydrous minerals in the slab may cause dehydration-induced faulting. Thus, the viscous flows, due to the sinking of the relic slab together with the dehydration-induced faulting can be seen as a possible triggering mechanism explaining the intermediate-depth seismicity in this region.

4.1.1 Distribution of seismicity in space and time

Because the data in the catalogue are of different quality, I plotted the distribution in

different colors to see where the ’best’ earthquakes are (Fig. 4.1a and b)

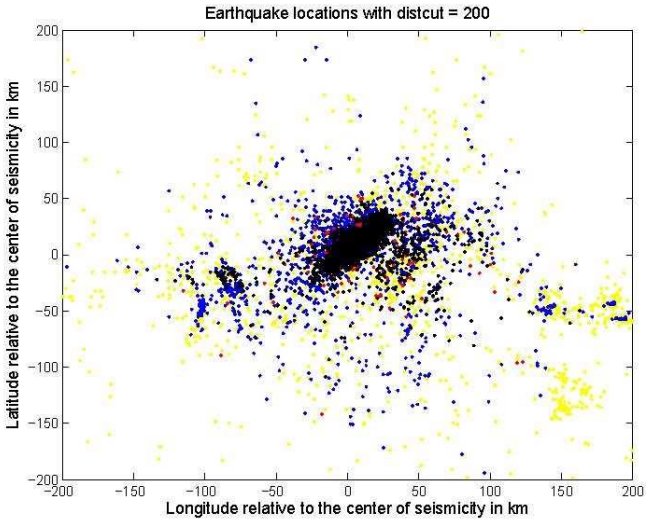

Fig. 4.1 a) Surface distribution of earthquakes within 200 km with different quality

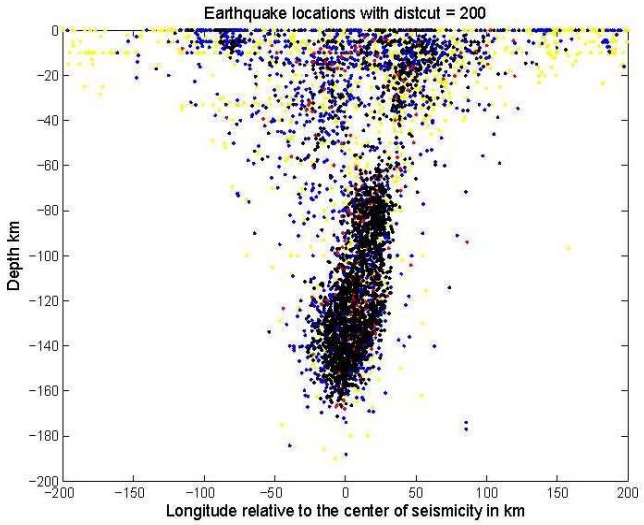

Fig. 4.1 b) Depth distribution of earthquakes within a distance of 200 km with different quality

Fig. 4.1: *Distribution of earthquakes within a distance of 200 km with different quality: quality ‘A’ in black, quality ‘B’ in red, quality ‘C’ in blue and quality ‘D’ in yellow, with a cut-off of 3.5; coordinates relative to centre of seismicity*

Fig. 4.1a and b show that the ’best’ earthquakes (quality ’A’) happen in more confined volume than the earthquakes with lower qualities. In Fig. 4.1b most of the quality ’A’ earthquakes are in the slab, showing that the data consisting of the deeper earthquakes are more reliable than for the ones at shallow depths.

To see how far the Vrancea Seismic Zone spreads, I plotted the distribution of all earthquakes of the Romplus-catalogue (Fig. 4.2a and b) within 200 km of the VSZ and deeper than 60 km. As seen in these figures, the earthquake distribution in space is very confined in the VSZ. In the plot of the depth distribution (Fig. 4.2b) the seismogenic part of the slab is quite clearly discernible. The different segments of the slab, A, B and C, proposed by e.g. Hurukawa et al. (2006) or Ardeleanu (1999), are not visible in Fig. 4.2b. The slab rather looks like a finger. However, the structure of the seismogenic part of the slab is revealed, when the earthquake coordinates are rotated according to the strike of the slab (see below). The nearly vertical seismogenic zone is clearly pictured, as well as the confined extent of the zone. According to the figures the VSZ spreads 240 km in the E-W-direction, 70 km in the N-W-direction, and 150 km in the depth-direction. The detaching slab is clearly visible. This shows that the seismicity of the VSZ is confined to a very small volume which also outlines a nearly vertical body with the shape of a parallelepiped. In the work of other authors, this led to the assumption of a subducting slab. Fan et al. (1998) applied body wave seismic tomography to study the structure beneath the Eastern and Southern Carpathians. This tomography revealed broad heterogeneity in the velocity structure in the region and a high-velocity body (100 to 170 km in depth) which was interpreted as a slab dipping near vertically, coinciding with the intermediate-depth earthquakes in the VSZ. This result of the tomography contrasts with the earlier mentioned study by Wenzel et al. (2002) who states that the slab reaches depths of at least 200 km.

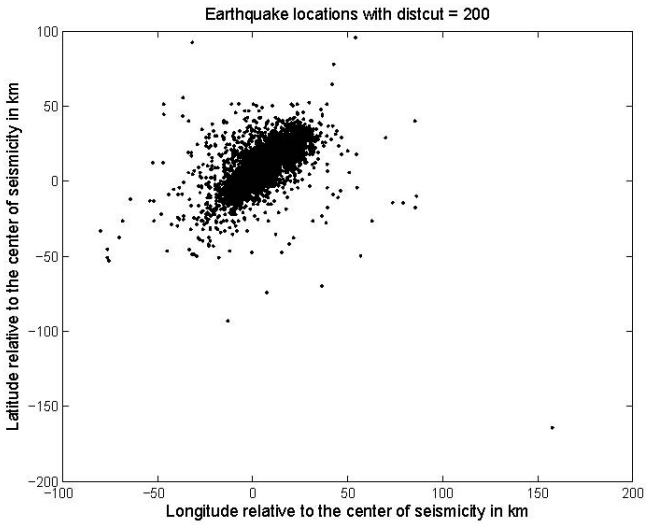

Fig. 4.2 a) Earthquake distribution along latitude and longitude

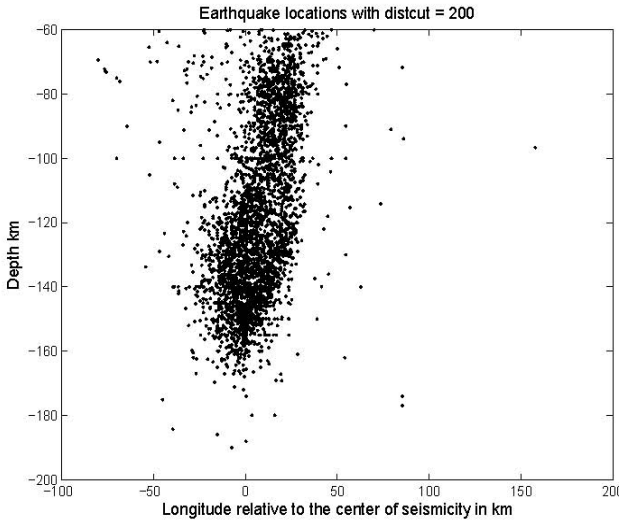

Fig. 4.2 b) Earthquake distribution along longitude and depth

Fig. 4.2: *Distribution of earthquakes within a distance of 200 km, deeper than 60 km with Mcut = 3.5; coordinates are relative to the centre of seismicity*

4.1.2 Slab geometry and strike

One of my goals of this work was to get a better picture of the geometry of the slab. To do this, I rotated the coordinate system, using a Matlab-command which computes the matrix singular decomposition and gives three different views on the geometry of the seismogenic part of the slab (see Appendix). The earthquakes at shallow depths do not seem to be well

located and it is not easy to conclude which of them are. To avoid these earthquakes, I used only the earthquakes of depth = 60*km* to determine the slab geometry. To get the strike I calculated the azimuth of the slab direction. The strike azimuth is 53°, Northeast. I then used the azimuth to plot the whole catalogue by rotating the epicenter coordinates. The largest spread in my resulting Matrix corresponds to the face of the slab, the second largest to the side and the smallest on the top of it (Fig. 4.3a, b and c). In all of these figures the most earthquakes are found to be in the slab. The downgoing seismogenic part of the slab itself is clearly visible. The shallow earthquakes have a broader distribution over approximately 400 km, while the earthquakes in the slab are confined to a lateral extend of about 50 km. In Fig. 4.3c it can be seen that there is a lot of seismicity in a depth range from 110 km to 160 km and very little seismicity between 40 km and 60 km of depth.

I also plotted the depth distribution of the rotated earthquakes only for events deeper than 60 km to get a better image of the slab (Fig. 4.4a and b).

From plane view (Fig. 4.4b), one can see that there are more earthquakes in the depth interval 120 km to 160 km than in the interval 60 km to 110 km, comparable to the segments A, B and C which are proposed by e.g. Hurukawa et al. (2006) or Ardeleanu (1999). It is also interesting to see if there are some special features in the distribution of magnitudes and if there are parts of the VSZ which have more medium and large earthquakes than other parts. I plotted the distribution of all earthquakes M_w = 5.0 from 1980 till the end of the catalogue to see where they have happened (Fig. 4.5a and b). There, the earthquakes with magnitudes 5, 6 and 7 can be seen in different colors. In Fig. 19a, the earthquakes with magnitudes 7.0 and greater seem to be only in a very confined space which coincides with the surface above the slab and Fig. 6.3b shows that these earthquakes did not happen in the crust, but in the slab. In contrast to this, earthquakes with magnitudes of 5 and 6 can be found in the crust as well as in the slab and are more spread out.

Thus, when rotated, the depth distribution of the earthquakes shows the segmentation as mentioned by Hurukawa et al. (2006) or Ardeleanu (1999). There seems to be an aseismic part of the slab between 40 km and 60 km of depth. After 60 km there is a strong clustering of earthquakes, suggesting the usage of a depth limit of 60 km. The introduction of a depth limit of 60 km is fortified by the lack of M7 earthquakes at crustal depths.

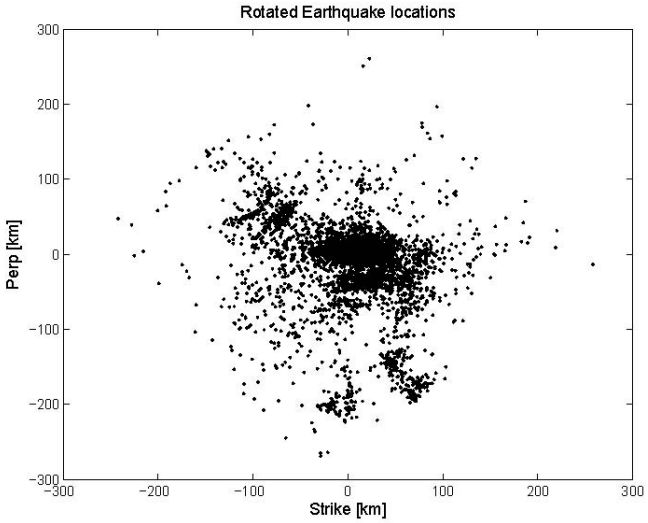

Fig. 4.3 a) Surface distribution after rotation

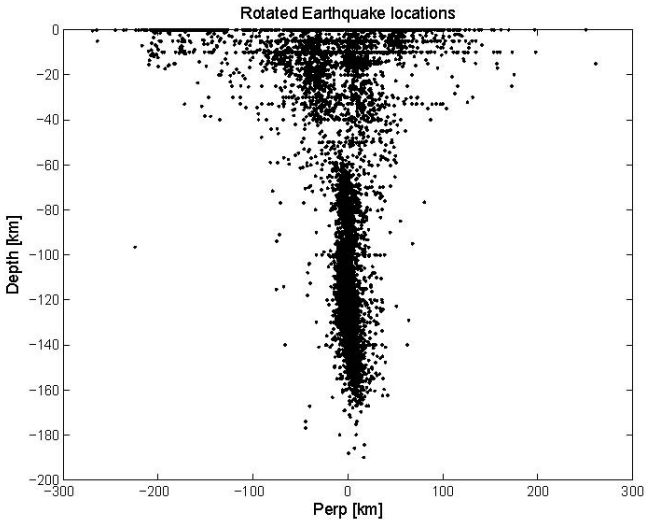

Fig. 4.3 b) Depth distribution after rotation perpendicular to the strike

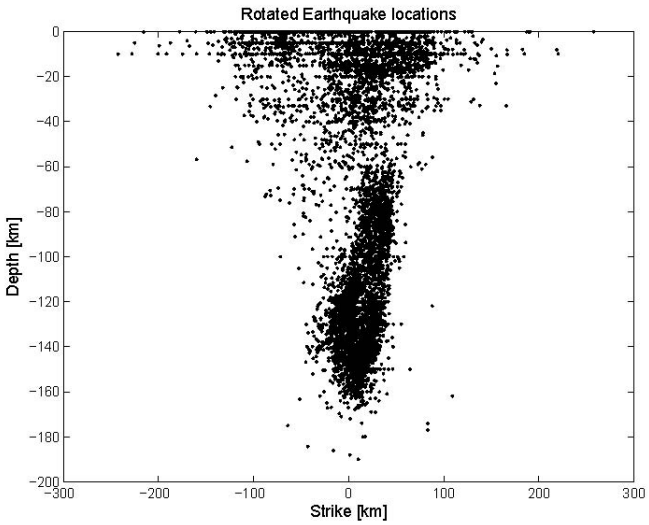

Fig. 4.3 c) Depth distribution after rotation along strike

Fig. 4.3: *Distribution of earthquakes after rotation*

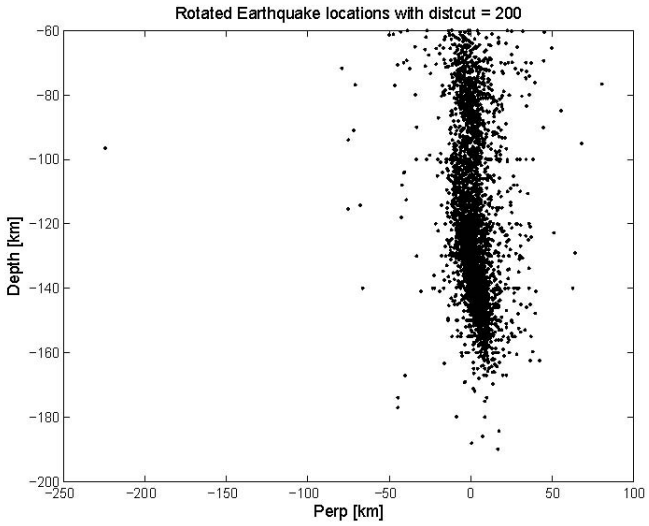

Fig. 4.4 a) Depth distribution of earthquakes after rotation within 200 km perpendicular to the strike; events deeper than 60 km

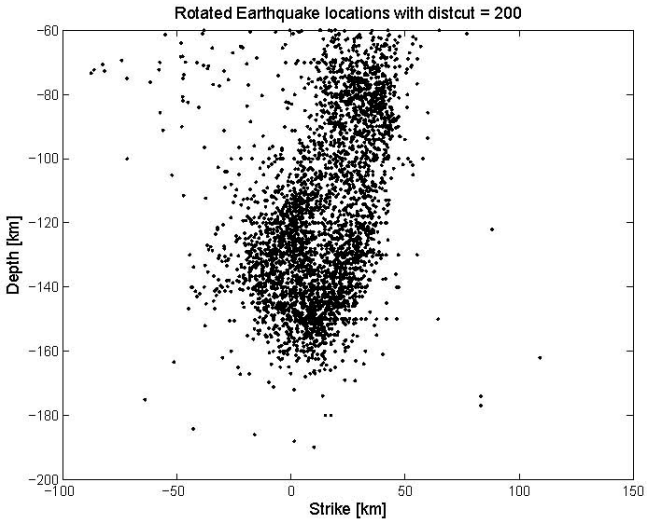

Fig. 4.4 b) Depth distribution of earthquakes after rotation within 200 km along strike; events deeper than 60 km

Fig. 4.4: *Distribution of earthquakes within depths of 60 km and deeper after rotation*

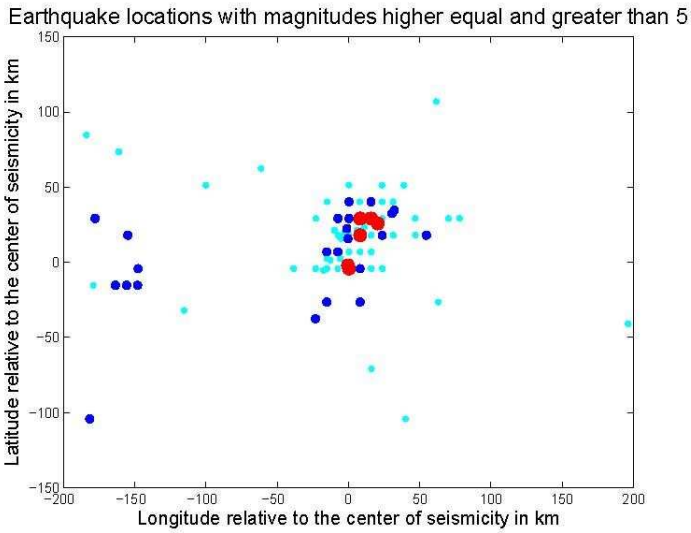

Fig. 4.5 a) Surface distribution of large earthquakes

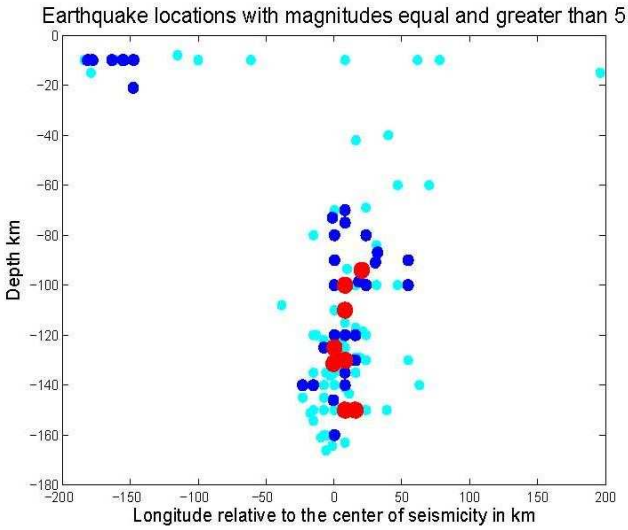

Fig. 4.5 b) Depth distribution of large earthquakes

Fig. 4.5*: Distribution of earthquakes with magnitudes equal and greater than 5 from 1980 till the end of the catalogue; M7 red stars M6 blue stars, M5 cyan stars; coordinates are relative to the centre of seismicity*

5. TEMPORAL DISTRIBUTION

5.1 The Work of Evison and Rhoades about the Ψ-Phenomenon

The work of Evison and Rhoades (2005) is about the precursory scale increase (Ψ) phenomenon, which has been identified in 47 large shallow earthquakes in the regions of California, Greece, Japan and New Zealand. This phenomenon consists of a sudden increase of seismicity to a new level, years or even decades before a new major shallow earthquake, and continues at that level until this new major earthquake happens. The future earthquake and its aftershocks occur within the area of increased seismicity. This level provides estimates of the magnitude and time of the major earthquake. Evison and Rhoades (2001) called this process long-term seismogenesis. The duration of Ψ is specific to the individual earthquake and scales with magnitude. In the Ψ-phenomenon the magnitude level of the increased seismicity is the same, on average, as that of the future aftershocks. Precursory seismicity includes two prominent features, quiescence and foreshocks. Quiescence was often been seen as a separate precursory phenomenon, and is a frequent feature of the Ψ-phenomenon. In the Ψ-phenomenon, foreshocks are seen as ordinary members of the long-term precursory seismicity. This phenomenon is attributed to the building of 'forecracks', 'maincracks', and 'aftercracks' (Evison and Rhoades, 2004). The authors state that the length of time intervening between crack formation and main shock has something to do with two effects. First, cracking causes an increase in strength by reducing fluid pressure. Secondly, the minor cracking renders the stress-field non-uniform across the major crack. The major fracture is thus inhibited from occurring until uniformity has been restored. This is caused by fracturing and then healing of the minor cracks. The three-stage faulting model, mentioned by Evison and Rhoades (2004), is another model different from the usual view of faulting. In contrast to the usual view, the Evison-Rhoadesmodel postulates that the cracking and fracturing stages can be separated by large intervals of time. The implications

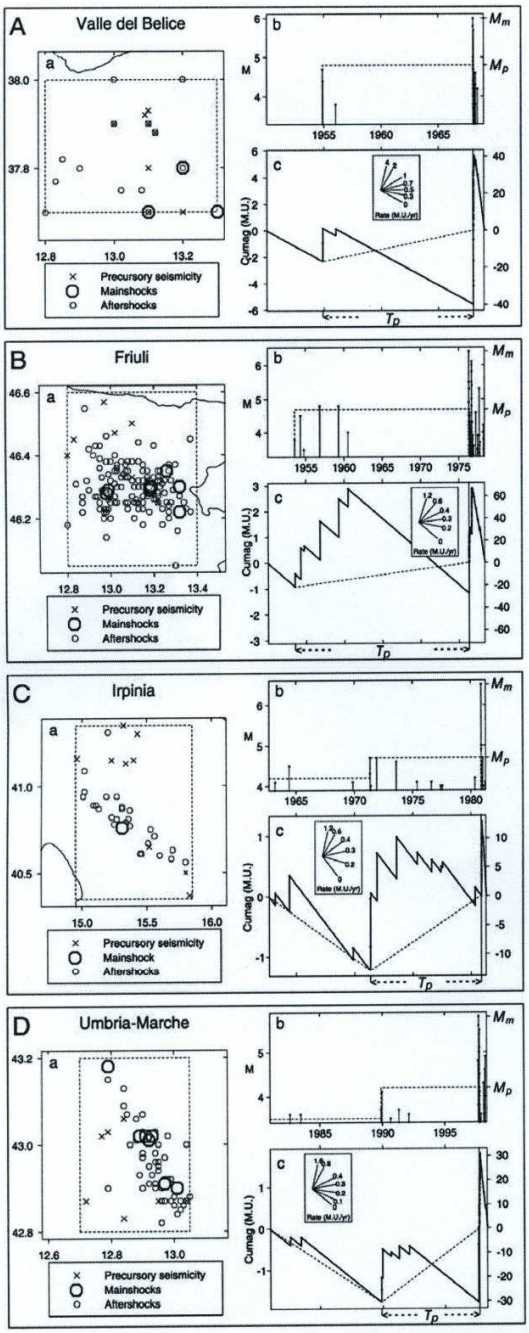

Fig. 10 The Ψ-phenomenon in (**A**) Valle del Belice, (**B**) Friuli, (**C**) Irpinia, (**D**) Umbria-Marche. Each example shows the following: (a) Epicentres. Dashed lines enclose precursor area A_P. (b) Magnitudes versus time. Dashed lines show prior and precursory magnitude levels, except where the prior level is below threshold. M_m is mainshock magnitude; M_P is precursor magnitude. (c) Cumag versus time. Dashed lines show precursory increase in seismicity rate (in (A) and (B) the prior rate coincides with the cumag). Protractor translates cumag slope into seismicity rate in magnitude units per year (M.U./yr). T_P is precursor time. (NB. The dashed lines in (b) and (c) are indicators of scale according to the Ψ-pattern, and are not a product of curve-fitting.)

Last Page: ***Fig. 5.1****: Example of the Ψ-Phenomenon, taken from the paper of Evison and Rhoades (2005)*

of the model are the following: First, it represents seismogenesis as beginning with a major event (the major crack formation), whereas swarms can occur any time during the precursory period. Second, the precursory seismicity does not have to occur in swarms. An example of the Ψ-phenomenon as they describe it in their work is given in Fig. 5.1.

The precursory seismicity can be seen where T_P starts, which is called the precursory time. It is characterized by a higher rate of seismicity in this time interval, which stops with the occurrence of the major earthquake. The graph shows the characteristic shape of the Ψ-phenomenon.

The authors mention that they found no differences in the average magnitude of the precursory seismicity and that of the aftershocks, and they state that the three-state faulting model gives an explanation. Cumag-plots (see below) show the increase of the seismicity rate until the major earthquake occurs. It consists of a prior and a precursory part. The time of the increase in seismicity rate is called the precursor time. The Cumag is based directly on the Gutenberg-Richter relation, where the prior and the precursory seismicities consists of two separated Gutenberg-Richter sets. The scale increase is an increase in magnitude level from that of the prior to that of the precursory set.

5.2 Cumag and the cumulative rate of occurrence, applied to the VSZ

The cumulative sum of the difference between each magnitude and the average magnitude plotted against time is called a Cumag-plot. The formula for the Cumag is

$$Cumag(j) = Cumag(j-1) + (Mw_j - M_{av}) \qquad (5.1)$$

where Mw_j is the magnitude of the earthquake j and M_{av} is the average magnitude. The

Cumag(N) is plotted against time t_N, which is the time of the N^{th} earthquake. The Cumag-plot can be used to find the appropriate cut-off magnitude for different times and see whether there have been changes in the seismicity rate. The Figure c) in the third part of Fig. 5.1 is a good example of the Cumag.

To see how the rate of occurrence changed at Vrancea, I converted the time in the catalogue into days plus fractions of days (Tj), with 1980 as starting time, omitting all earthquakes before this year . Then, I used following formula for the normalized rate R_j:

$$R_j = j - (T_j * R) \qquad (5.2)$$

N is the total number of earthquakes and R is the average rate over the whole catalogue. R_j is plotted against T_j, the time of the j^{th} earthquake. The Cumag and the cumulative rate of occurrence are shown in Fig. 5.2a and b. Fig. 5.2a shows changes in mean magnitude, Fig. 5.2b changes in the rate of occurrence with time.

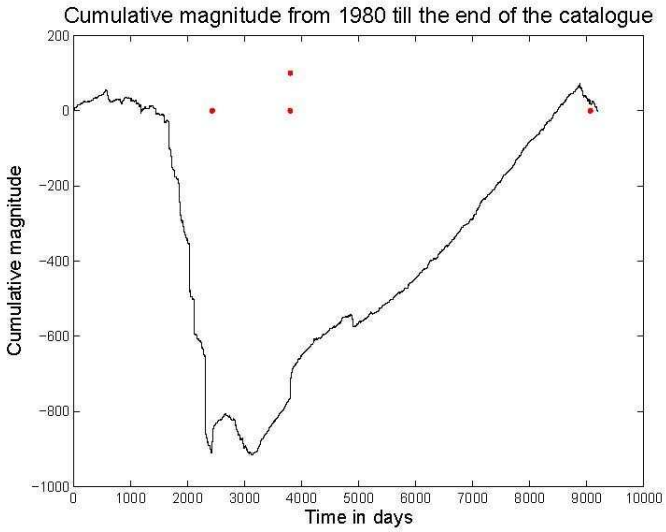

Fig. 5.2 a) Cumag for all earthquakes after 1980

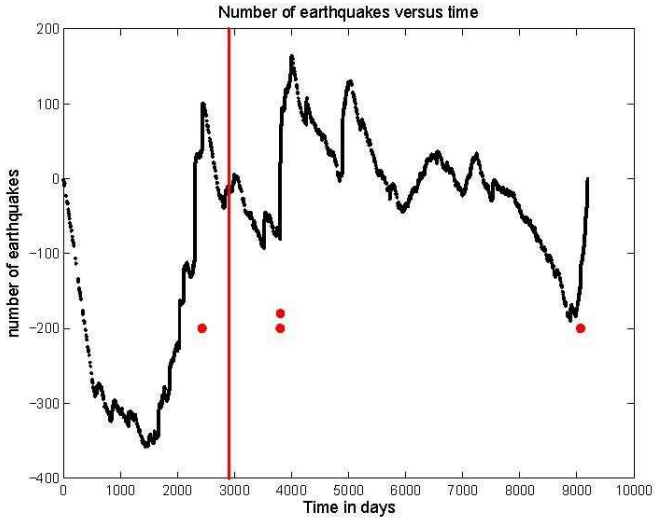

Fig. 5.2 b) Normalized rate Rj against time of earthquakes with magnitudes above 3.5; red line showing 2900 days, red dots showing earthquakes with Mw ≥ 6

Fig. 5.2: *a) Cumag after 1980, b) rate of occurrence after 1980; red dots showing earthquakes with Mw ≥ 6; red line showing 2900 days*

I plotted Cumags for all earthquakes from 1980 till the end of the catalogue with a cut-off magnitude of 3.5 (Fig. 5.3a). Fig. 5.3b shows the Cumag only for the time between 1980 and November 1986, as well as for the time interval between November 1986 and the end of the catalogue (Fig. 5.3c). The reason for plotting these intervals is that it is still not sure what the cut-off magnitude should be for this part of the catalogue as well as the change in the b-value, which could affect the Cumag.

Fig. 5.4a and b show the temporal evolution of the rate of occurrence for two different time intervals. Fig. 5.4a shows the rate for the time between November 1986 and the end of the catalogue, Fig. 5.4b the same for the time between 580 after the beginning of 1980 and the end of the catalogue. The plot 5.4b was made because of the striking feature in Fig. 5.2b, showing a steep decline of the rate of occurrence in this time interval after 1980.

The next figure (Fig. 5.5) shows the same rate as Fig. 5.4b but without the major earthquakes and their supposed aftershocks. The magnitudes of the time intervals which were cut out of Fig. 5.4b are now shown in Fig. 5.6a and b. The intervals are 2430 to 2490 days and 3800 to 3850 days, respectively. They show the magnitude of the main shocks and the smaller earthquakes which followed them.

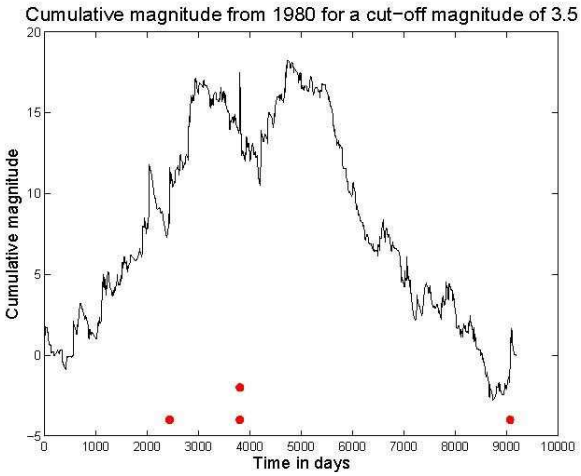

Fig. 5.3 a) Cumag for all earthquakes with magnitudes of 3.5 and above

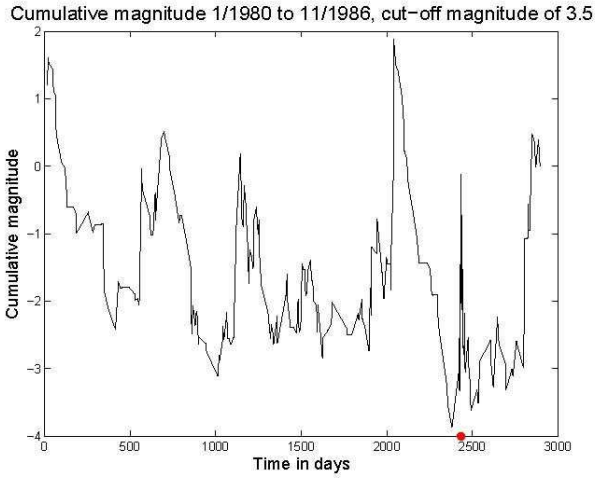

Fig. 5.3 b) Cumag for the first 2900 days after 1/1/1980 with magnitudes of 3.5 and above

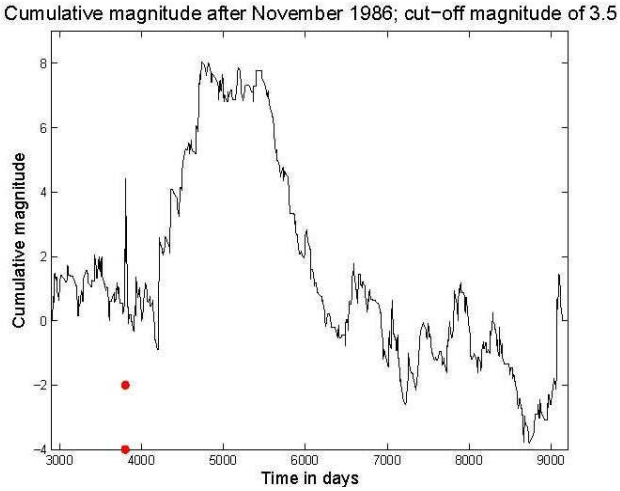

Fig. 5.3 c) Cumag from November 1986 till the end of the catalogue and magnitudes of at least 3.5

Fig. 5.3: *Cumag for all earthquakes with magnitude equal and greater than 3.5; dots correspond to large earthquakes; a) till end of catalogue, b) first 2900 days from 1980, c) from 1986 till the end of catalogue*

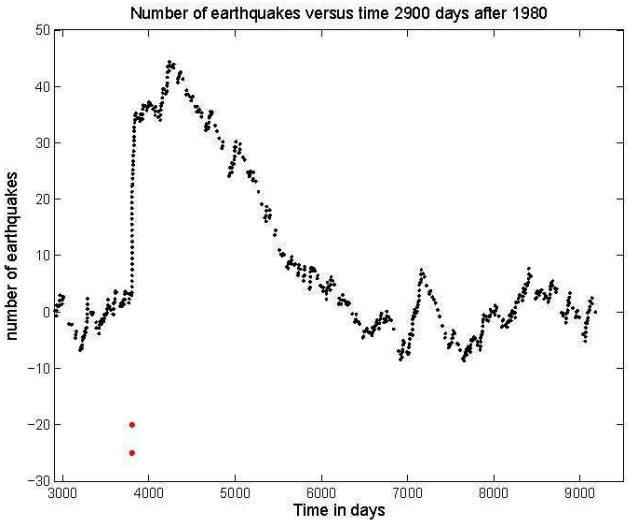

Fig. 5.4 a) Number of earthquakes against time 2900 days after 1980

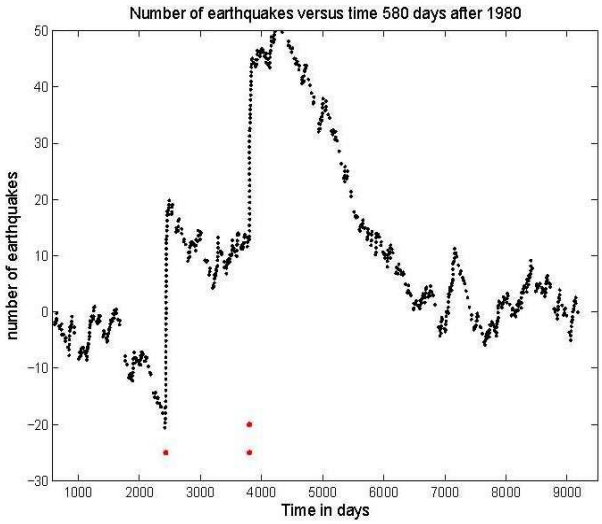

Fig. 5.4 b) Number of earthquakes against time 580 days after 1980

Fig. 5.4: *Number of earthquakes with a magnitude cut-off of 3.5 against time; red dots correspond to large earthquakes; a) from 1/1/1980 till November 1986, b) 580 days after 1/1/1980 till end of catalogue*

5.2.1 Description of the results

In the plot for all earthquakes of the catalogue (Fig. 5.2a), which happened within a distance of 200 km, the typical features of the three-stage faulting model can be seen. There is a clear prior seismicity until the first major earthquake (first red dot on the left). It is not quite clear what happens in the time between the first and second major earthquakes, but after

the second red dot, the seismicity rate increases almost steadily till the last major earthquake of the catalogue. I did not draw any conclusions from this plot as there is a change in the cut-off magnitude during the time interval in the plot. Fig. 5.3a shows the Cumag for a cut-off magnitude of 3.5 and has an unusually high number of larger earthquakes in the first quarter of the plot. After the second and third major earthquakes on May 30th and May 31st, 1990, respectively, the rate normalizes again. There is a larger peak before the first major earthquake. This is caused by another larger earthquake with a magnitude close to 6. This peak is followed by an increase caused by the earthquake of 1986. The rate still increases afterwards and then starts to fall at about 2500 days. The sharp spike in this plot is caused by the second and third major earthquake after which the rate falls only for a short time before rising again. Not until 4700 days after 1/1/1980 does the rate start falling. The decrease continues until the last major earthquake in the catalogue. The vertical red line in Fig. 5.2b marks the 2900 days after the first of January 1980. I did this because I found a remarkable feature in the Cumag. The interesting feature in Fig. 5.2b is the time interval of about 500 days before the major earthquake, marked by the red dot. However, this interval of 500 days is too short for a magnitude 7 event according to Evison and Rhoades. This led to the conclusion that there are missing earthquakes in this time interval and hence was excluded. After 580 days, there are a few lows which are followed by a sudden increase of the earthquake rate. This could be a sign of aftershocks. The last low seems to have no physical cause and could be associated with the new data acquisition and processing systems, installed in 2004. Also, it seems as there would be much more earthquakes than average following each larger event. This could be due to higher attention payed on this region after a major earthquake. Fig. 5.3c shows the Cumag for the time after November 1986. The sharp peak is again the two earthquakes in May 1990 and the following peak is caused by three earthquakes later in the same year which all have magnitudes of 5.5 and 5.6, which rise the value of the average magnitude at this point of the catalogue.

There is also an increase of the b-value around this time, which was discussed in chapter 3. Fig. 5.2b and 5.4a show a strong increase in the rate of occurrence at about 2400 and 3900 days after the beginning of the year 1980. These features have clearly to do with the three major earthquakes which occurred around this time and are shown as red dots.

5.2.2 Conclusions of the Cumag-plots

As typical for the Ψ-phenomenon mentioned by Evison and Rhoades, there seems to be a precursory seismicity and an increase in the rate of seismicity until the major earthquake as postulated by the authors. There is an earthquake of magnitude 5.8 on the first of August, 1985 and several earthquakes with magnitudes between 4.2 and 4.8 which fall in the time interval of the unusually high number of larger earthquakes. The earthquake on 1/8/1985 is the reason for the peak prior to the first red dot in Fig. 5.3a and 5.3b. I also found out that there are six earthquakes with a magnitude between 5.0 and 5.6 in the time between the third and the last major earthquake, with three of them following the third in a short time. This explains the higher rate after the third major earthquake. These plots are also used to make conclusions about the cut-off magnitude. The unusually high Cumag in the first quarter of Fig. 5.3a could mean that the cut-off magnitude for the first 2900 days after the 1/1/1980 is higher than 3.5. Another reason could be the b-value which changes by about 0.2 units in November 1986 (see chapter 3). From Fig. 3.2a I concluded that the cut-off magnitude for this part of the catalogue should be not much lower than 3.5, because the b-value seems to fall for magnitudes smaller than 3.5. To be really sure about the magnitude completeness of the intervals in the catalogue, I used a cut-off magnitude of 3.5 for the first 2900 days after 1/1/1980, to be consistent with the Fig. 3.3b .

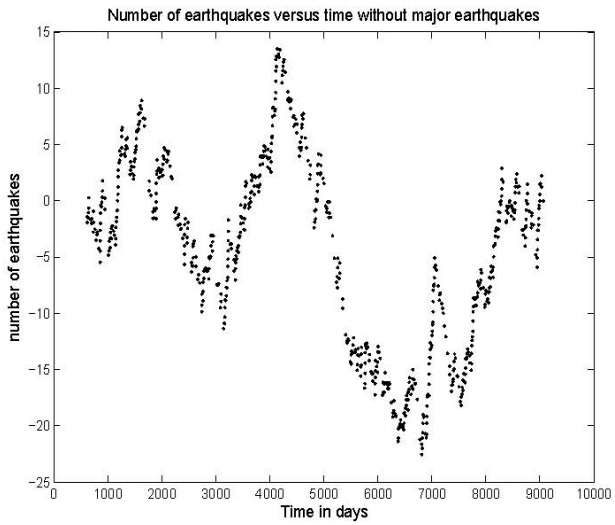

***Fig. 5.5**: The rate of earthquakes after 1980 reduced by the earthquakes of 1986 and 1990 and their aftershocks (see. Fig. 5.6)*

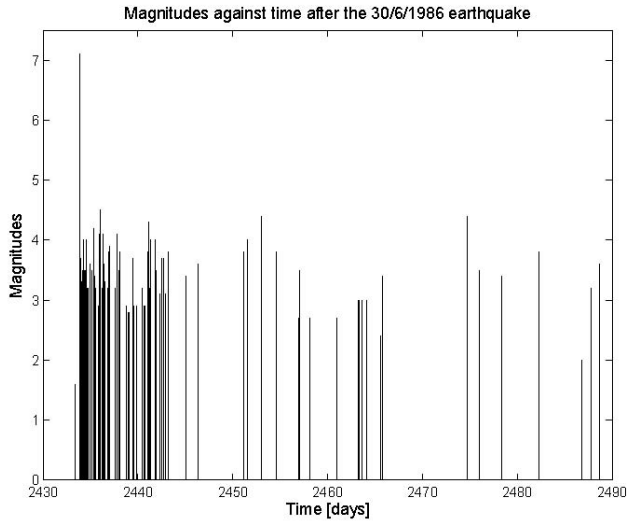

Fig. 5.6 a) Magnitude against time after the earthquake of 1986

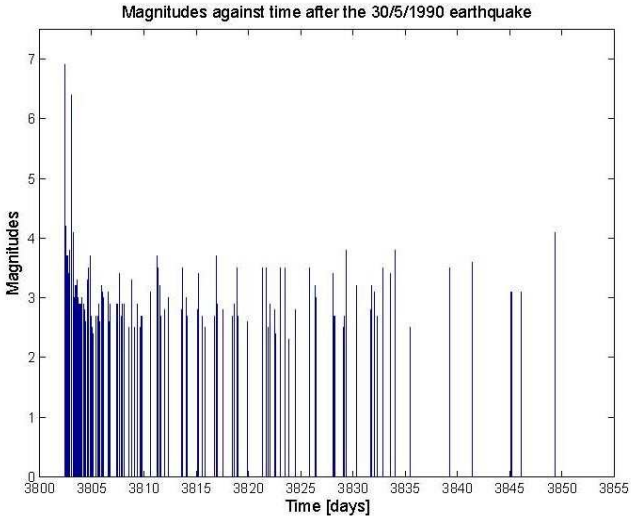

Fig. 5.6 b) Magnitude against time after the earthquakes of 1990

Fig. 5.6: *Magnitude against time after the major earthquakes of a) 1986 and b) 1990*

6. OMORI'S LAW AND EARTHQUAKE CLUSTERING

In 1935, Charles Richter and Beno Gutenberg developed the Richter scale. This scale was first only used for local earthquakes. Then, body and surface wave scales were introduced. But both are underlie saturation for high earthquake magnitudes. Thus, the moment magnitude scale was introduced in 1979 by Thomas C. Hanks and Hiroo Kanamori as a successor to the Richter scale and is used to compare the released energy. Mw is dimensionless and depends on the seismic moment M_0. This scale has the advantage that the magnitudes do not saturate.

On the Richter scale, the magnitude of an earthquake is proportional to the log of the maximum amplitude of the earth's motion. This is one of the two fundamental earthquake laws. The other is Omori's law, which gives information about the behavior of aftershocks.

6.1 Earthquake Clustering, fore-and aftershocks and their identification

6.1.1 Earthquake Clustering

What follows is part of Dieterich's (1999) discussion of earthquake clustering. A characteristic feature of earthquakes is their clustering. Thus, we can speak about fore-shocks, main shocks and aftershocks. The nucleation in time and space controls the time and place of occurrence, so that non-linear dependence of nucleation times on stress changes can affect the spatial and temporal patterns of earthquake occurrence. Dieterich states that earthquake nucleation on faults with rate-and state-dependent fault properties has this characteristic, and to represent details and statistical patterns of earthquake clustering. Various phenomena, such as foreshocks, main shocks and aftershocks, have common origins related to time-and stress-dependent earthquake nucleation. The nucleation process is preceded by a long interval (months to years) of slowly accelerating

slip on a fault patch of finite dimensions. When the nucleation process starts, perturbation of the time of the onset of the earthquake instability is very sensitive to the magnitude of the stress perturbation and the unperturbed time to the instability. Dieterich says that clustering is due to the sensitivity of nucleation times to stress changes induced by prior earthquakes. Kagan et al. (1991) state that short-term clustering is significantly stronger than long-term clustering, and especially strong for earthquakes of small and medium size. There is also a difficulty in analyzing long-term variations of seismicity, because we lack the data and model for them. Short-term clustering is especially obvious for shallow earthquakes, but intermediate and deep earthquakes have aftershocks, too (Kagan, 1991). Recent studies (e.g. Ogata et al., 2002, Kagan, 1991) relied on the model of a Poisson cluster process where earthquake occurrence is represented as a random field of earthquake sequences, where main shocks follow a stationary Poisson process and their dependent events are distributed according to a probabilistic law. Kagan et al. (1991) say that the long-term behavior of main shocks could be quasi-periodic, Poissonian, or clustered. Periodic models would predict a higher probability of an earthquake after a long, 'quiet' period, while clustering models would predict lower than the Poissonian probability. Kagan et al. (1991) mention also the fractal class of models, or scale-invariant distributions of time intervals. They say that the time distribution of earthquakes and aftershocks is scale-invariant. These fractal, or power-law distributions have a mean inter-occurrence time, standard deviation, and coefficient of variation which all tend to infinity as the observation time increases. This could be called fractal clustering. Kagan et al. (1991) mention studies that all show that there is clustering of major events over long time intervals which can extend over thousands of years (e.g. Ambraseys, 1971, 1989; Lee and Brillinger 1979; Ambraseys and Melvilee 1982; Vere-Jones and Ozaki 1982; Ogata 1988). Quasi-periodicity can be explained, according to Kagan et al. (1999), by stresses which cause earthquakes slowly build up due to the plate movements after each event. Before the stress reaches a critical value, strong earthquakes are less likely. But the existence of large aftershocks shows that large main -

shocks do not reduce the stress to a 'safe' level.

In their study, Kagan et al. (1991) see time-space clustering as a universal phenomenon which has two parts: (1) a short-term, strong clustering of shallow earthquakes, which consists of foreshock -main shock -aftershock sequences, and (2) long-term, weak clustering for all main shocks in all depth ranges. Both clustering processes should be governed by a power-law distribution, which means that they are fractal. Shallow earthquakes show strong temporal clustering. This clustering has a fractal temporal dimension of 0.5, which characterizes shallow earthquake occurrence (Kagan et al. (1991) and references therein). Kagan et al. (1980) found that earthquake sequences in depths between 70 and 140 km have a rate of clustering that is smaller by a factor of about 10 compared to shallow earthquakes. For earthquakes deeper than 140 km, this rate is close to zero.

6.1.2 Foreshocks

Foreshocks can be seen as promising short-term predictors for large earthquakes. Maeda (1996) cites Jones (1985) who worked with a Californian data set and who suggested that the occurrence of an earthquake with a magnitude equal and larger than 3.0 increases the hazard within a small space-time window by several orders of magnitude above the background level. This increase was combined with long-term probability from the background seismicity rate to evaluate the probability of a large earthquake on the San Andreas Fault. Merrifield et al. (2004) and Savage et al. (2000) studied foreshock probabilities in New Zealand and found relatively high probabilities (4.5 ± 0.7%) that an event is a foreshock. If the mainshock is required to have a magnitude at least one unit larger than the foreshock, the probability drops to 0.8 ± 0.3. Maeda (1996) mentions the work of Yoshida et al. (1994) who suggested that clustered activity indicates a buildup of the regional stress fields and may have relation with a large earthquake. The procedure of Maeda (1996) consisted of eliminating small aftershocks, segmenting the region, selecting possible foreshocks, and estimating the probabilities with regard to the occurrence of mainshocks in a certain period after the possible foreshock. He did the latter by investigating whether the mainshock

occurred in a certain space, defined as the segment where proposed foreshocks had occurred and in a certain time interval after these foreshocks. He found that the relational distance between foreshock and mainshock increases with magnitude. Maeda also found an optimal number of earthquakes having occurred in a defined space-time window, thus foreshocks are less likely if this number is exceeded.

6.1.3 Aftershocks

Fore-and aftershocks are the most important type of earthquake clustering and aftershocks seem to contribute 30 to 40 per cent to the total number of recorded earthquakes (Molchan et al., 1992). They contain significant information about the rupture process. Aftershocks are earthquakes that follow an earthquake of equal or larger magnitude. They are an example for earthquake triggering and the aftershock process does not end abruptly. Aftershocks do have necessarily to be near to the location of the main shock, but can be distributed around this location and even on different faults. This is possible due to stress redistribution (e.g. Baumbach et a., 2003).

Kagan (2004) gives a discussion about the law of Omori on which the following part will be based. Aftershocks are earthquakes that happen in the vicinity of a major shock and have a smaller magnitude than the major earthquake. Aftershock behavior is described by Omori's Law, which is an empirical relation for the temporal decay of aftershock rate. Omori's law says that the rate of aftershocks dies off quickly with time. The rate of aftershocks is proportional to the inverse of time since the main shock. In 1894 Omori formulated his law for aftershock rate decay:

$$n(t) = \frac{K}{t} \qquad (6.1)$$

These patterns describe only the mass behavior of aftershocks: the actual times, numbers and locations of the aftershock are 'random'. The values of the parameters are obtained by

fitting the equation (6.1) to the data after the main shock occurred. The other main law describing aftershocks is Bath's Law, which states that the magnitude of an aftershock is approximately one unit less than its mainshock. In 1957 Utsu suggested that aftershock decay occurs in a shorter time than assumed by Omori's law. He found the formula

$$n(t) = \frac{K}{(t+c)^p} \tag{6.2}$$

which fits better, with *p* slightly more than 1 and *c* is between 0.01 and several days. The parameter *c* was introduced to explain the seeming saturation of aftershock rate close to the origin time of a mainshock. Short-term aftershocks deviate from the modified Omori's law due to the limited possibilities of registration, such as the detection threshold, false interpretation, and the earthquake source process. Kagan (2004) proposes that *c* approximates 0 for strong earthquakes. But $c = 0$ implies a singularity, which means an infinite energy release at the origin time. Kagan (2004) discusses the issue of time completeness of aftershock sequences thoroughly and find that both local and global earthquake catalogues are significantly incomplete in terms of aftershocks occurring close in time relative to the main shock. From a statistical point of view Kagan (2004) thus concludes that the parameter *c* is not likely to be a physical property of the earthquake process.

6.1.4 Identification of fore-and aftershocks

There are several aftershock identification methods with different goals. Molchan et al. (1992) describe the most popular techniques: The hand procedure is a visual identification of earlier aftershocks and is used to analyze large well-studied earthquakes, but becomes arguable for later and distant aftershocks, and has to be formalized for data processing. The window method is the simplest formalization of the hand method. Aftershocks of a main shock are identified within space-time windows:

$$t_0 < t < t_0 + T, |g - g_0| < D, M < M_0,$$

(Molchan et al., 1992). where t, g, M are time, epicenter coordinates and magnitude. D and T are window thresholds for space and time, respectively, which depend on the main shock magnitude. The catalogue can be analyzed in chronological order or in decreasing order of magnitude. To eliminate each main shock and its fore-and aftershocks leads to the recurrent rule of main shock identification. Simultaneous identification of fore-and aftershocks causes uncertainty in the identification of main shocks, depending on the choice of main shock ordering, by time or by magnitude. Molchan et al. (1992) state that the spatial window sizes are rather similar and for $M_0 = 6$ they have the order of the accuracy of epicenter location, although this seems not always to be the case (see. Utsu et al. 1955). The elimination of spatial coordinates leads to the mathematical model, the summation of weakly dependent flows of events. Under very general conditions the resulting flow ought to be Poissonian. This method is very simple and suitable for data processing. But it does not include specific aftershock location features, e.g., offset of the aftershock zone center with respect to the main shock epicenter. This may result in losing a lot of aftershocks. Cluster methods define the methods of nearness of events and the nearness of clusters of events in time and space. Thus, the catalogue can be divided into non-overlapping clusters. There are several near-event definitions and methods for using physical information. Formal methods see earthquakes as homogeneous space-time objects which should be divided

into well-separated groups with high inner concentrations of elements, for which the single-cluster analysis is often used. It connects elements of the original set by a chain of minimum length, with removing all the edges longer than a critical value. The result is to split the chain into isolated points and clusters. Non-formal methods start with a model and identify aftershocks in the context of that model. Fore-and aftershocks are considered as chains or branching trees of causally connected events with given statistical properties. These methods use the window method to define a local nearness of events. For each next event its spatial and temporal proximity has to be evaluated. Thus, each subsequent event is linked with the largest event or with the last one in each cluster. Overlapping clusters are joined. Then, there is modeling and statistical estimation. The seismic process is described by a model and the parameters are estimated by statistical methods, e.g., the maximum likelihood. It is seen as the most natural but it is also limited by studying general cluster properties only. In this context, there are two models which should be discussed The ETES (Epidemic Type Earthquake Sequence) model is based on the Gutenberg-Richter law and on Omori's law and it assumes that all earthquakes may be simultaneously main shocks, aftershocks, and foreshocks. Each one triggers aftershocks with a rate that increases proportionally to about $10^{\alpha m}$, with magnitude m and a decay rate according to Omori's law. An aftershock sequence is seen as the sum of a cascade of events in which each event can trigger more events. The global seismicity rate is the sum of the background rate (mostly a spatially inhomogeneous Poisson process) and the sum of dependent events of the past earthquakes. It is also assumed that aftershocks can have their own aftershocks and so on (see Helmstetter et al., 2006). The ETAS-model is based only on the Gutenberg-Richter and Omori laws and assumes that each earthquake above a magnitude threshold m_0 can trigger direct aftershocks, with a rate that increases as ~ $10^{\alpha M}$ with its magnitude and decays with time according to the Omori law. Regarding the fact that large earthquakes can trigger direct aftershocks, which follow the Gutenberg-Richter and Omori Laws, many studies use the ETAS-model to calculate α of the relation of the rate increase of ~ $10^{\alpha M}$

using a maximum likelihood method. Molchan et al. (1992) also mention Prozorov's iterative method, in which main shocks are considered in decreasing order of magnitude, obeying time chronology when the magnitudes are equal. By using a spatial window S of size $D(M_0)$, a portion of statistically significant aftershocks are found. An event is seen as an aftershock if

$$n(S\delta t) = R\lambda_b(S)|\delta t|$$

where $n(S\delta t)$ is the number of events within $S\delta t$ volume, $|\Delta t|$ is the length of a time interval, $\lambda_b(S)$ is the expected number of background events within S per unit time, and R is a threshold, varied in the range of 3 to 100. Preliminary aftershock identification ends as soon the condition above fails or the identification time exceeds the threshold T. If the number of these aftershocks is greater than 10, the aftershock zone S is updated. Several elliptic zones with different sizes k_i are used for the identification, so that at the end, the aftershocks belong to the pyramid $V = Sk_i \Delta t_i$. This procedure takes into account spatial aftershock localization and it is possible to later assess the number of false aftershocks. The method is very sensitive to R, where high values lead either to the division of an aftershock sequence into separate clusters of earlier and later events, or many aftershocks may be lost. Molchan et al. (1992) propose a new approach to the identification of aftershocks. They say that it is impossible to identify aftershocks without any error. Either false events are captured or true ones are lost, when the space-time windows are chosen. The authors suggest to use the trade-off between those two errors to get a new formulation of the aftershock identification problem. The propose a 'loss function' γ which depends on the two kind of errors and is an increasing function. The goal is to minimize γ. The loss function produces a set of aftershock identification methods depending both on the loss function and on the aftershock distribution model assumed. But aftershock identification methods are restricted by the main shock magnitude range.

Foreshocks have made an obvious contribution among the earthquake predictions with hazard-mitigating effect and social manifestation, for example, the M_S = 7.2 Menglian earthquake and the M_S = 5.6 Xiuyan earthquake in China (see Wang et al., 2004). It is often necessary to make it clear if a moderate-strong earthquake is generalized foreshock or a direct foreshock and whether it contains medium and short-term information about a strong

earthquake. The authors argue that, with this judgment, it then should be possible to change the three element prediction to a one element prediction (time) (see discussion about the work of Evison and Rhoades, 2004), which means that the time before a major earthquake can be separated into three stages, with a prior and a precursory part and the main shock itself. Particularly important is the judgment of a direct earthquake. In recent years, digital seismology is developing more and more attention is being paid to studying initial earthquake rupture. The foreshock mechanism and the condition of the source medium are now very important subjects of studying. Wang et al. (2004) cite the definition of a foreshock from Mei and Feng (1993), in which a ”foreshock refers to the shocks occurred in the focal zone before the main earthquake and are associated with the main earthquake [....].” Foreshocks mostly occur several minutes or days before the main event, in the same focal zone, resulting from the same destabilizing variation in the focal zone (Lu, 1985). These definitions refer to the direct foreshock . The generalized foreshock is an extension of the definition of direct foreshocks. The authors cite Lu et al. (1985), who described the generalized foreshock as ”the single shock, shock swarm, or their combination that occurred a long period (months, years) before an earthquake sequence in a larger distance (tens or hundreds of kilometers to the focus) and related to the development of the earthquake sequence.” (see Evison and Rhoades, 2004) The definition of foreshocks by Wang et al. (2004) has a clearer limitation on time than on space. To analyze the characteristics of space and time intervals the authors use a statistic. They take a magnitude range of M_L = 4.0 - 5.9 for both direct and generalized foreshocks. Magnitudes smaller than 4 are not used because the smaller the shock, the larger the probability of random occurrence. Also, the portion of random coupling in its relationship to the main earthquake will increase with decreasing magnitude. The authors define the ’doubtful’ foreshock in time and space as the time interval to the main event is ΔT = 360 days, and the distance to the future major event is ΔR = 350 km, and a magnitude difference to the major earthquake of not less than 0.5 units. The authors mention the characteristics of the spatial relationship of direct foreshocks and main event and say that the longer the spatial distance is, the larger will be the circular area for statistics. If the statistic ’area’ is also considered in the same time, the scale of ’doubtful’ foreshock will decrease with increasing radius of the circular area. The scale is measured in percent and gives a probability of the ’doubtful’ foreshock. Wang et al. (2004) propose 30 days for a time window and 50 km for a space window.

6.2 Seismic Moment

The relation between magnitude *m* and seismic moment *M* can be written as

$$m = \frac{2}{3} log_{10} M - 6.0$$

and the seismic moment is calculated by

$$M = \mu u L W$$

with μ as the elastic shear modulus, u the slip vector, L the length and W the width of the rupture plane. The seismic moment release rate is estimated to be 8 x 10^{18} *Nm*/*yr* (Wenzel et al., 1999a), which is comparable with Southern California, and manifests itself in 3 to 5 major and highly damaging earthquakes in a century, with the last and very severe, above mentioned earthquake at March 4, 1977, which took the lives of 1.500 people, destroyed and damaged 32,000 apartments and 33 high buildings (MŁntyniemi et al. (2003) and references therein) and caused a seismic loss corresponding to more than 2 Billion US Dollars (Van der Hoeven (2003)). References in Kagan (2002) stated that for small and moderate earthquakes, the seismic moment is proportional to l^d, with d = 3 with l the length of the fault, and that this law would break down for larger earthquakes with M = 6, with d = 2 for large and d = 1 for great earthquakes.

7. TEMPORAL BEHAVIOUR OF EARTHQUAKES, SEISMIC HAZARD AND EARTHQUAKE MODELING

This chapter gives an overview about earthquake theory and what has been done recently. Probabilistic Seismic Hazard Analysis is discussed and the Poisson Process and the Seismic Gap Model are mentioned because of relevance to the results discussed in the next chapter.

7.1 Fractal behaviour

Earthquakes are described in deterministic or stochastic models. In the first case, rupture process is seen as a combination of delta functions with smooth distributions of slip over time and space. But these models fail to explain the temporal complexity of the rupture, the occurrence of aftershocks, and the geometric complexity (Kagan, 2004). In the late 1980s, models where constructed that use scale-invariant and fractal formalism. These models see earthquakes as individual events, too. In the 1990s, earthquakes were represented as a large collection of subevents with a fractal distribution of their sizes. The propagation of a rupture is imagined as jumping from one subevent to another (see references in Kagan (2004)). And Kagan proposed each subevent as a cluster of elementary dislocations. So, the fractal model replaces the delta function singularities by weaker power-law singularities. Kagan (1991) states that the physical parameters of subducting slabs, such as temperature, slab age, or pressure are not enough to explain the details of their earthquake distribution, and that this distribution in time and space is controlled by random factors which exhibit fractal behavior. It could be that the mantle convection in the neighborhood of subducting slabs is non-uniform, which causes strains in the slab which cannot be accommodated

plastically. So the distribution of such regions may have a fractal pattern. Kagan (2005) and references therein) also states that the spatial distribution of epicenters and hypocenters can be described by a fractal, scale-invariant relation with the correlation dimension $\Delta = 2.2 - 2.3$.

7.2 Earthquake Triggering

There are several forces that can trigger earthquakes. First of all, the movement of tectonic plates relative to another and other processes cause strain to build in earthquake fault zones around the world. Various obstacles such as the resistance of rock layers to smoothly slip past one another cause that strain energy to build to high levels in some fault zones. When enough strain is accumulated, some of the stored energy is released in the form of an earthquake. Large earthquakes can produce permanent instabilities in a fault zone and can influence the time to the next earthquake. When an earthquake triggers an earthquake at a remote distance, one speaks of dynamic triggering. The physical origin of dynamic triggering remains one of the least understood aspects of earthquake nucleation. Johnson et al. (2005) state that the dynamic strain amplitudes from a large earthquake are very small once the waves have propagated more than several fault radii. But if a fault is already weak, seismic waves can cause fault slip. There are several dynamic triggering mechanisms possible. Most of them are based on fluid-mechanical interaction in the fault gouge. Proposed mechanisms include increase pore pressure associated with:

- the compaction of saturated fault gouge (liquefaction), leading to
- failure cyclic fatigue of the gouge from the oscillatory wave and a 'sub-critical crack growth' mechanism in which chemical reactions are accelerated by the wave stresses

Johnson et al. (2005) suspect that dynamic elastic nonlinearity of fault gouge might have an influence in triggering, because they observed temporary decrease in modulus (material softening) under the influence of wave excitation at seismic strains. Almost all larger earthquakes are followed by aftershocks, but it still is not clear how many of them are caused by the passage of seismic waves and how many are triggered by the rearrangement of the Earth's crust during the main shock (static triggering). Dynamic stresses are larger, but temporary, lasting only as long as the crust is influenced by seismic waves. Static stress changes are smaller, but permanent and are the only ones to decrease seismicity rates. Thus, earthquake suppression is seen as a means to study the cause of earthquake triggering (Parsons, 2005). Parsons shows that if seismic waves can alter some frictional contacts in neighboring fault zones, dynamic triggering might cause delayed triggering and an Omori-law response. The author argues that the question whether earthquakes are more often triggered by dynamic triggering than by static triggering is very important to the methods used to forecast earthquake probabilities. Aftershocks and earthquake triggering are often explained by laboratory fault analogs and rate-and state-dependent friction (Dieterich, 1979). Dynamic triggering models show that earthquakes can be triggered if a stress pulse emitted by a main shock increases another fault's slip speed ('rate') above a threshold value. This pulse can also enhance triggering by reducing the 'state' of a fault (frictional increase with contact age). This should occur through slip-induced renewal of contacts, which could be time-delayed. Parsons (2005) suggests that the fault state is also changed by minor 'damage' to fault contacts induced by passing seismic waves. By changing the critical slip distance D_c in rate-state slip speed calculations, Parsons shows that the time to failure can be changed. Triggering would be delayed until the evolution to failure is complete. He can replicate an Omori-law response to dynamic triggering, if fault contacts are disturbed according to a power law with smaller contacts occurring in exponentially greater numbers. Therefore, an approximately uniform reduction of D_c across the power-law distribution is important to create an Omori-law sequence. He suggests that seismic waves most likely affect D_c by strain-induced compaction and/or fluid migration.

Helmstetter et al. (2005) estimated the importance of small and large earthquakes for static stress changes and for earthquake triggering. They assumed that earthquakes are triggered by static stress changes and that earthquakes are located on a fractal network of dimension

D. Their model suggests that the number events triggered by earthquakes with magnitude *m* and the stress change which is thus induced on other locations increase proportionally with *m* as $10^{Dm/2}$. The authors also state that the stronger the spatial clustering, the larger the influence of small earthquakes on stress changes and earthquake triggering. If earthquake magnitudes follow the Gutenberg-Richter law with $b > D/2$, small earthquakes collectively dominate stress transfer and earthquake triggering. When $D/2 \approx b$,small earthquakes are about as important to earthquake triggering as larger ones.

7.3 Poisson Process and Poisson Model

The Poisson process is a stochastic process which is defined in terms of the occurrences of events. This process, given as a function of time N(t), represents the number of events since $t = 0$. The number between time *a* and time *b* is given as $N(b) - N(a)$ and has a Poisson distribution. It is a continuous-time process. A homogeneous Poisson process is characterized by a rate parameter λ and the number of events in a time interval [t, t+τ] and follows a Poisson distribution with the parameter λτ. This relation is given as

$$P\big[N\big((t+\tau)-N(t)\big)=k\big]=\frac{e^{-\lambda\tau}*(\lambda\tau)^{k}}{k!} \qquad \text{k = 0,1……}$$

The homogeneous Poisson process is characterized by its rate parameter λ, which is the expected number of events that occur per unit time. The rate parameter may change over time, where the generalized rate function is given as $\lambda(t)$. The expected number of events between time *a* and time *b* is

$$\lambda_{a,b}=\int_{a}^{b}\lambda(t)dt$$

The number of events in the time interval [a,b] follows a Poisson distribution with associated parameter $\lambda_{a,b}$

$$P\left[\left(N(b) - N(a)\right) = k\right] = \frac{e^{\lambda_{a,b}} * (\lambda_{a,b})^k}{k!} \qquad k = 0,1\ldots.$$

The characteristics of the Poisson process are its orderliness, which implies that events do not occur simultaneously and its memorylessness, which implies that the events are independent of each other. These characteristics mean that the time between consecutive events are independent random variables.

In the Poisson model there is only one parameter, the average rate of earthquake occurrence, λ. The Poisson probability density is given by

$$f_{Poiss}(t) = \lambda * e^{\lambda * t}$$

To model the temporal occurrence of earthquakes, the Poisson process has been used extensively (see references in Hong and Guo (1995)). Reasons are its simplicity and easy application.

7.4 Seismic Gap Model

The characteristic earthquakes, assumed in the seismic gap hypothesis, are presumed to have similar rupture areas and magnitudes for each fault segment. They should have similar hypocenters, similar displacement distributions, and similar source-time functions (Jackson et al. (2006)).The Working Group on California Earthquake Probability stated the characteristic earthquake hypothesis in 1988:

"*A fault segment is said to have a characteristic earthquake if it repeatedly slips in earthquakes of similar magnitude and if those earthquakes dominate the stress release for that segment*. "

This hypothesis is justified from general, geological, physical, and mechanical considerations, which are subject to various, sometimes even contradictory interpretations (Kagan (1993). Kagan also states that this thesis is not specified enough to undergo formal testing. The Seismic Gap Model, which was developed by McCann et al. (1979) and Nishenko (1989, 1991), states that these characteristic earthquakes are quasi-periodic with a characteristic recurrence time. Plate boundaries are seen as divided into segments, each with a characteristic earthquake, which is strong enough to dominate the seismic moment release, so that the stress, which is built up through plate movements, is substantially reduced. So the earthquake hazard is smaller, directly after an characteristic earthquake and increases with time, as plate movement goes on. Evidence for characteristic earthquake could be the result from selection biases:

- short instrumental history
- errors and biases in estimating the size or frequency of the largest earthquakes from paleoseismic records
- selection bias of the spatial extend of a seismic zone

(Jackson et al. (2006) and references therein). McCann and Nishenko (1979, see references in Rong et al. (2003)) proposed six categories of seismic potential for major plate

boundaries in and around Pacific regions. The red category or 1 denotes the highest seismic potential; the orange category or 2 denotes the second highest potential; the green category or 6 denotes the lowest potential; the yellow category or 3 denotes regions with incomplete historic records but with a potential for large earthquakes; the hatched category or 4 denotes regions for which plate motion is subparallel to the arc; and the purple category or 5 denotes the regions without historic records of great earthquakes. But Rong et al. (2003) found out that the red zones show less seismicity than the orange or green zones. Kagan et al. (1995) tested the new seismic gap hypothesis, which considers recurrence time and characteristic earthquakes specific to each plate boundary segment. They found out that this thesis predicts too many earthquakes for the following reasons: (1) the forecasts were made for some zones specifically because they had two or more earthquakes in the previous centuries, which biased the estimated earthquake rate; (2) the time before the first event and after the last one on a segment was excluded; and (3) it was assumed that all slip in each zone is released in characteristic earthquakes of the same size. In contrast to the Seismic Gap Model, Jackson et al. (2006) propose a model which assumes earthquakes to follow a Poisson process and the magnitudes to follow a tapered Gutenberg-Richter distribution.

7.5 Recent Work

In the model of Helmstetter et al. (2006), which is a method to estimate earthquake probabilities in Southern California using the Epidemic Type Aftershock Sequence Model (e.g. Kagan and Knopoff 1987; Ogata 1988; Kagan and Jackson, 2000) , the seismicity rate is the sum of a constant background seismicity and of the aftershocks of past earthquakes.

The ETAS model is a stochastic point process used to obtain short-term earthquake forecasts which include dependent events like foreshocks and aftershocks (see references in Helmstetter et al., 2006). For the aftershocks Omori's law is valid. The spatial distribution of aftershocks following a small main shock is modeled by an isotropic adaptive kernel. For the ones following a larger main shock, they smooth the density of early aftershocks to model the density of the future aftershocks. Helmstetter et al. assume that the earthquakes follow the Gutenberg-Richter relation with an uniform b-value. They made several observations:

(1) aftershocks vary with respect to regional tectonics, (2) the time decay behavior of the aftershocks varies between shallow and deeper earthquakes, (3) at large time separations the aftershock rate drops off more quickly than a power law decay, and (4) intermediate and deep earthquakes show very little clustering. In a similar model (Console et al., 2003) the occurrence rate density is displayed as a sum of two terms, the first represents the independent activity and depends only on space. The second consists of three terms: magnitude, time, and location of the past earthquakes. The time is represented by the modified Omori law and the magnitude and location are found with the maximum likelihood method.

Hsu et al. (2006) modeled the afterslip in Sumatra using a rate-and-state-dependent friction law. They suggested the postseismic displacement as resulting from rate-strengthening brittle creep and found out that this displacement should increase approximately linear with the logarithm of time.

7.6 Probabilistic Seismic Hazard Analysis

Probabilistic Seismic Hazard Analysis (PSHA), which is mentioned and used widely (e.g. Tormann, 2005) is the effort to quantify the potential for ground shaking due to earthquakes at a certain site and for the time period of interest. The probability at a given site may appear to be low (e.g., 1/10 000), but it still is critical as it is these numbers that help such

things as earthquake insurance rates and building codes (Barros et al., 2003). Short-term hazard analysis due to earthquake clustering is still slow in its development. The hazard due to these phenomena has strong daily fluctuations and does not typically remain for the time period of interest in the traditional PSHA mapping. Thus, it is not used for the development of building codes, but helps in recovery efforts after large earthquakes. Tormann (2005) gives an overview of the PSHA and its development. A first attempt to quantify the probabilities of future aftershocks was made by Reasenberg and Jones (1989) . They conveyed the expected number of aftershocks of a given size and the next step has to expand it into the PSHA framework. After the work of Reasenberg and Jones it was shown that there are spatially and temporally systematic changes in both magnitudes and productivity of earthquakes. The first scientific framework for seismic hazard assessment was based on the theory of plate tectonics. Prior, earthquake catalogues were used as representative empirical guides to the sources of hazard. Probability is a good tool to describe seismic processes and hazard, and it can also be used to model sources derived from epicenters, to calculate the next earthquake in the vicinity of the past one, whose distance scale should be dependent on the magnitude. Within the kernel estimation methodology (see next section) the magnitude dependence of the spatial distribution is represented by the bandwidth, which scales with the fault size. At the beginning, the PSHA was developed for engineering purposes to measure the earthquake hazard on certain sites. Today, time dependence due to foreshock and aftershock triggering is incorporated. PSHA is used to calculate a quantitative estimate of the likelihood of exceeding a given threshold of earthquake-caused ground motions in a certain region during a certain time period. Rates of earthquake occurrences (Poissonian) are estimated and the associated ground motions are calculated from an attenuation model. The influence of each earthquake is multiplied by the rate with which the event could occur. The probability of a certain ground motion in a certain time is calculated by summing over all events. By assuming a Poisson process, this approach is time-independent. Cornell (1968) developed the methodology of

PSHA to provide average return periods of ground motions for engineering reasons. He used the annual number of earthquakes exceeding a certain minimum magnitude. With the integration over all individual influences of the potential earthquake sources resulted in a probability distribution of the maximum intensity. In PSHA it is common to take into account the uncertainty in estimates of ground motion from attenuation relationships, when the annual frequencies of exceedance are calculated. The ground motion is then the median of a log-normal distribution that is characterized by a standard deviation. In 1996, geoscientists of the US Geological Survey and the California Department of Conservation (today California Geological Survey) published seismic hazard maps of horizontal peak ground accelerations for California. They used a record of 200 years of historical seismicity and active fault data and took into account the recurrence rates of potential earthquakes in each earthquake source and the potential ground motions for each of them. According to different slip rates and different availability of paleoseismic data, the applied magnitude-frequency distributions varied. Modeling was based on the characteristic earthquake model of the seismic gap theory and the exponential Gutenberg-Richter relationship. When the earthquake distributions were calculated, attenuation relationships were used to estimate the ground motion distribution for each earthquake with a certain magnitude, distance, and rupture mechanism. A few years later, the methodology was improved and it was shown that the maps over-and underestimated the hazard on certain places of the San Andreas Fault.

7.6.1 Kernel Estimation

What follows is an explanation of the kernel estimation by Stock and Smith (2002). The representation of seismic sources in area zone is a common way to reduce data in the PSHA. But the assumption of uniform seismicity in these zones and the Euclidian geometry of the zones do not match the fractal spatial distribution of the seismicity. The spatial extent and the correlations of earthquakes of different size are ignored. Thus, kernel estimations

are used, which are based on the concepts of fractal geometry and self-organized criticality, and have a bandwidth scaling with the magnitude. With kernel estimations, hypocenters of earthquakes are redistributed in space. The kernel function and its bandwidth give the shape and the amount of redistribution. Stock and Smith (2002) used an adaptive kernel with a spatially varying bandwidth, to filter temporal sequences to produce mainshock occurrence representations. Thus, multiple mainshock-aftershock sequences are reduced to one single earthquake.

7.6.2 Recent work in PSHA

Radulian et al. (2002) used a deterministic approach to compute seismic hazard in terms of peak ground motion values on a grid covering Romania. They used the input of two parameters, one related to the source, the other to structure modeling. Van der Hoeven (2003) carried out a hazard analysis in the VSZ and considered only earthquakes with focal depths greater than 60 km. They regard this depth as the boundary between crustal and subcrustal activity. Additionally, they omitted dependent events (foreshocks, aftershocks and swarms of earthquakes). Their approach is parametric-historic and the hazard is expressed in terms of peak ground acceleration (PGA), or acceleration response spectra, where knowledge of the form of the attenuation curve is needed. After this, they computed the expected ground motions for several sites, to create seismic hazard maps for the VSZ. Their results indicate a b-value of 0.78(±0.01) and, for example for Bucharest, PGA values of $0.30g \approx 2.9m/s^2$ for the shallowest earthquakes, $0.24g \approx 2.4m/s^2$ for the ones at the depth of 120km and $0.20g \approx 2.0m/s^2$ for the deepest earthquakes.

Stirling et al. (2002), whose methodology is based on the one of Cornell (1968), defined a three-dimensional grid of a-values and the parameter b and the maximum cutoff magnitude of the Gutenberg-Richter distribution were defined from the zonated surrounding region and then smoothed across the zone boundaries. They used geologic data and historical earthquakes to define the locations, magnitudes, the tectonic type, and frequencies of

earthquakes that could be produced in each source. Then they estimated the ground motions that could be produced by the sources. Their method combines defining continuous distributions of seismicity parameters with the traditional method of defining large area sources and the associated seismicity parameters (see references in Stirling et al., 2002). The PSHA combines the modeled seismicity data with geological data, which contains information of the location and recurrence times of 305 active faults and attenuation relationships for peak ground acceleration developed specifically for New Zealand. Their methodology for the treatment of distributed seismicity is an improvement, because it preserves the smooth transitions of seismicity rates within and across zone boundaries, avoiding edge effects. Stirling et al. (2002) used the standard methodology of PSHA. They calculated the annual frequencies of exceedance for a given site for a suite of ground motion levels, using magnitude, recurrence rate, earthquake type, and source-to-site distance predicted by the source model. After this, they estimated the maximum acceleration level that is expected to be exceeded in different time intervals. They assigned every fault a particular slip type, because of the different attenuation expressions for each slip type. The new geological data set was constructed on the basis of the old one and then extended. It contains 205 faults, with slip type, dip, dip direction, maximum and minimum depth, slip rate, displacement, maximum magnitudes (the most likely maximum magnitude), and recurrence intervals. Different techniques are used, depending on the quality and quantity of the data, to determine the maximum magnitude and the recurrence intervals. With the spatial seismicity distribution of events greater than 5.25, locations and recurrence rates of distributed seismicity are estimated on a three dimensional grid (spacing of 0.1°) of point sources over New Zealand. For each gridpoint, the recurrence rate is estimated by calculating the a-and b-value of the Gutenberg-Richter relationship. After that, the incremental rates of magnitudes are calculated for each 0.1 increment of magnitude from 5.25. The methodology of Stirling et al. (2002) is now used for the development of building codes in New Zealand.

The STEP model, developed by Gerstenberger (2003) is ready to be used in real time and combines traditional long term background hazard analysis based on geological data and historic seismicity with short-term models. In this model, each earthquake is considered as a mainshock and the full aftershock probability model is applied. Thus, more than one event can contribute to the aftershock hazard, but it only shows the highest rate produced by any event. Gerstenberger uses three aftershock models, depending on the available data. The simplest one was developed by Reasenberg and Jones, 1989 and 1994 ,and considers only the magnitude of the mainshock. If a sufficient number of aftershocks are observed, a sequence specific model is calculated, which the parameters estimated for the sequence. The most complex model is applied, when the aftershock sequence shows a spatial heterogeneity. It calculates its parameters on each node of the grid independently.

Tormann (2005) modeled the prospective foreshock probability decay as a function of origin time and epicentral distance from a potential foreshock, and the magnitude difference between foreshock-mainshock pairs. She suggests that foreshocks follow similar statistical laws to the time dependence of aftershocks. Tormann takes into account the number of possible foreshocks and the magnitude difference between foreshock and mainshock. She founds out that the probability values for foreshocks are similar between different foreshock magnitudes. Furthermore, the Gutenberg-Richter relation seems to apply to the magnitude distribution in foreshock-mainshock pairs, too. The spatial decay is independent of the magnitude distribution, the foreshock probabilities decrease approximately to the inversion of time. Tormann calculates the seismic hazard as a combination of the Poissonian background hazard, the foreshock probability influence and the aftershock hazard. Bommer et al. (2005) use logic trees as a tool to deal with the uncertainties associated with the inputs in the PSHA. They have become a standard feature in the PSHA. For example, there is aleatory variability, i.e. the scatter associated with empirical relationships. The most important aleatory variability is associated with ground-motion prediction equations, represented by the standard deviation of the logarithmic residuals of the predicted parame-

ters. And then there are epistemic uncertainties which reflect the incomplete knowledge of seismicity, rupture characteristics, and seismic energy. And there are epistemic uncertainties in the characteristics of the seismic source zones, the model of recurrence, or the maximum magnitude. For epistemic uncertainties, logic trees are used. In each step for which there is an epistemic uncertainty, separate branches of a logic tree are added for each of the feasible choices. To each a normalized weight is assigned that reflects the confidence that this is the most correct model, and mostly, the weights are centered on a best estimate. Then, the hazard analysis follows each of these branches, each analysis producing a single hazard curve. By multiplying the weights along all the branches, the weighting of each hazard curve is found. This allows the definition of a mean curve, a median curve and curves for different confidence intervals. But the number of hazard calculations can become very large, so it is avoided to use branches with very small differences between the options and when these options result in very similar nodes.

Kagan et al. (2002) used the Harvard CMT catalogue and expressed their forecasts as the rate density, which is assumed, for the long-term forecast, to be proportional to a smoothed version of past seismicity. The estimated rate density depends linearly in the magnitude of the past earthquakes and on a negative power of the epicentral distance, up to 100 km. No explicit time dependence is assumed. The short-term forecast is expressed as a rate density in location, magnitude, and time and changes from one day to the next. Kagan (2002) applied the forecast to mainshocks, aftershocks, secondary aftershocks and mainshocks with foreshocks. For the long-term forecast, they smoothed the past earthquake catalogues of seismic moment solutions, using kernel functions. The short-term forecasts are based on the short-term earthquake clustering. Seismicity is approximated by a Poisson cluster process, in which clusters of earthquakes are statistically independent and the rupture propagation is approximated by a stochastic space-time critical branching process.

8. MODEL APPLICATION AND CONDITIONAL PROBABILITIES

8.1 The model of Smith and Christophersen

Smith and Christophersen (2006) developed a new probability function for earthquake recurrence times, based on the empirical distribution function of inter-event times. The model consists of two terms, with the first term an Omori's law of aftershock decay of the form of $\frac{1}{t}$, but modified with modulating exponential functions to remove the singularity at 0 and ∞. The second term is an exponential (Poisson) model. The causally related proportion of events and the Poisson time constant are the only two important parameters in that model. The model gives a probability distribution for the time to the next earthquake above a specified magnitude conditional on the time since the last event. Christophersen (2000) proposed elliptical areas A, in which 90% of the aftershocks of a mainshock of magnitude M occurred. A was found by $log_{10}A = M - 3.39$ (8.1)

$$log_{10}A = M - 3.39 \tag{8.1}$$

and the maximum distance *d* between earthquakes within such an ellipse was calculated via

$$d = 2a = 4\sqrt{\frac{10^{M-3.39}}{\pi}} \tag{8.2}$$

which was used to construct a region of potentially related events, being called super clusters.

The frequency of superclusters was found to follow a power law. Then, they plotted the cumulative distribution of inter-event times and found one part which is a linear function of (log)time and a second part, which corresponds to the occurrence of new earthquakes. In this work, superclusters were not used as the distribution of the VSZ earthquakes is already very confined.The model initially had the form

$$f(t) = \frac{A}{t^p} + \frac{B}{t^q} \tag{8.3}$$

But because of non-integrable singularities at both *t* = 0 and *t* = 8 additional terms were used. The final model can be written as

$$f(t) = w_1 f_0 \left(1 - \exp\left(\frac{-t}{t_s}\right)\right) \exp\left(\frac{-t}{t_1}\right) t + w_2 \left(\frac{1}{t_0}\right) \exp\left(\frac{-t}{t_0}\right) \tag{8.4}$$

Where normalizing constants f_0 and $\frac{1}{t_0}$ are introduced, so that $w_1 + w_2 = 1$. The term $(1 - \exp\left(\frac{-t}{t_s}\right))$ is approximately 1 for times *t* greater than a few multiples of t_s. The term $\exp\left(\frac{-t}{t_1}\right)$ and $\exp\left(\frac{-t}{t_0}\right)$ are approximately 1 for times that are a modest fraction of t_1 and t_0. Smith et al. (2006) state that these exponentials do not disrupt the power-law behaviour at shorter times. f_0 is approximated by

$$f_0 = \frac{1}{E_1\left(\frac{a}{t_1}\right) + \ln\left(\frac{a}{t_s}\right) + \gamma + E_1\left(\frac{a}{t_1}\right)} \tag{8.5}$$

where $E_1(x)$ is the exponential integral (e.g. Abramowitz amd Stegun, 1965, p228, 5.1.1 and p230 5.1.39)

$$E_1 = \int_0^\infty \frac{\exp(-u)}{u}\, du \tag{8.6}$$

γ is Euler's constant 0.57721566, and *a* is a constant chosen so that $t_s \ll a \ll t_1$. f_0 is not sensitive to *a*.

The closed form for the model in equation 8.4 is

$$F(t) = w_1\left(1 - f_0 E_1\left(\frac{t}{t_1}\right) + w_2\left(1 - \exp\left(\frac{-t}{t_0}\right)\right)\right) \tag{8.7}$$

t_s can be either a period immediately after a main shock during which some aftershocks may not have been detected or a transient time after initiation of the rupture of the main shock during which the aftershock-causing process builds up. w_1 is the proportion of aftershocks, w_2 the proportion of new events. t_0 and t_1 have to be determined from the data. I took $t_0 = t_1$.

Applying the model to New Zealand data, Smith and Christophersen (2006) found that the conditional probabilities falling relative to the Poisson law, when the time since the last earthquake increased, and suggested that this partially explains seismic gaps.

8.2 Maximum Likelihood Method

To calculate the parameters of the model, I used the Maximum Likelihood Method (MML). What follows is a description of the method by Pisarenko (1970). The advantages of the MML are its universality and that its estimators are the most efficient under general conditions. $x_1,....x_n$ is a sample of random variables whose probability distribution depends on parameters $\alpha_1....\alpha_m$. The parameters can vary in some domain A. The density function of random variables exists and is denoted by $f(z_1,...z_n|\alpha_1....\alpha_m)$. Substituting for the arguments of this density, the likelihood function for the parameters $\alpha_1....\alpha_m$ is

$$L = f(x_1,....x_n|\alpha_1,...\alpha_m)$$

The maximum likelihood estimators of the parameters $\alpha_1....\alpha_m$ give the maximum value to the function for L. If this function is differentiable, then its maximum in the domain A is achieved in the point where

$$\frac{\partial f(x_1,...x_n|\alpha_1,...\alpha_m)}{\partial \alpha_k} = 0 \qquad k = 1,\ldots m \qquad (8.8)$$

Sometimes it is more convenient to consider the system of equations:

$$\frac{\partial log f(x_1, \ldots x_n | \alpha_1, \ldots \alpha_m)}{\partial \alpha_k} = 0 \qquad k = 1, \ldots m$$

The last equations are called the likelihood equations. The problem of finding the maximum likelihood estimator for $\alpha_1 \ldots \alpha_m$ is reduced to solving the last system.

8.3 Application of the model of Smith and Christophersen to the VSZ

With a depth cut-off of 60 km and a data set starting in the year 1980, I used the equation 8.4 to compare the model with the data. Parameters w_1 and t_0 where found with the Maximum Likelihood Method. I first used a magnitude cut-off of 3.5. The maximum likelihood values for w_1 and t_0 can be seen in Fig. 8.1, with $t_0 = t_1$. The arbitrary starting time t_S has a value of 0.025 days.

From this Fig. 8.1, which was found by grid search, it can be seen that the data contain 13 ± 5% aftershocks and the inter-event time for new earthquakes is 13 ± 1 days.

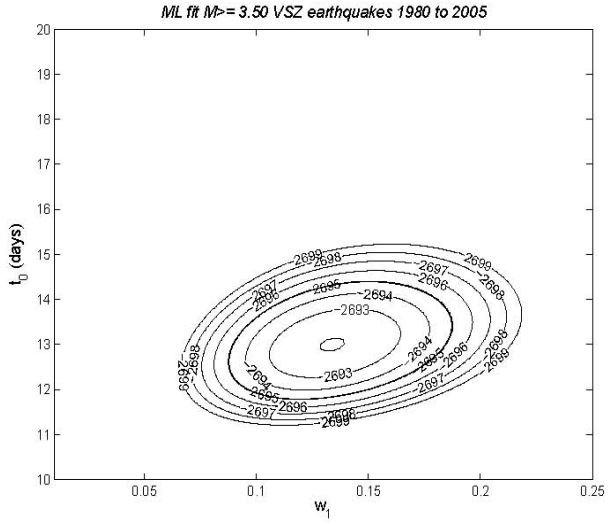

Fig. 8.1: *Maximum likelihood fit for w_1 and t_0 using a magnitude cut-off of 3.5, a depth cut-off of 60 km, starting at 1980; thick black line represents 95% confidence level*

Fig. 8.2a and b show the comparison of the data (solid black line) with the model of Smith and Christophersen (2006) (bright blue) and the Poisson model (dashed black line) for a logarithmic and a linear time scale.

In Fig. 8.2a the model and the data are compared on a logarithmic time scale. The model, shown as blue line, fits the data (solid black line) very well. The dashed line is a pure Poisson model, which is used for comparison. Fig. 8.2b shows the same plot on a linear time scale. Up to ten days after the major earthquake, there are more earthquakes than predicted by the pure Poisson model. Then, earthquakes show Poissonian behaviour for about 3 to 5 days. Finally, there are less earthquakes than expected, which is a behaviour similar to the seismic gap model. Thus, the earthquakes cluster right after the major event, but after several days there seems to be not enough stress to give rise to new earthquakes.

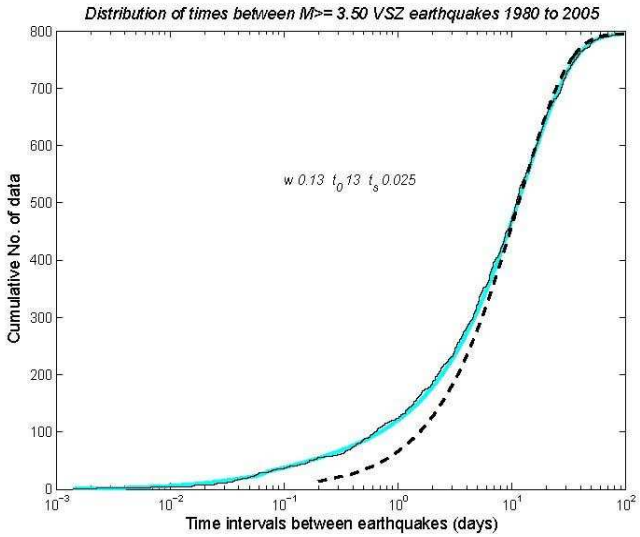

Fig. 8.2 a) Distribution of the inter-event times in a logarithmic scale, using a magnitude cut-off of 3.5, a depth-cut-off of 60 km, starting 1980

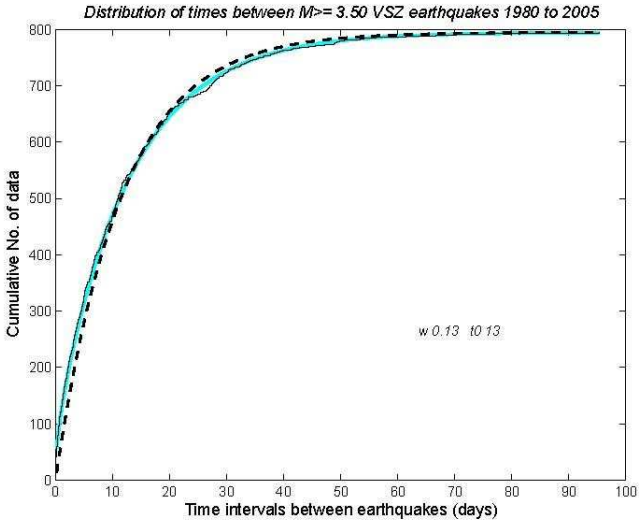

Fig. 8.2 b) Distribution of the inter-event times in a linear scale, using a magnitude cut-off of 3.5, a depth cut-off of 60 km, starting 1980

Fig. 8.2: *Distribution of inter-event times, using a magnitude cut-off of 3.5, a depth cut-off of 60 km, starting 1980; blue = model, black = data, dashed line = pure Poisson model*

To see how big the differences are between model and data, I plotted the difference between model and data against the inter-event times (Fig. 8.3).

The differences start to increase after one day and reach their peak about 30 days after the major event. The largest difference between model and data is 1.5%, shown as the highest peak in Fig. 8.3.

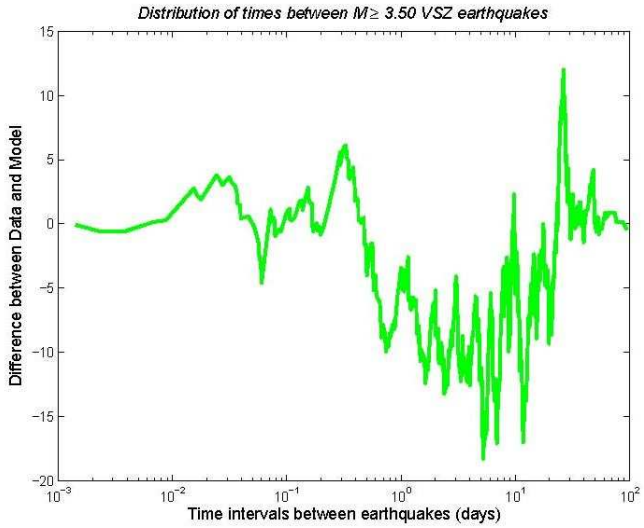

Fig. 8.3: *Differences between model and data for M ≥ 3.5 earthquakes*

I plotted the maximum likelihood value, comparisons of data and model and the differences between them for several cut-off magnitudes (Fig. 8.4 -8.8).

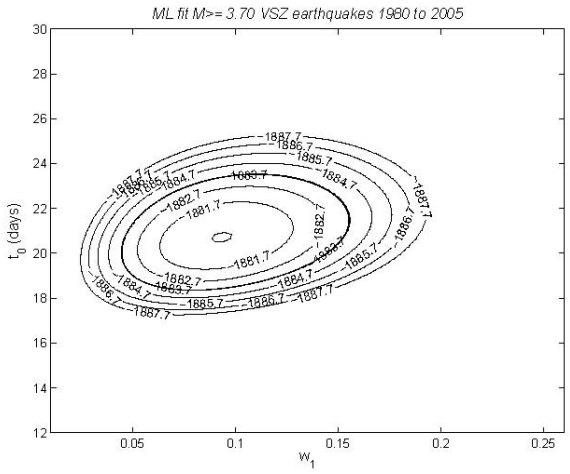

Fig. 8.4 a) Maximum Likelihood Values for w_1 and t_0 for a cut-off magnitude of 3.7, a depth cut-off of 60 km, starting 1980

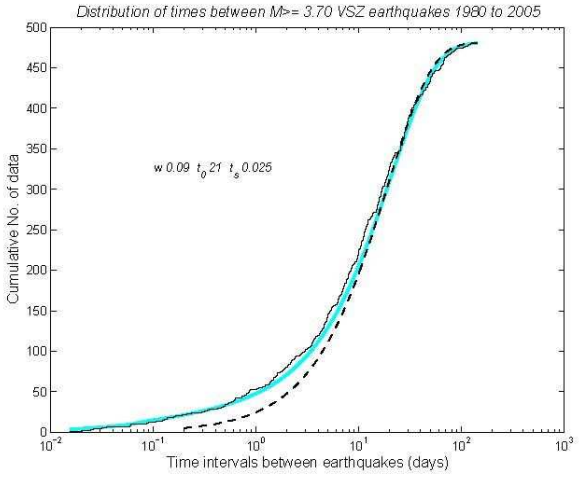

Fig. 8.4 b) Distribution of inter-event times in a logarithmic scale, using a magnitude cut-off of 3.7, a depth cut-off of 60 km, starting 1980

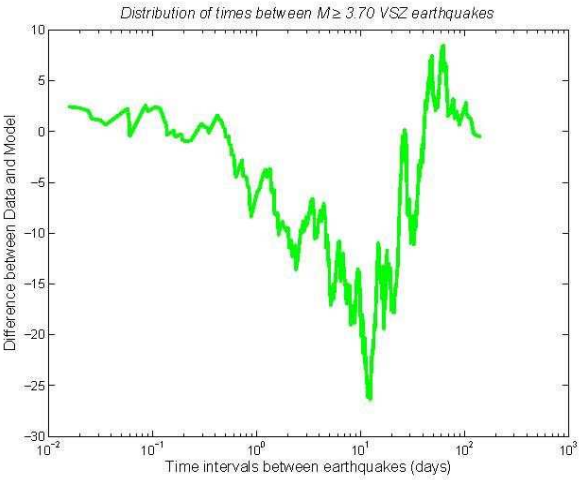

Fig. 8.4 c) Difference between model and data for M ≥ 3.7 earthquakes

Fig. 8.4: *a) Maximum Likelihood Values, b) model and data comparison, c) differences between model and data for earthquakes after 1980, deeper than 60 km and above a magnitude of 3.7*

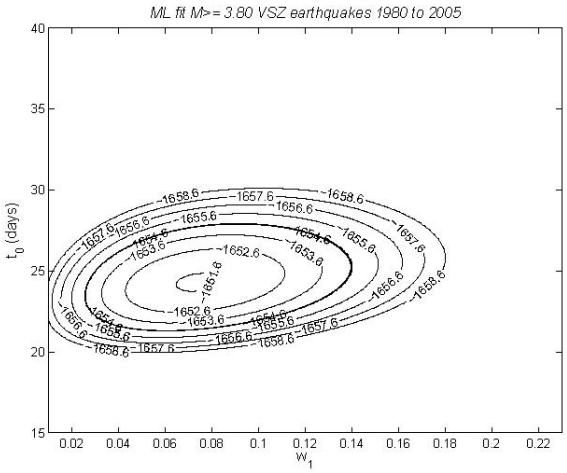

Fig. 8.5 a) Maximum Likelihood Method for w_0 and t_0 with a magnitude cut-off of 3.8, a depth cut-off of 60 km, starting 1980

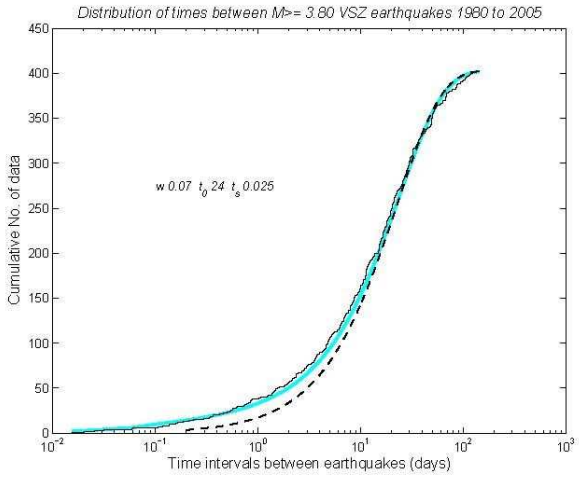

Fig. 8.5 b) Distribution of inter-event times in a logarithmic scale, using a magnitude cut-off of 3.8, a depth cut-off of 60 km, starting 1980

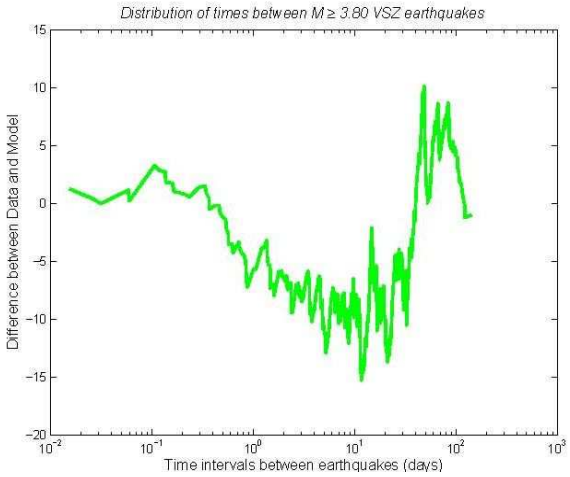

Fig. 8.5 c) Differences between model and data for Mcut ≥ 3.8

Fig. 8.5: *a) Maximum Likelihood Values, b) model and data comparison, c) differences between model and data for earthquakes after 1980, deeper than 60 km and above a magnitude of 3.8*

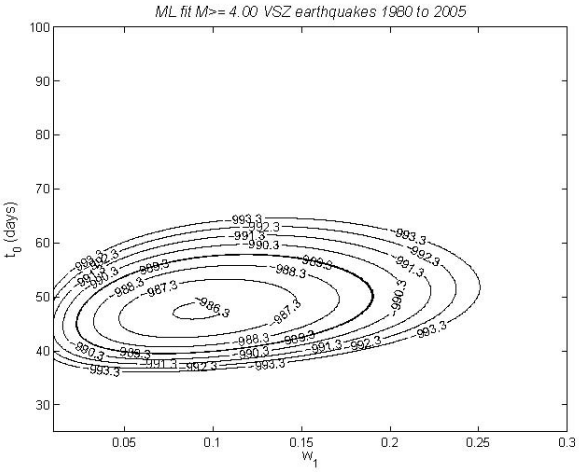

Fig. 8.6 a) Maximum Likelihood Values for w_0 and t_0 with a magnitude cut-off of 4.0, a depth cut-off of 60 km, starting 1980

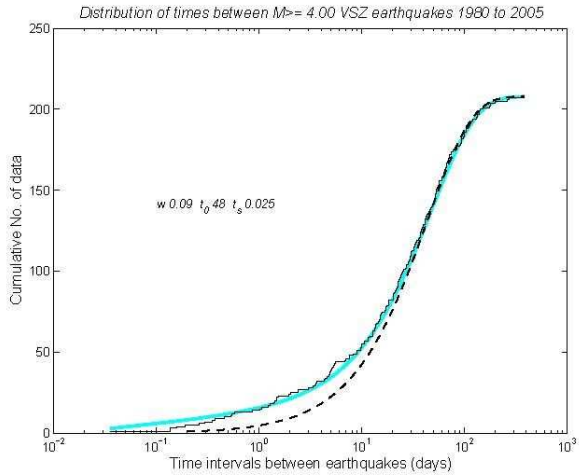

Fig. 8.6 b) Distribution of inter-event times in a logarithmic scale, using a magnitude cut-off of 4.0, a depth cut-off of 60 km, starting 1980

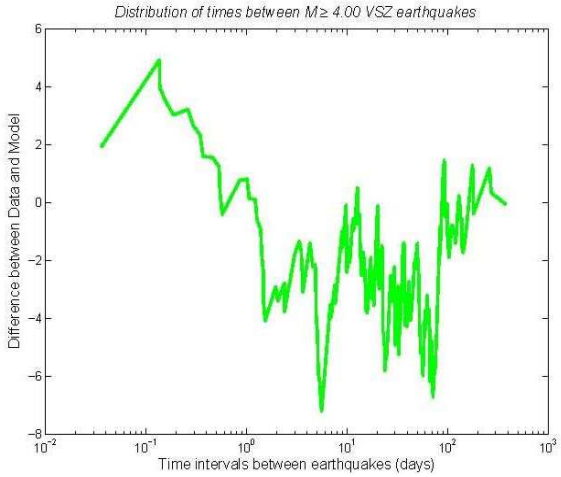

Fig. 8.6 c) Differences between model and data for Mcut ≥ 4.0

Fig. 8.6: *a) Maximum Likelihood Values, b) model and data comparison, c) differences between model and data for earthquakes after 1980, deeper than 60 km and above a magnitude of 4.0*

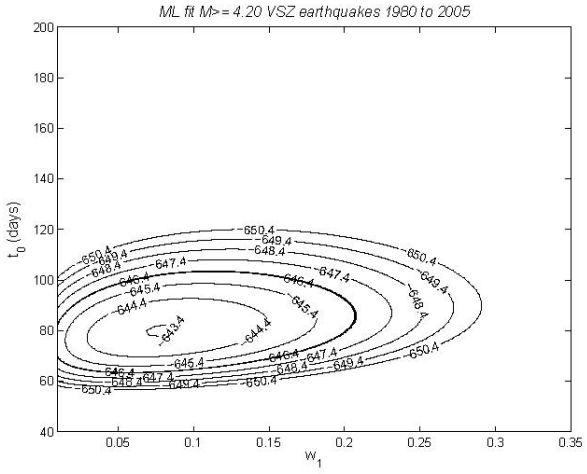

Fig. 8.7 a) Maximum Likelihood Values for w_0 and t_0 with a magnitude cut-off of 4.2, a depth cut-off of 60 km, starting 1980

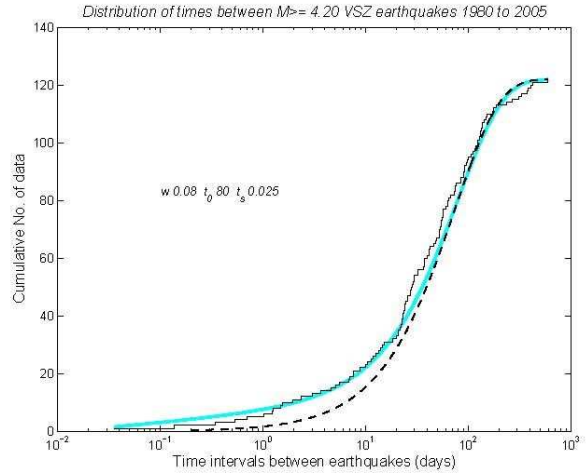

Fig. 8.7 b) Distribution of inter-event times in a logarithmic scale, using a magnitude cut-off of 4.2, a depth cut-off of 60 km, starting 1980

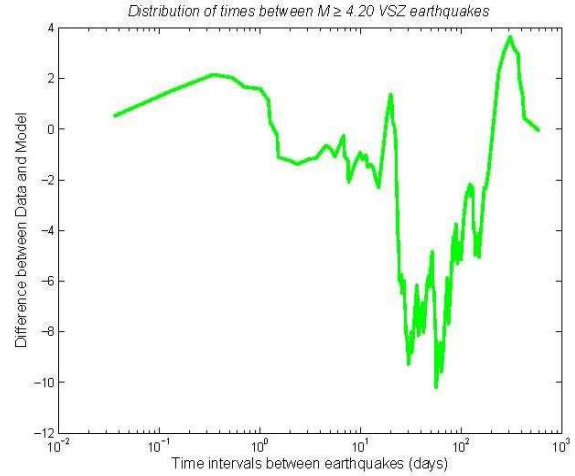

Fig. 8.7 c) Differences between model and data for Mcut ≥ 4.2

Fig. 8.7: *a) Maximum Likelihood Values, b) model and data comparison, c) differences between model and data for earthquakes after 1980, deeper than 60 km and above a magnitude of 4.2*

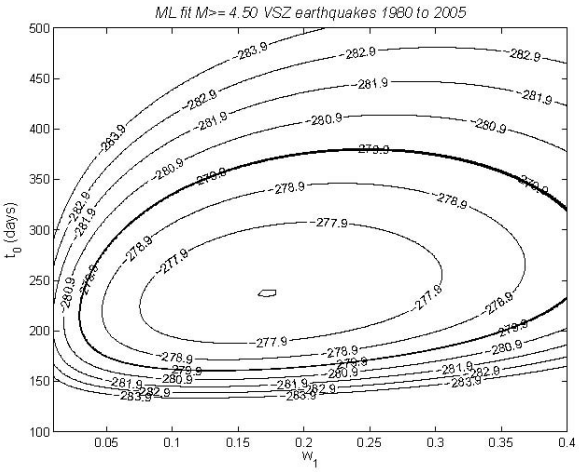

Fig. 8.8 a) Maximum Likelihood Values for w_0 and t_0 with a magnitude cut-off of 4.5, a depth cut-off of 60 km, starting 1980

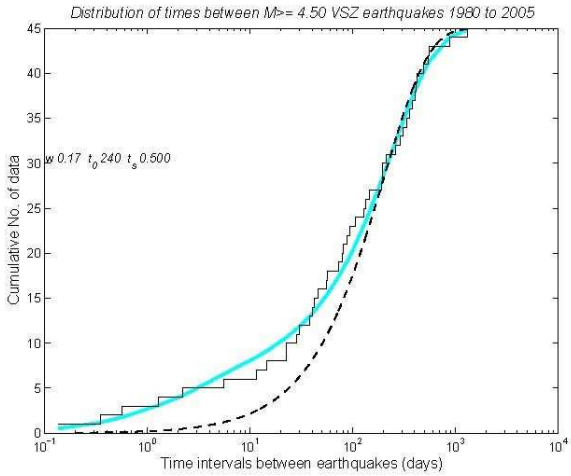

Fig. 8.8 b) Distribution of inter-event times in a logarithmic scale, using a magnitude cut-off of 4.5, a depth cut-off of 60 km, starting 1980

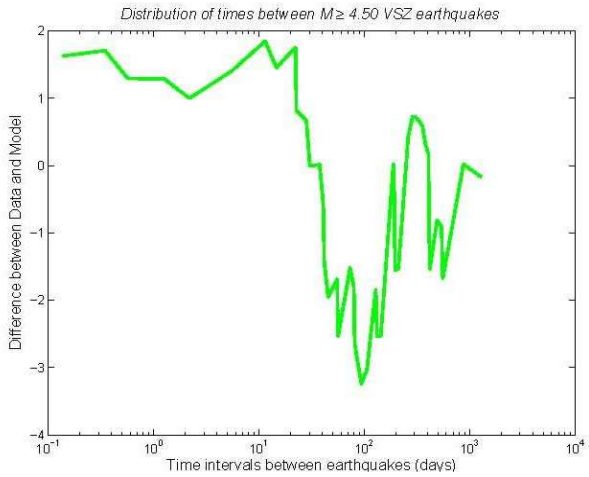

Fig. 8.8 c) Differences between model and data for Mcut ≥ 4.5

Fig. 8.8: *a) Maximum Likelihood Values, b) model and data comparison, c) differences between model and data for earthquakes after 1980, deeper than 60 km and above a magnitude of 4.5*

No. of data	Mcut	ML w	ML t_0 [days]	t_s [days]	error w ± (95%)	error t_0 ± (95%)
795	3.5	0.13	13	0.025	0.07	1
481	3.7	0.09	21	0.025	0.07	2
403	3.8	0.07	24	0.025	0.06	4
208	4.0	0.09	48	0.025	0.10	9
122	4.2	0.08	80	0.025	0.10	20
45	4.5	0.17	240	0.050	0.19	100

The table shows are the parameter values for several magnitude cut-offs.

The errors are taken from the 95% confidence limit shown in the plots 8.1, 8.4a -8.8a. The inter-event time for new earthquakes which is given by the parameter t_0 increases, the percentage of aftershocks decreases and their respective errors increase with increasing cutoff magnitude. For larger data sets the fit of the model seems to be almost independent of the t_s. The decreasing amount of data is quite probably the reason for the increasing error ranges with increasing magnitude cut-off and the less good fit between model and data.

To see if the inter-event times, which were calculated by the Maximum Likelihood Method, are consistent with the Gutenberg-Richter law, I plotted t_0 against the cut-off magnitudes used above (Fig. 8.9). I also added the value of t_0 for a magnitude cut-off of 7 by taking the average inter-event time for M7 earthquakes from the catalogue.

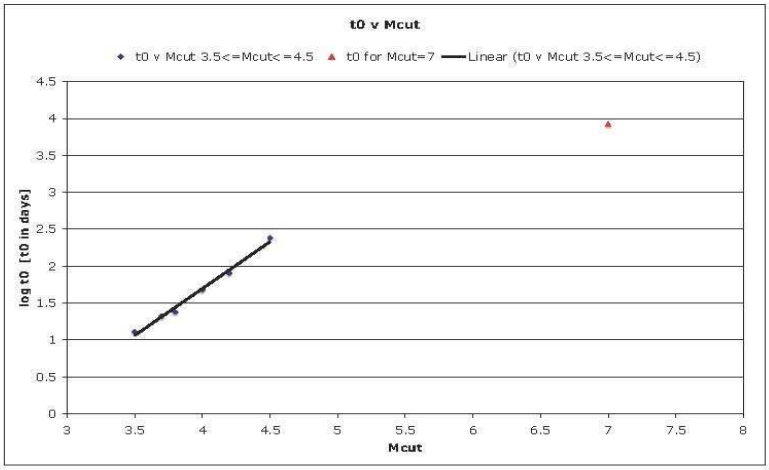

***Fig. 8.9**: Inter-event times for several magnitude cut-offs*

Fig. 8.9 is a straight line which should be expected if the data are consistent. But the interesting thing is, when the formula

$$y = 0.0004e^{2.9181x} \tag{8.10}$$

with *x* standing for the magnitude, is used for a magnitude 7 earthquake, an inter-event time is calculated which is far longer than observed in the past. The formula leads to a recurrence time of M7 earthquakes of 814 years, which is much too long compared to the recurrence times which where found in the catalogue. This means that there are by far more magnitude 7 earthquakes than should be expected from the Gutenberg-Richter law. The Gutenberg-Richter relation in Fig. 3.7b showed a bulge at magnitude 7, which is a hint that there are more M7 earthquakes than normal. The recurrence time for the M7 earthquake in Fig. 8.10 is much shorter than the one forecast by equation 8.10. An average recurrence time of 23 years, which corresponds to about 9000 days, was found from the catalogue for all M7 earthquakes since 1800.

8.3.1 Aftershocks of the large earthquakes in 1986 and 1990

I applied the model to two smaller data sets. I only used the major earthquakes of 1986 and 1990 and the earthquakes which followed in the next 60 and 50 days, respectively.

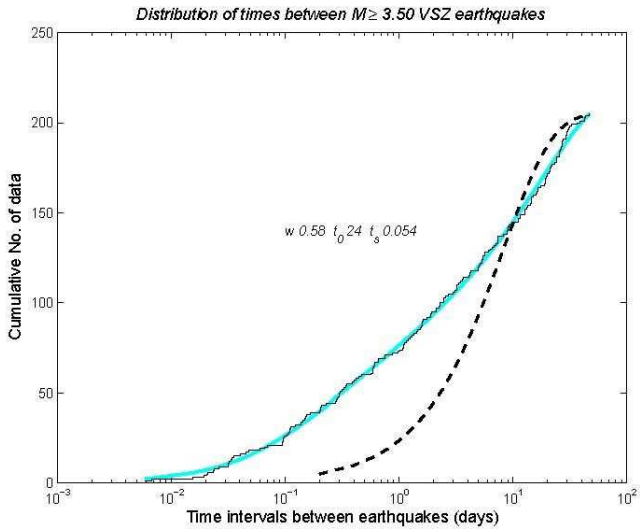

Fig. 8.10 a) Distribution of inter-event times in a logarithmic scale for the 1990 aftershocks, using a magnitude cut-off of 3.5, a depth cut-off of 60 km

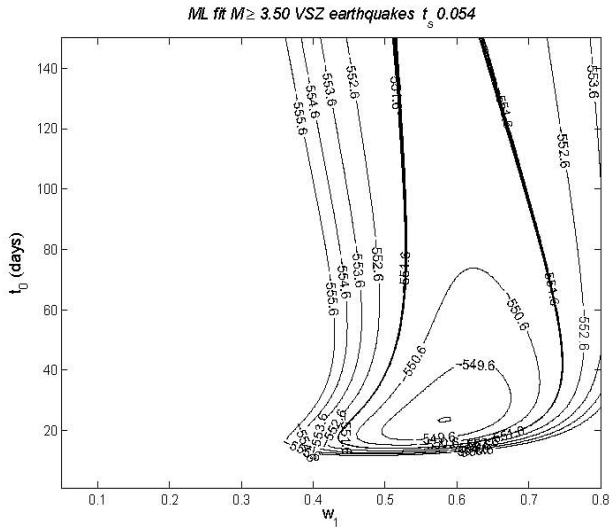

Fig. 8.10 b) Maximum Likelihood Values of w_1 and t_0 for the 1990 earthquakes

Fig. 8.10: *a) Distribution of inter-event times for the 1990 earthquakes, b) Maximum Likelihood Values for w_1 and t_0, using a magnitude cut-off of 3.5, a depth cut-off of 60 km; blue = model, black = data, dashed line = pure Poisson model*

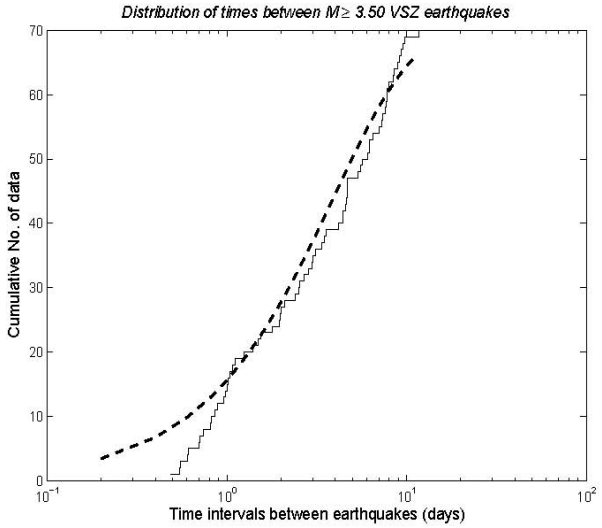

Fig. 8.11: *Distribution of inter-event times in a logarithmic scale for the 1986 aftershocks, using a magnitude cut-off of 3.5*

Fig. 8.10a shows that the model for the 1990 earthquakes fits the data very well. The data consist of 58 ± 15% aftershocks. In Fig. 8.10b it can be seen that t_0 has a large error range. This could have something to do with the small amount of data, which consists of only 60 earthquakes. The result in Fig. 8.11 is different. The 1986 data do not match with the model well. The number of earthquakes is less than Poissonian in the first day after the major event. From this, we conclude that aftershocks were missed in the first day or few days after the main shock.

For the 1990 event t_S has a value of 0.054. Thus, the amount of data seems to have an influence on this parameter as it increases with decreasing number of data or with increasing magnitude.

8.3.2 Shallow earthquakes

Using a magnitude cut-off of 3.5, I plotted data, model and a pure Poisson model for shallow (not deeper than 60 km) earthquakes (Fig. 8.12a, b, c).

The model matches the data well, with an aftershock percentage of 14 ± 13%, a recurrence time for new earthquakes of 258 ± 150 days and a t_S of 0.025 days. The reason for the large error ranges is probably the small amount of data, which consists of only 40 earthquakes.

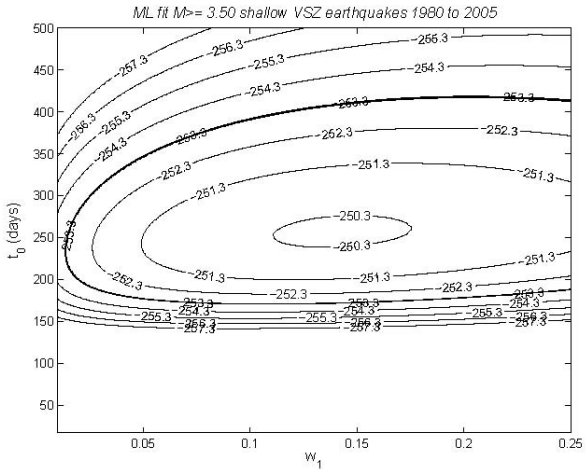

Fig. 8.12 a) Maximum Likelihood Values for w_1 and t_0 for shallow earthquakes, using a magnitude cut-off of 3.5; starting 1980

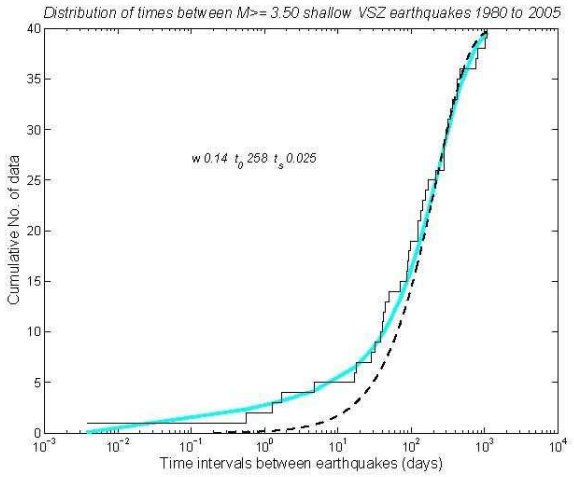

Fig. 8.12 b) Distribution of inter-event times in a logarithmic scale of shallow earthquakes, using a magnitude cut-off of 3.5; starting 1980

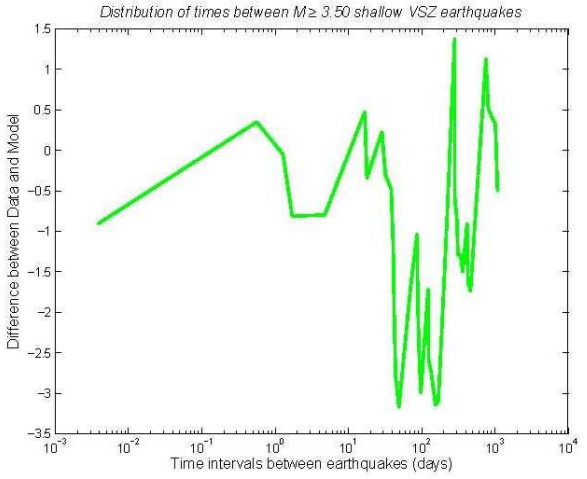

8.12 c) Difference between model and data for shallow Mcut ≥ 3.5 earthquakes

***Fig. 8.12**: a) Maximum Likelihood Values for w_1 und t_0, b) distribution of inter-event times and c) differences between model and data for shallow earthquakes, using a magnitude cut-off of 3.5, starting 1980*

8.4 Conditional probability distribution function

I computed the probability distributions for the time to the next earthquake conditional on the time t_L since the last. To do this I used the following formula:

$$F(t|t_L) = \frac{F(t+t_L)-F(t_L)}{1-F(t_L)} \tag{8.11}$$

Hence,

$$f(t|t_L) = \frac{f(t+t_L)}{1-F(t_L)} \tag{8.12}$$

for t_L = 0 this reverts to being f(t).

I calculated the model and the Poisson model as well as the corresponding ratios of model and Poisson probabilities for several times t_L (0, 0.1, 0.6, 1.0 and 5 days) for all earthquakes after 1980 with a cut-off magnitude of 3.5, deeper than 60 km. The ratio of the model probability to the one of the Poisson model shows when the model predicts more earthquakes and when it predicts as much as the Poisson model. Fig. 8.13a, b -8.17a, b show the ratios for several values of t_L for the data set from 1980, with a magnitude cut-off of 3.5 and depth greater than 60 km.

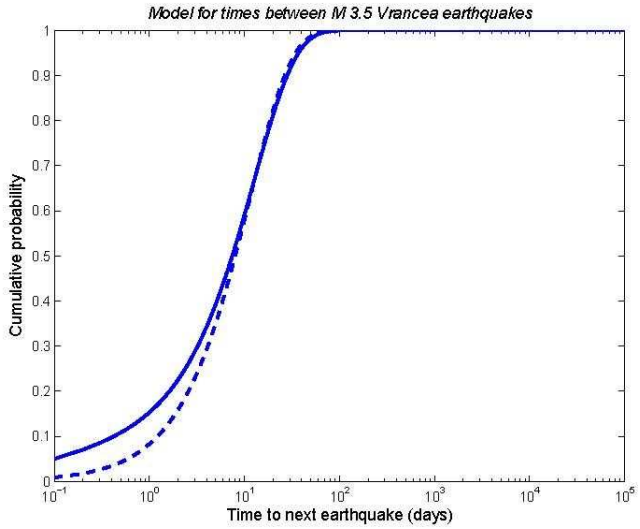

8.13 a) Distribution of inter-event times in a logarithmic scale, using a cut-off magnitude of 3.5, a depth cut-off of 60km, starting 1980, t_L is 0 days

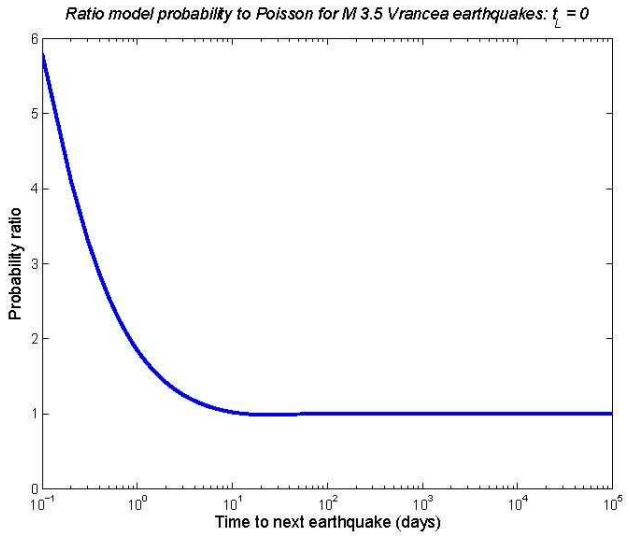

Fig. 8.13 b) Ratio model probability to Poisson, magnitude cut-off is 3.5, depth cut-off is 60 km, starting 1980, t_L is 0 days

***Fig. 8.13**: a) Model distribution of inter-event times for M3.5 earthquakes with a t_L of 0 days and b) ration model probability to Poisson for a t_L of 0 days, solid line = model, dashed line = pure Poisson model*

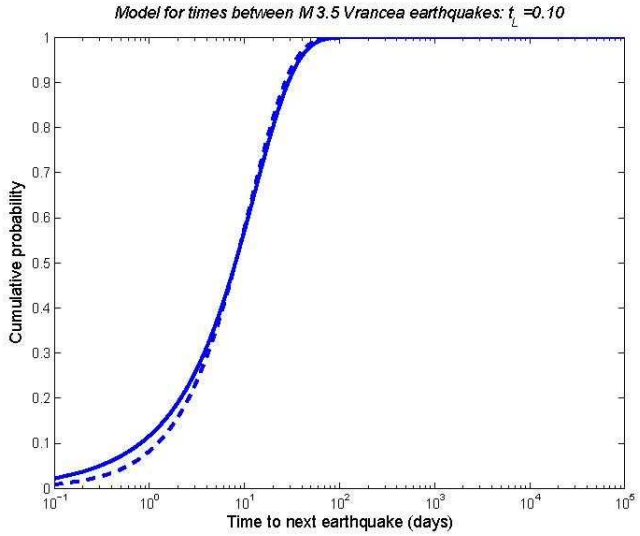

8.14 a) Distribution of inter-event times in a logarithmic scale, using a cut-off magnitude of 3.5, a depth cut-off of 60km, starting 1980, t_L is 0.10 days

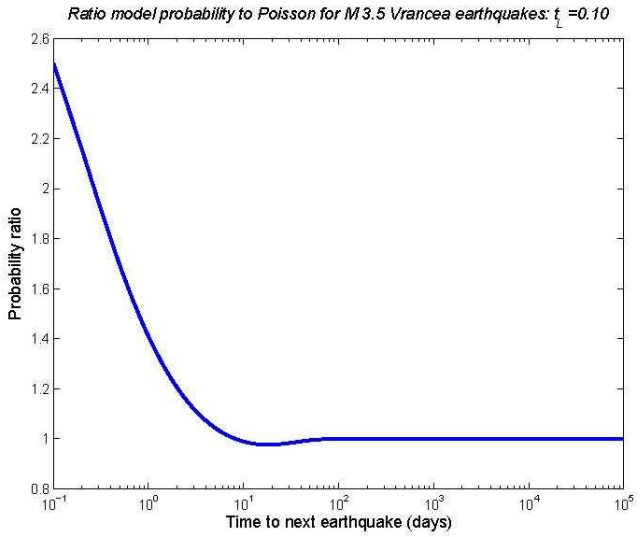

8.14 b) Ratio model probability to Poisson, magnitude cut-off is 3.5, depth cut-off is 60 km, starting 1980, t_L is 0.10 days

***Fig. 8.14**: a) Model distribution of inter-event times for M3.5 earthquakes with a t_L of 0.10 days and b) ration model probability to Poisson for a t_L of 0.10 days, solid line = model, dashed line = pure Poisson model*

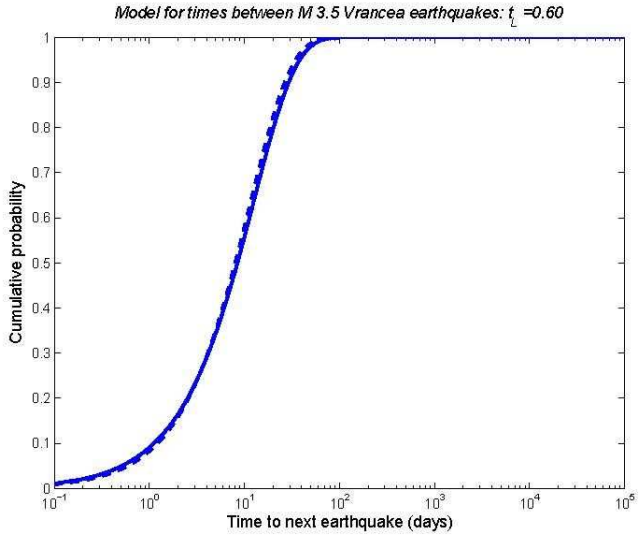

8.15 a) Distribution of inter-event times in a logarithmic scale, using a cut-off magnitude of 3.5, a depth cut-off of 60km, starting 1980, t_L is 0.60 days

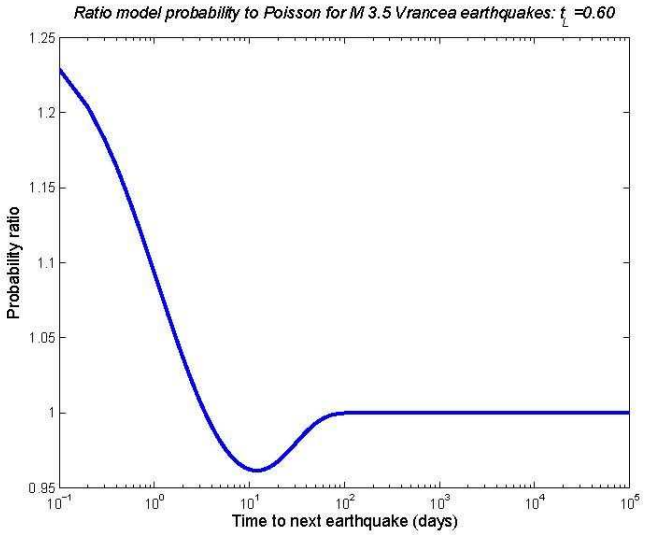

8.15 b) Ratio model probability to Poisson, magnitude cut-off is 3.5, depth cut-off is 60 km, starting 1980, t_L is 0.60 days

***Fig. 8.15**: a) Model distribution of inter-event times for M3.5 earthquakes with a t_L of 0.60 days and b) ration model probability to Poisson for a t_L of 0.60 days, solid line = model, dashed line = pure Poisson model*

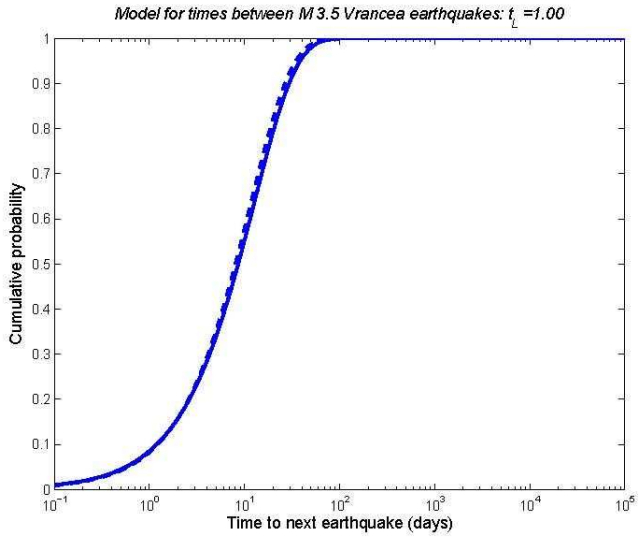

8.16 a) Distribution of inter-event times in a logarithmic scale, using a cut-off magnitude of 3.5, a depth cut-off of 60km, starting 1980, t_L is 1.0 days

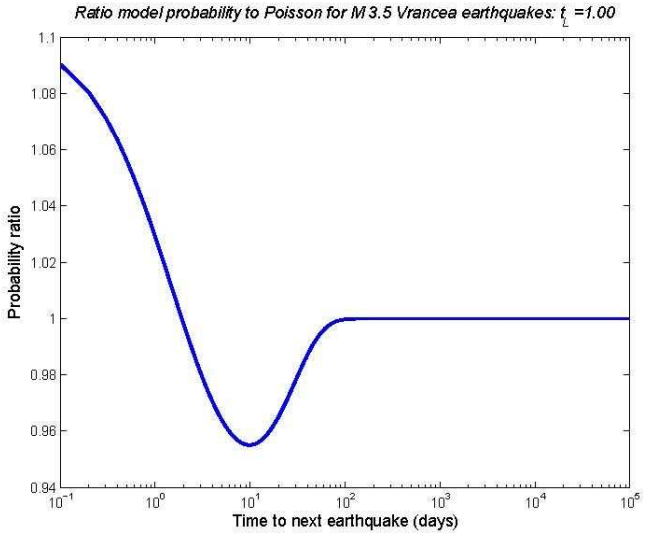

8.16 b) Ratio model probability to Poisson, magnitude cut-off is 3.5, depth cut-off is 60 km, starting 1980, t_L is 1.0 days

***Fig. 8.16**: a) Model distribution of inter-event times for M3.5 earthquakes with a t_L of 1.0 days and b) ration model probability to Poisson for a t_L of 1.0 days, solid line = model, dashed line = pure Poisson model*

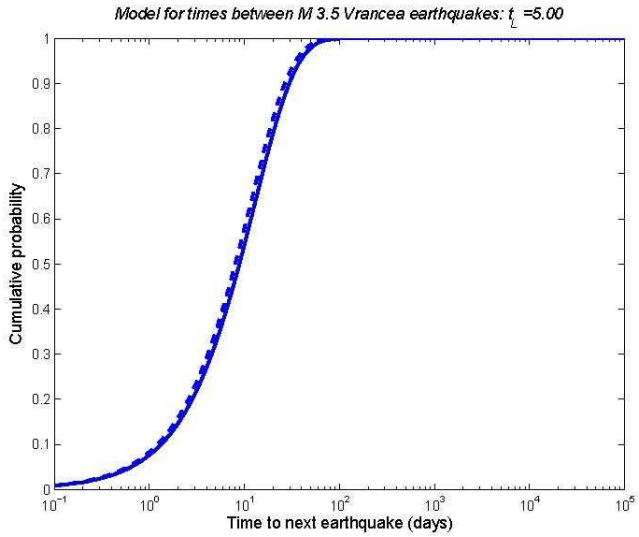

8.17 a) Distribution of inter-event times in a logarithmic scale, using a cut-off magnitude of 3.5, a depth cut-off of 60km, starting 1980, t_L is 5.0 days

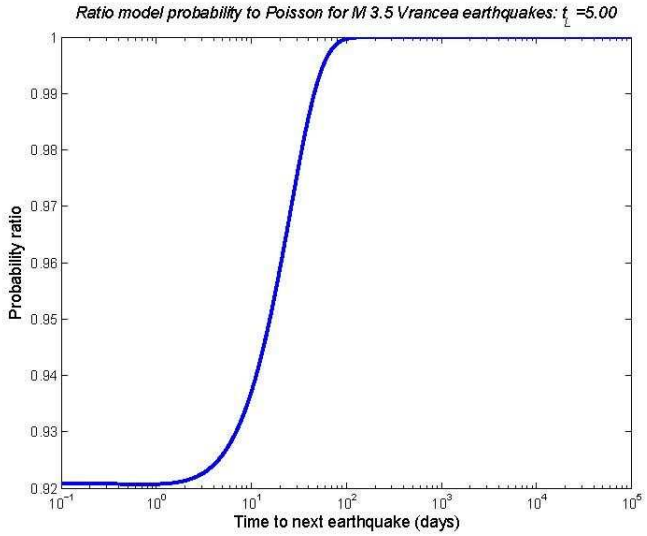

8.17 b) Ratio model probability to Poisson, magnitude cut-off is 3.5, depth cut-off is 60 km, starting 1980, t_L is 5.0 days

Fig. 8.17*: a) Model distribution of inter-event times for M3.5 earthquakes with a t_L of 5.0 days and b) ration model probability to Poisson for a t_L of 5.0 days, solid line = model, dashed line = pure Poisson model*

From Fig. 8.13a -8.17a model (equation 8.4) and Poisson model gradually converge with time, with signs of clustering after the major earthquake and almost identical behaviour after one day. The ratio between the model probabilities, seen in Fig. 8.13b -8.17b, changes with time, too. When t_L = 0 there are about six times more earthquakes than predicted by the Poisson model. After one day, the probabilities for both models are the same. With increasing time the model predicts less earthquakes than predicted by the Poisson model, clearly visible in Fig. 8.17b, where there are first a few earthquakes more than expected and then less events from one to about hundred days after the major earthquake. This behaviour again shows the clustering shortly after the major earthquake and the change to a behaviour according to the seismic gap model after several days. t_L = 1 day seems to be the critical turning point for the whole catalogue, where earthquake behaviour can be seen as Poissonian. This means that aftershock occurrence is generally unlikely one day after the major earthquake, given that there has not been a new major earthquake in this time interval. Fig. 8.17a and b show model and conditional probability 5 days after the major earthquake. Model and Poisson model do not show many differences. In Fig. 8.17b the model predicts less earthquakes than expected by the Poisson model in the first 10 days. The following 90 days, the seismicity increases until it is Poissonian 100 days after the major earthquake. This plot does not show any sign of aftershock behaviour anymore, which confirms the conclusion that there are no significant aftershocks after the first day following the main shock.

The second data set was the one consisting of the 1990 aftershocks. Here, I plotted model (equation 8.11) and pure Poisson model as well as the ratio of their probabilities for the times t_L = 0,1,5,10 days (Fig. 8.18a, b -8.22a, b).

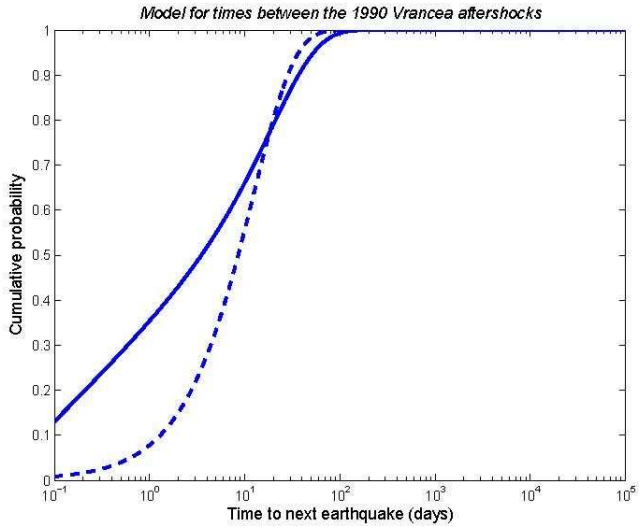

8.18 a) Distribution of inter-event times in a logarithmic scale for the 1990 aftershocks and a t_L of 0 days

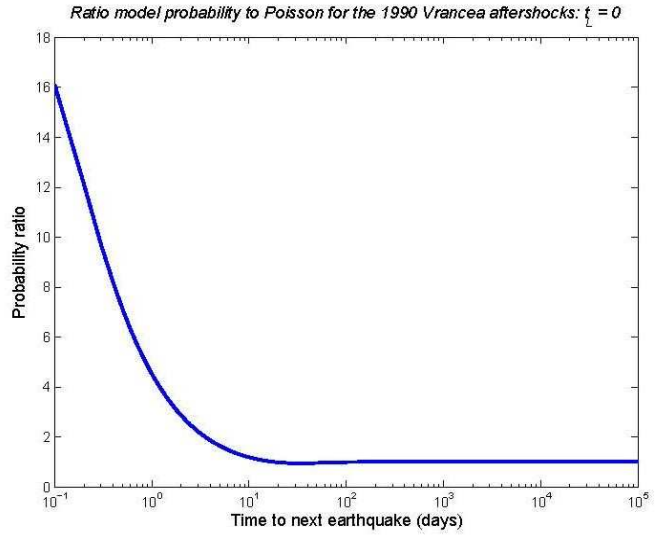

8.18 b) Ratio model probability to Poisson for the 1990 aftershocks and a t_L of 0 days

Fig. 8.18: *a) Distribution of inter-event times of the 1990 aftershocks with a t_L of 0 days and b) ratio model probability to Poisson for a t_L of 0 days; solid line = model, dashed line = pure Poisson model*

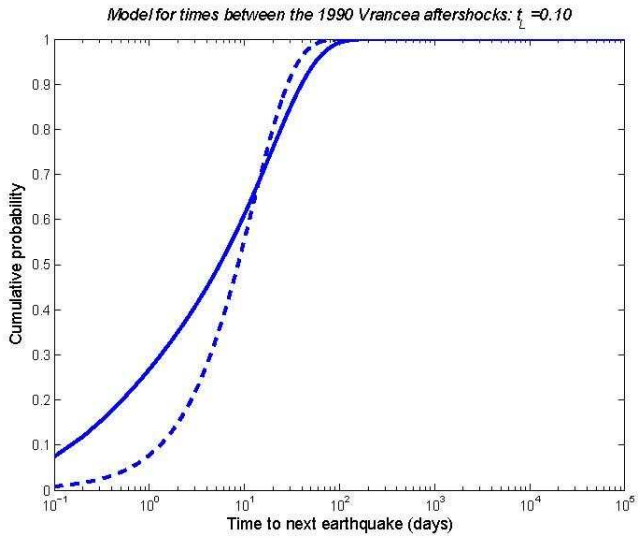

8.19 a) Distribution of inter-event times in a logarithmic scale for the 1990 aftershocks and a t_L of 0.10 days

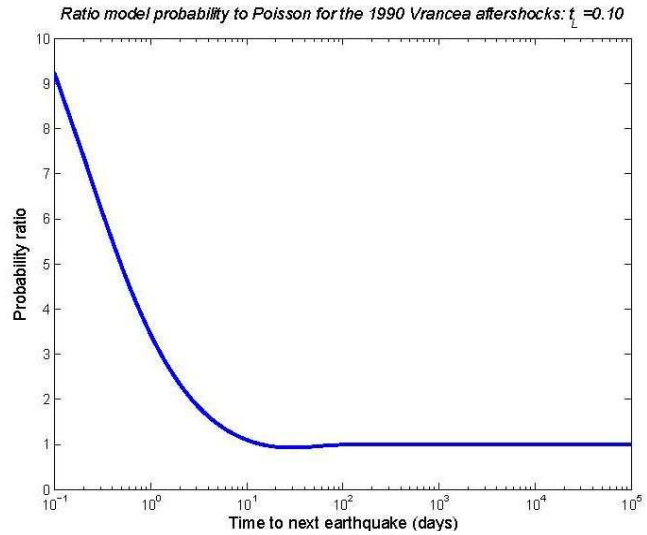

8.19 b) Distribution of inter-event times in a logarithmic scale for the 1990 aftershocks and a t_L of 0.10 days

Fig. 8.19: *a) Distribution of inter-event times of the 1990 aftershocks with a t_L of 0.10 days and b) ratio model probability to Poisson for a t_L of 0.10 days; solid line = model, dashed line = pure Poisson model*

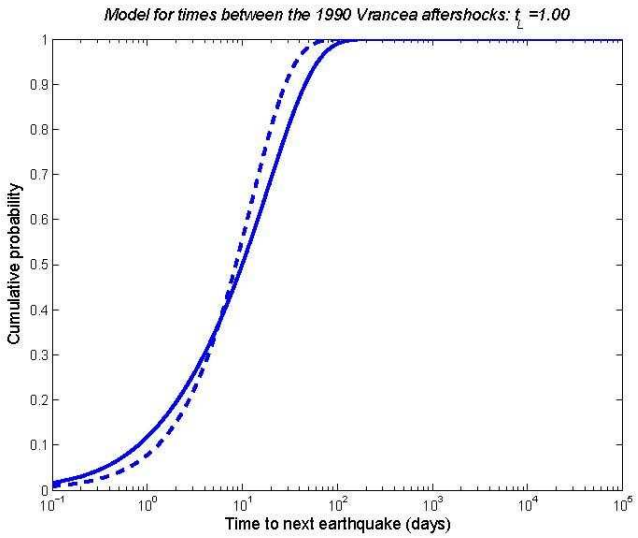

8.20 a) Distribution of inter-event times in a logarithmic scale for the 1990 aftershocks and a t_L of 1.0 days

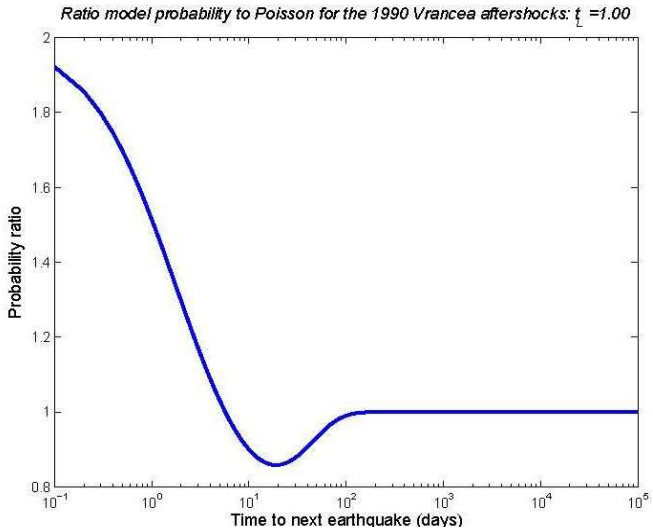

8.20 b) Distribution of inter-event times in a logarithmic scale for the 1990 aftershocks and a t_L of 1.0 days

Fig. 8.20: *a) Distribution of inter-event times of the 1990 aftershocks with a t_L of 1.0 days and b) ratio model probability to Poisson for a t_L of 1.0 days; solid line = model, dashed line = pure Poisson model*

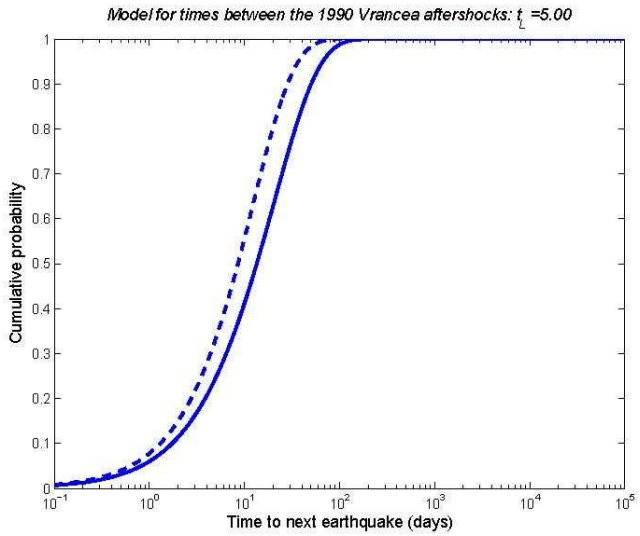

8.21 a) Distribution of inter-event times in a logarithmic scale for the 1990 aftershocks and a t_L of 5.0 days

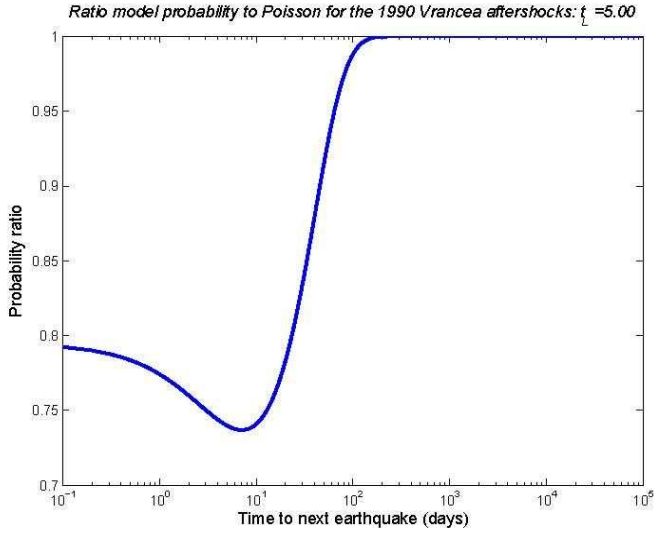

8.21 b) Distribution of inter-event times in a logarithmic scale for the 1990 aftershocks and a t_L of 5.0 days

Fig. 8.21: *a) Distribution of inter-event times of the 1990 aftershocks with a t_L of 5.0 days and b) ratio model probability to Poisson for a t_L of 5.0 days; solid line = model, dashed line = pure Poisson model*

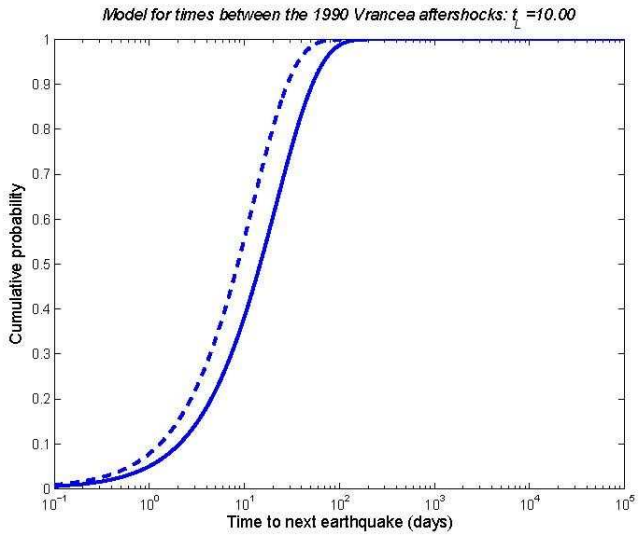

8.22 a) Distribution of inter-event times in a logarithmic scale for the 1990 aftershocks and a t_L of 10.0 days

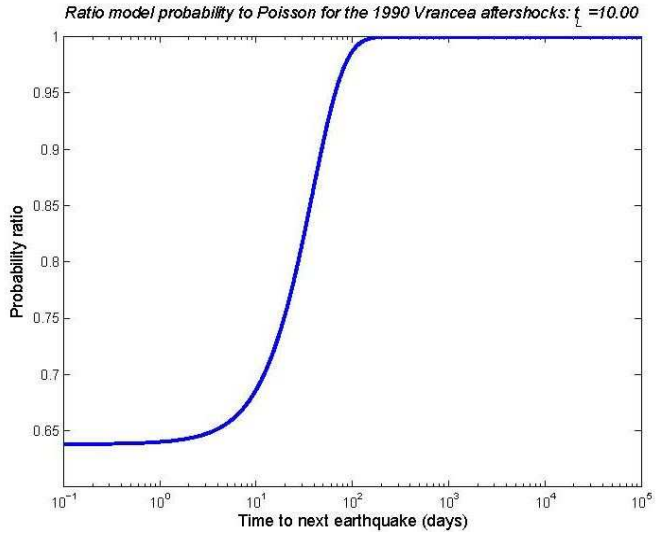

8.22 b) Distribution of inter-event times in a logarithmic scale for the 1990 aftershocks and a t_L of 10.0 days

Fig. 8.22: *a) Distribution of inter-event times of the 1990 aftershocks with a t_L of 10.0 days and b) ratio model probability to Poisson for a t_L of 10.0 days; solid line = model, dashed line = pure Poisson model*

In the Fig. 8.18a -8.22a the model first shows the clustering behaviour after the major earthquake. With increasing time t_L the number of earthquakes is less than Poissonian. In Fig. 8.22a there are clearly less earthquakes than expected according to Poisson. The ratio in Fig. 8.18b, 8.19b and 8.20.b is quite similar to the figures made for the whole time from 1980, but in Fig. 8.18b the model predicts even 16 times more earthquakes than in the Poisson model. Striking is the similarity of the graph between Fig. 8.14b and 8.19b (t_L of 0.1 days). The major difference is that, in the first 24 hours after the major earthquake there are 2.5 times (Fig. 8.14b) compared to 9 times (Fig. 8.19b) more earthquakes than in the Poisson model. This certainly has to do with the magnitude of 6.9 of the 1990 earthquake, while Fig. 8.14b was made for the whole data set after 1980 (including magnitude and depth cut-offs). This similarity in the graph is also seen in Fig. 8.15b and Fig. 8.20b for a t_L of 1 day, starting with 1.09 and 1.9 times more earthquakes than the Poisson model, respectively. Fig. 8.21.b and 8.22b show the probability ratio for 5 and 10 days, respectively and look quite different. Both figures show that there are less earthquakes in the first 100 days after the main shock before the seismicity goes back to being Poissonian.

I conclude that aftershock occurrence is likely to take place in the first 24 hours after the main shock. In this time interval people should stay alert because of a heightened probability that further major earthquakes occur. Then, seismicity slowly goes back to a nearly Poissonian behaviour with even less seismicity in the first 100 days after the main event. I also conclude that the 1990 earthquake and the behaviour of its aftershocks should be considered as a model for future M7 earthquakes.

9. DISCUSSION AND CONCLUSIONS

Working with the Romplus catalogue for VSZ earthquakes and using a new probability function for the recurrence times, we studied the temporal behaviour of these earthquakes.

The Vrancea Seismic Zone in Romania is a source area for large earthquakes and a potential hazard for eastern and southeastern Europe. There occurred several large earthquakes, especially in the last 70 years, which caused a lot of damage and even casualties. Because of insufficient stability of construction, buildings collapse more easily than they do elsewhere. In the past, large parts of Bucharest were damaged and high economic losses were caused, especially when compared to Romania's poverty. In 1977, 1500 people died and 35,000 buildings were damaged during a M7 earthquake. Thus, there is a lot of work done to get a better view on the earthquake potential. Scientists try to find out more about the behaviour of Vrancean earthquakes and their recurrence times. People try to give probabilities for next major earthquakes which could affect the country severly. This project is about a new method to study recurrence times and to get information about the temporal behaviour of earthquakes in the VSZ. To model the data, it is very important that one can be sure about the completeness of the catalogue and the data which are used. There is always a cut-off magnitude under which it can not be sure that all earthquakes where detected. Missing earthquakes can influence the model and cause results which are not trustworthy or which lead to wrong conclusions about the danger or the earthquake potential in the study area. The first thing we looked at, was the quality of the data of the Romplus catalogue. This catalogue is a compilation of several sources and spans the time from 984 to 2005. It consists of more than 8000 earthquakes. The quality of the data was given as 'A', 'B', 'C', 'D' and '=', where 'A' is the best quality, 'D' the worst and the equal sign refers to the lack of any statement about the quality. We looked at the relation of quality to several other factors like the RMS residual, the number of stations or the biggest azimuth angle of separation (GAP). We concluded that further work should only include qualities 'A',

'B' and 'C'. Without the earthquakes with qualities 'D' and '=', half of the catalogue still was left. To exclude earthquakes of magnitudes, which were only partly detected, a magnitude cut-off had to be found. An important tool in finding the cut-off magnitude is the b-value. The b-value is the slope of the graph of the Gutenberg-Richter law which gives the relation between the number of earthquakes and the occurrence of magnitudes. The b-value should have a global value of 1.0. We plotted the Gutenberg-Richter relation first for the whole catalogue. There are more large sized earthquakes than expected by the relation. Assuming that the Gutenberg-Richter law applies for the data, the b-value was plotted against the cut-off magnitude to see at which magnitude value the b-value starts to fall. When the b-value falls under 1.0 it means that earthquakes were not detected and thus are missing in the catalogue. The magnitude at which the b-value starts to fall, should be the correct cut-off. This led to the conclusion that the right magnitude cut-off for our data is 3.5. By plotting the same for a data set from November 1986 to the end of the catalogue, we observed an increase of the b-value by about 0.2 units. We could not draw any conclusion about the reason for this change but there exist several theories about b-value changes, ranging from the state of stress after major earthquakes to detection problems. Interestingly, a 7.2 earthquake happened only a few month earlier, which could be the cause for the increase. The cut-off magnitude decreased after this earthquake to a value of 3.2, but -to be consistent - we used 3.5 as magnitude cut-off for all times.

The stations in Romania were upgraded in the last 20 years. Before this upgrading, the detection threshold was much higher and many earthquakes were missed. We concluded that data prior to the year 1980 should not be taken into consideration for modeling. Furthermore, the average magnitude has a stable value after 1980, except of the first 580 days after 1980, which led to the conclusion that even at these times, earthquakes were missed. Trying to find the cut-off magnitude for shallow earthquakes (depth = 60km) we found that there have to be severe bias in magnitude calculation. The b-value has a value of 1.0 at about the cut-off magnitude for the deep earthquakes but then starts to increase

steeply for smaller magnitudes. The highest value for *b* lies at about 2.4. Then, the b-value shows a sharp decrease. We inferred a cut-off magnitude of 3.6, and, because of rounding effects, used the value 3.5 for modelling the shallow earthquakes. With these conclusions concerning the cut-off magnitude and depth and time limits, Gutenberg-Richter relations for several time and depth intervals were plotted. The plots were made for the whole catalogue time as well as for the earthquakes after 1980. We also plotted the Gutenberg-Richter relation for earthquakes shallower and deeper as 60 km. For both time and depth intervals there are clearly too many magnitude 7 earthquakes than should be expected from by Gutenberg-Richter law. This is an indication that major earthquakes in Vrancea have a characteristic behaviour. To get a better view on the slab and the earthquake distribution, we rotated the earthquake coordinates with a distance cut of 200 km. The plots showed the earthquakes in the slab very clearly. The confined volume in which the earthquakes happen is clearly visible as well as the aseismic part of the slab between 40 km an 60 km and the clustering of earthquakes after 60 km of depth. Judging from the plots that resulted from the rotation, the VSZ has the most earthquakes in a volume of the approximate size of 100 km x 100 km x 180 km. Using a single matrix decomposition, we could calculate the strike as to be 53°. Thus, we could get a view along strike and perpendicular to the strike. Furthermore, we found out that all the magnitude 7 earthquakes happened in the slab and that only the slab earthquakes show clustering behaviour. Because of this, we decided to also introduce a depth limit of 60 km for modeling. To get some information about the temporal behaviour of the earthquake in the Romplus catalogue, we made Cumag and Cusum plots, which show changes in the mean magnitude and changes in the rate of occurrence of earthquakes, respectively. The Cumag, which is the cumulative sum of the difference between each magnitude and the average magnitude, showed the increase of the mean magnitude after each larger earthquake. This means that there were more larger earthquakes after the major events. In the Cusum plot the rate of occurrence after the 1990 major earthquakes increased visibly. This means that there are detected aftershocks after these two earthquakes, which occurred on consecutive days. In the Cusum plot there are changes in the rate

before and after the 7.2 earthquake of 1986. The rate of occurrence was much too low, especially in the first 500 days after 1980, probably because of missing earthquakes. After the 1986 earthquake, from November 1986 on, the rate shows a different behaviour. This indicates that earthquake detection was insufficient before November 1986. Having found the constraints for the catalogue and being sure about catalogue completeness, we could start modeling. We used a model which was developed by Euan Smith and Annemarie Christophersen in 2006. The model was already applied to New Zealand data. It is a new probability function for recurrence times based on the empirical distribution function of inter-event times. It consists of two terms: 1) a term which represents the Omori law of aftershock decay and 2) a term consisting of an exponential Poisson model. The results of the model, calculated with the Maximum Likelihood Method, show the percentage of aftershocks in the data as well as the inter-event times for the earthquakes above the used magnitude cut-offs. We applied the model to the Romanian data. First, we used the earthquakes after 1980 and with a depth minimum of 60 km and several magnitude cut-offs. The model fitted the data well, but an especially good fit was found for a cut-off of 3.5. According to the model, this data set consists of 13 ± 5% aftershocks and has an inter-event time of 13 ± 1 days. We also found the fitting values for higher magnitude cut-offs, but with increasing cut-off the were also increasing uncertainties. The Maximum Likelihood values of the inter-event times of different cut-off magnitudes were plotted against cut-off magnitude. As expected from the Gutenberg-Richter relation, this led to a straight line and showed that these values are consistent and reliable. The inter-event times are increasing and the proportion of aftershocks is decreasing with increasing magnitude cut-off. Although a still good fit was found between model and data, there were increasing uncertainties in w and t_0 with increasing magnitude cut-off. We also used smaller data sets. The first data set consisted of the 1990 earthquake and its aftershocks. The model again fitted very well and calculated 58 ± 15% for the proportion of aftershocks. The inter-event time has a large error range because of the small size of data used. The data set of the 1986 earthquake did not match

at all. Comparing the data with a pure Poisson model, it can be concluded that the aftershocks of the 1986 earthquake were not detected, which caused the differences between model and data. Finally, we compared model and data for shallow earthquakes with a cut-off magnitude of 3.5. The proportion of aftershocks lies at 14 ± 13%, the recurrence time for new events is 258 ± 150 days and *ts* is 0.025 days. The fit between model and data is quite well, but the error range is high, due to a small amount of data. We also plotted the ratio of the conditional probabilities of the model and the Poisson model for the data set consisting of all deep earthquakes after 1980 and with a magnitude cut-off of 3.5 and then for the 1990 aftershocks. For small times after the last earthquake, these ratios show clustering behaviour and with increasing time since the last there are less earthquakes than expected until the seismicity goes back to be Poissonian after about 100 days. This observation matches the result of the model for both data sets. Thus, model and conditional probabilities predict clustering behaviour in the first 24 hours after the main shock, a following decreased seismicity and finally Possonian behaviour after 100 days. This led to the conclusion that the aftershock behaviour is only relevant in the first 24 hours following a main shock. The results also lead to the suggestion that the 1990 earthquake and its aftershocks can be regarded as a kind of model for future Vrancea earthquakes, as they seem to be representative for Vrancean seismicity. The maybe most important conclusion of this work is that the M7 earthquakes of the VSZ have a different behaviour from the smaller ones. The model could predict recurrence times for medium sized earthquakes, but the predicted recurrence time for the damaging M7 earthquakes is 814 years and thus much too long compared to ’real’ recurrence times in the catalogue. Thus, we can not use the model for major events in the VSZ and instead have to consider the catalogue, which gives more realistic information about the recurrence times of M7 earthquakes. It follows that M7 should be studied more closely in the future.

10.APPENDIX

10.1 Rotation of the earthquake coordinates

I wrote longitude, latitude and depth -converted into kilometers -in a matrix X and calculated the product A = XX' to get a square, symmetric and real matrix A, which consists of the squared longitude, latitude and depth in the diagonal, and products of these elsewhere. Symmetric means that $A_{ij} = A_{ji}$ for all elements which are not in the diagonal. I then used the Matlab-command svd to get a new matrix U. The columns of this new matrix U give the new coordinate system which should allow a better view on the slab. This gave me three different views: one of the plain view, one of the spread along the slab and one of the strike of it. The matrix Λ is:

$$\begin{pmatrix} 1.314 & 0 & 0 \\ 0 & 0.327 & 0 \\ 0 & 0 & 0.064 \end{pmatrix} * 10^6$$

The values $\sum_{i=1}^{3} s_{ii}$ give the variance of the spread in the three different directions on the slab, with the first value as the largest , and the last the smallest one.

10.2. Romplus Catalogue

year	month	Day	hour	minute	second	latitude	longitude	depth
1990	5	30	10	40	6.4	45.83	26.89	90.0
1990	5	30	10	48	32	45.67	26.94	67.2
1990	5	30	10	49	45.7	45.94	26.8	94
1990	5	30	11	2	21	45.79	26.84	93.9
1990	5	30	11	7	51.5	45.86	26.8	99.6
1990	5	30	11	9	41.8	45.73	26.88	86.1
1990	5	30	11	10	23.3	46.01	26.88	93.7

Example for the Romplus catalogue – part One

magnitude	no. of stations	NA	NM	RMS	time error	loc error	loc error	depth error
6.9	12	14	0	0.2	0.6	2.7	2.2	6.4
3.4	6	10	4	0.98	2.7	14.2	14	33.5
3.5	8	12	5	0.97	2.5	14.9	12.7	25.1
3.9	8	12	6	0.38	1.4	8.9	6.8	10.1
3.6	10	17	8	0.46	1.3	11	4.8	9.7
2.7	6	8	3	0.57	2.3	10.4	11.2	25
2.9	5	7	2	0.21	1.3	6.1	9.8	8.4

Example for the Romplus catalogue – part Two

NA = number of phases

NM = number of magnitudes per station

Bibliography

Aki K., 1965, *Maximum likelihood estimates of b in the formula log N = a-bM and its confidence limits*, Bull. Earthquake Res. Inst., Tokyo Univ., **43**, 237-239

Allen C.R., 1976, *Responsibilities in earthquake prediction*, Bull. Seism. Soc. Am., **66**, 6, 2069-2074

Anderson H., Webb T., 1994, *New Zealand seismicity: patterns revealed by the upgraded National Seismograph Network*, New Zealand Journal of Geology and Geophysics, **37**, 477-493

Ardeleanu L., 1999, *Statistical models of the seismicity of the Vrancea Region, Romania*, Natural Hazards, **19**, 151-164

Barros L.R., Chase J.G., Hunt S., 2003, *Probabilistic Seismic Hazard Analysis of semi-active controlled 9-story steel moment-resisting structure*, 16th ASCE Engineering Mechanics Conference

Baumann M., Grosser H., Romero Torres G., Rojas Gonzales J. L., Sobiesiak M., Welle W., 2003, *Aftershock pattern of the July 9, 1997 Mw=6.9 Cariaco earthquake in Northeastern Venezuela*, Tectonophysics, **379**, 1-4, 1-23

Bazacliu O., Radulian M., 1999, *Seismicity variations in depth and time in the Vrancea (Romania) subcrustal region*, Natural Hazards, **19**, 165-177

Bommer J.J., Scherbaum F., Bungum H., Cotton F., Sabetta F., Abrahamson N.A., 2005, *On the use of logic trees for ground-motion prediction equations in seismic hazard analysis*, Bull. Seis. Soc. Am., **95**, No. 2, 377-389

Bowman D.D., Sammis C.G., 2004, *Intermittent criticality and the Gutenberg-Richter distribution*, Pure appl. geophys., **161**, 1945-1956

Console R., Murru M., Lombardi A.M., 2003, *Refining earthquake clustering models*, **108**, B10 , doi:10.1029/2002JB002130

Davey F.J., Henyey T., Holbrook W.S., Okaya D., Stern T.A., Melhuish A., Henrys S., Anderson H., Eberhart-Phillips D., McEvilly T., Uhrhammer R., Wu F., Jiracek G.R., Wannamaker P.E., Caldwell G., Christensen N., 1998, *Preliminary results from a geophysical study across a modern continent -continent collisional plate boundary -the Southern Alps, New Zealand* , Tectonophysics, **288**, 221-235

Dieterich J.H., 1999, *Earthquake nucleation and its relationship to earthquake clustering* ,

U.S. Geological Survey

Eberhart-Phillips D., Reyners M., 1997 *Continental subduction and three-dimensional crustal structure: the northern South Island, New Zealand* J. Geophys. Res. ,**102** ,B6, 11,843-11,861

Evison F.F., Rhoades D.A. , 2005, *Multiple-mainshock events and long-term seismogenesis in Italy and New Zealand*, New Zealand Journal of Geology and Geophysics, **48**, 423-536

Evison F.F., Rhoades D.A., 2004, *Demarcation and Scaling of long-term seismogenesis*, Pure appl. geophys., **161**, 21-45

Fan G., Wallace T., Zhao D., 1998, *Tomographic imaging of deep velocity structure beneath the Eastern and Southern Carpathians, Romania: Implications for continental collision* , J. Int. Geophys.,**103**, B2, 2705-2723

Felzer K., 2006, *Calculation and confidence intervals of the Gutenberg-Richter b* Geller R.J., Jackson D.D., Kagan Y.Y., Mulargia F., 1997, *Earthquakes can not be predicted*, Science, **275**, 5306, DOI: 10.1126/science.275.5306.1616

Godano C., Pingue F., 2000, *Is the seismic moment-frequency relation universal?*, Geophys. J. Int., **142**, 193-198

Hank T.C., Kanamori H., 1979, *A moment magnitude scale*, J. Geophys. Res., **84**, 2348-2350

Helmstetter A., Kagan Y.Y., Jackson D.D., 2006, *Comparison of short-term time-independent earthquake forecast models for Southern California*, **96**, 90-106

Helmstetter A., Kagan Y.Y., Jackson D.D., 2005, *Importance of small earthquakes for stress transfers and earthquake triggering*, J. Geophys. Res., **110**, No.5, doi:10.1029/2004JB003286

Hong L.-L., Guo S.-W., 2005, *Nonstationary Poisson model for earthquake occurrences*, Bull. Seis. Soc. Am., **3**, 814-824

Hsu Y.-J., Simons M., Avouac J.-P., Galetzka J., Sieh K., Chlieh M., Natawidjaja D., Prawirodirdjo L., Bock Y., 2006, *Frictional afterslip following the 2005 Nias-Simeuleu earthquake, Sumatra*, Science, **312**, 1921

Hurukawa N., Popa M, Radulian M., 2006, *Where and when will the next M7 Vrancea (Romania) intermediate-depth earthquakes occur?*, Geophysical Research Abstracts, Vol. **8**, 01581

Ismail-Zadeh A.T., Panza G.F., Naimark B.M., 1996, *Stress in the descending relic slab*

beneath Vrancea, Romania, United Nations Educational Scientific and Cultural Organization and International Atomic Energy Agency, International Center for Theoretical Physics

Jackson D.D., Kagan Y.Y, 2006, *The 2004 Parkfield Earthquake, the 1985 prediction, and characteristic earthquakes: Lessons for the future*, **96**, 397-409

Johnson P.A., Xiaoping J., *Nonlinear dynamics, granular media and dynamic earthquake triggering*, 2005, Nature , **437**

Kagan Y.Y., 1999, *Universality of the seismic moment-frequency relation*, Pure appl. geophys., **155**, 537-573

Kagan Y.Y., Jackson D.D., Liu Z., 2005, *Stress and earthquakes in Southern California, 1850-2004*, J. Geophys. Res., **110**, No. 5, doi:10.1029/2004JB003313

Kagan Y.Y., 2005, *Earthquake slip distribution: a statistical model*, J.Geophys. Res., **110**, No.5, doi:10.1029/2004JB003280

Kagan Y.Y., 2004, *Short-term properties of earthquake catalogues and models of earthquake source*, Bull. Seis. Soc. Am., **94**, No.4, 1207-1228

Kagan Y.Y., 2002, *Aftershock zone scaling*, Bull. Seis. Soc. Am., **92**, No.2, 641-655

Kagan Y.Y., Jackson D.D., 2002, *Probabilistic forecasting of earthquakes*, Geophys. J. Int., **143**, 438-453

Kagan Y.Y., 1997, *Are earthquakes predictable?*, Geophys. J. Int., **131**, 505-525

Kagan Y.Y., Jackson D.D., 1995, *New seismic gap hypothesis: five years after* , J. Geophys. Res., **100**, B3, 3943-3959

Kagan Y.Y., 1993, *Statistics of characteristic earthquakes*, Bull. Seis. Soc. Am., **83**, 7-24

Kagan Y.Y., 1991, *Seismic moment distribution*, Geophys. J. Int., **106**, 123-134

Kagan Y.Y., Jackson D.D., 1991, *Long-term earthquake clustering*, Geophys. J. Int., **104**, 117-133

Kagan Y.Y., Houston H., 2005, *Relation between main shock rupture process and Omori's law for aftershock moment release rate*, Geophys. J. Int., **163**, 1039-1048

Kagan Y.Y., Knopoff L., 1980, *Dependence of seismicity on depth*, Bull. Seis. Soc. Am., **70**, No.5, 1811-1822

Kagan Y.Y. Houston H., 2005, *Relation between main shock rupture process and Omori's law for aftershock moment release rate*, University of California, Postprints, Paper 1600

Kagan Y.Y., 2004, *Short-term properties of earthquake catalogs and models of earthquake source*, Bull. Seis. Soc. Am., **94**, 1207-1228

Kagan Y.Y., Knopoff L., 1987, *Statistical short-term earthquake prediction*, Science, **236**, 1563-1567

Maeda K., 1996, *The use of foreshocks in probabilistic prediction along the Japan and Kuril trenches*, Bull. Seis. Soc. Am., **86**, 242-254

Maentyniemi P., Mˆarza V.I., Kijko A., Retief P., 2003, *A new probabilistic seismic hazard analysis for the Vrancea (Romania) Seismogenic Zone* , Natural Hazards, **29**, 371-385

Martin M., Wenzel F., 2006, *High-resolution body-wave tomography beneath SW Romania – II Imaging of a slab detachment scenario*, Geophys. J. Intern, **163**(3), 579-595

Matsumura S., 2005, *Seismic Activity Changes progressing simultaneously with Slow-Slip in the Tokai Area*, Tectonophysics, **417**, Issues 1-2, 5-15 Merrifield A., Savage M.K., Vere-Jones D., 2004, *Geographical distributions of prospective foreshock probabilities in New Zealand*, New Zealand Journal of Geology and Geophysics, **47**, 327-339

Molchan G.M., Dmitricva O.E., 1992, *Aftershock identification: methods and new approaches*, Geophys J. Int., **109**, 501-516

Musson R.M.W., Tsapanos T., Nakas C.T. ,2002, *A power-law function for earthquake interarrival time and magnitude*, **92**, 1783-1794

Necea D., Fielitz W., Matenco L., 2005, *Late Pliocene-Quaternary tectonics in the frontal part of the SE Carpathians: insights from tectonic geomorphology*, Tectonophysics, **410**, 1-4, 137-156

Ogata Y., Zhuang J., Vere-Jones D., 2002, *Stochastic declustering of space-time earth-quake occurrences*, Journal of the American Statistical Association, **97**, 458, 369-379

Ogata Y., 1988, *Statistical models for earthquake occurrence and residual analysis for point processes*, J. Am. Statist. Assoc., **83**, 9-27

Onescu M.C., Marca V.I., Rizescu M., Popa M., 1998, *The Romanian earthquake catalogue between 984-1996* in: Vrancea Earthquakes, Wenzel F., Lungu D., & Novak O. (eds.), Kluwer Academic Publishers, Dordrecht, Netherlands, 1998

Parsons T., 2002, *Global Omori's Law rate decay of triggered earthquakes: large aftershocks ouside the classical aftershock zone*, J. Geophs. Res., **107**, B9, doi:10.1029/2001JB000646

Parsons T., 2005, *A hypothesis for delayed dynamic earthquake triggering*, Geophys. Res. Lett., **32**, L04302, doi:10.1029/2004GL021811

Pisarenko V. F., 1970, *Some applications of the Maximum Likelihood Method in*

seismology, Geophys. J. R. astr. Soc., **21**, 307-322

Radulian M., Vaccari F., Mandrescu N., Moldoveanu C.L., Panza G.F., 2002, *Seismic hazard in Romania associated to Vrancea subcrustal source: deterministic evaluation*, United Nations Educational and Cultural Organization and International Atomic Energy Agency, available at *http* : //*www.ict p.trieste.it/ pub*o*ff*

Radulian M., Bonjer K.-P., Popescu E., Popa M., Ionescu C., Grecu B., 2007, *The October 27th, 2004 Vrancea (Romania) earthquake*, Orfeus Newsletter, **7**, No. 1

Reyners M., 1998, *Plate coupling and the hazard of large subduction thrust earthquakes at the Hikurangi subduction zone, New Zealand*, New Zealand Journal of Geology and Geophysics, 1998, **41**, 343-354

Rong Y., Jackson D.D., Kagan Y.Y., 2003, *Seismic gaps and earthquakes*, J. Geophys. Res., **108**, B10, 2471, ESE-6, 1-14, doi:10.1029/2002JB002334

Savage M.K., Rupp S., 2000, *Foreshock probabilities in New Zealand*, New Zealand Journal of Geology and Geophysics, **43**, 461-459

Shcherbokov R., Turcotte D.L., Rundle J.B., 2004, *A generalized Omori's law for earthquake aftershock decay*, Geophys. Res. Lett., **31**

Smith E.G.C., Christophersen A., 2006, *A new formulation of Omori's law for aftershock decay in models for earthquake occurrence conditional on the time since the last earthquake*, personal contact

Sornette D., Knopoff, 1997, *The paradox of the expected time until the next earthquake*, Bull. Seis. Soc. Am., **87**, 789-798

Sperner B., Lorenz F., Bonjer K., Hettel S., Mueller B., Wenzel F., 2001, *Slab break-off abrupt cut or gradual detachment? New insights from the Vrancea Region (SE Carpathians, Romania)*, Terra Nova, **13**, 172-179

Stirling M.W., Berryman K.R., Wesnousky S.G., 1998, *Probabilistic seismic hazard analysis for New Zealand*, New Zealand Journal of Geology and Geophysics, **41**, 355-375

Stirling M.W., McVerry G.H., Berryman K.R., 2002, *A new seismic hazard model for New Zealand* Bull. Seis. Soc. Am., **92**, No.5, 1878-1903

Stock C., Cmith E.G.C., 2002, *Comparison of seismicity models generated by different kernel estimations*, Bull. Seis. Soc. Am., **92**, No.3, 913-922

Tebbens S.F., Burroughs S.M., 2003, *Temporal Truncation as an explanation for the change in b-value preceding large earthquakes*, Geophysical Research Abstracts, 5

Tormann T., 2005, *Dynamic seismic hazard model for New Zealand*, Master Thesis, Victoria University of Wellington, New Zealand

Utsu T., Seki A., 1955, *Relation between the area of aftershock region and the energy of the main shock*, J. Seismol., Soc. Japan, 233-240

Van der Hoeven A.G.A., 2003, *Crustal motions in the Eastern Carpathians (Vrancea) measured by GPS* , Projectreport

Volant P., Grasso J.-R., Chatelain J.-L., Frogneux M., 1992, *b-Value, Aseismic Deformation and Brittle Failure within an Isolated Geologcal Object: Evidences from a Dome Structure loaded by Fluid Extraction*, Geophys. Res. Lett., **19**, 11, 1149-1152

Wang L., Chen P., Wu Z., Bai T.M *Characteristics of foreshock and its identification*, Acta Seismologica Sinica, **18**, No 2, 180 -188

Wenzel F., Sperner B., Lorenz F., Mocanu V., 2002, *Geodynamics, tomographic images and seismicity of the Vrancea region (SE-Carpathians, Romania)*, EGU Stephan Mueller Special Publication Series, 3**,** 95-104

Wenzel F., *Perspective in modern seismology*, Lecture notes in Earth Sciences, **105**, Springer, 2005

Wesnousky S.G., 1994, *The Gutenberg-Richter or Characteristic Earthquake Distribution, which is it?,* Bull. Seis. Soc. Am., **84**, 1940-1959